NASA CR 121217

N73-26286

MULTIPLE JET STUDY

FINAL REPORT

by

R. E. Walker

and

D. L. Kors

Aerojet Liquid Rocket Company
Sacramento, California 95812

Prepared for

National Aeronautics and Space Administration

NASA Lewis Research Center
Contract NAS3-15703
J. D. Holdeman, Project Manager

1. Report No.	2. Government Accession No.	3. Recipient's Catalog No.
NASA CR-121217		

4. Title and Subtitle	5. Report Date
MULTIPLE JET STUDY - FINAL REPORT	June 1973
	6. Performing Organization Code

7. Author(s)	8. Performing Organization Report No.
R. E. Walker and D. L. Kors	
	10. Work Unit No.

9. Performing Organization Name and Address	11. Contract or Grant No.
Aerojet Liquid Rocket Company P. O. Box 13222 Sacramento, California 95813	NAS 3-15703
	13. Type of Report and Period Covered
12. Sponsoring Agency Name and Address	Contractor Report
National Aeronautics and Space Administration Washington, D. C. 20546	14. Sponsoring Agency Code

15. Supplementary Notes

Project Manager, James D. Holdeman, Air Breathing Engines Division,
NASA Lewis Research Center, Cleveland, Ohio 44135

16. Abstract

Test data is presented which allows determination of jet penetration and mixing of multiple cold air jets into a ducted subsonic heated mainstream flow. Jet-to-mainstream momentum flux ratios ranged from 6 to 60. Temperature profile data is presented at various duct locations up to 24 orifice diameters downstream of the plane of jet injection. Except for two configurations, all geometries investigated had a single row of constant diameter orifices located transverse to the main flow direction. Orifice size and spacing between orifices were varied. Both of these were found to have a significant effect on jet penetration and mixing. The best mixing of the hot and cold streams was achieved with spacing between the orifices equal to one half of the duct height. For this spacing, variation in orifice size changed the mean exit temperature level, but did not significantly alter the shape of the distributions. The mixing at the various test conditions was evaluated using an energy exchange parameter developed in this program. Comparison of the results of this study with existing single jet data indicates that single jet correlations do not adequately describe the multiple jet results.

17. Key Words (Suggested by Author(s))	18. Distribution Statement
Jet Mixing; Jet Penetration; Jets in Crossflow; Combustion Gas Dilution; Temperature Distribution	Unclassified - Unlimited.

19. Security Classif. (of this report)	20. Security Classif. (of this page)	21. No. of Pages	22. Price*
Unclassified	Unclassified	104	$3.00

* For sale by the National Technical Information Service, Springfield, Virginia 22151

FOREWORD

The work described herein was conducted by the Aerojet Liquid Rocket Company under NASA Contract NAS3-15703; the period of performance was 31 March 1972 through 31 March 1973. Dr. J. D. Holdeman, NASA-Lewis Research Center, was the NASA Project Manager.

Mr. D. M. Campbell and Mrs. N. M. Kosko of the Engineering Computer Services Department, ALRC provided invaluable assistence in setting up the computerized data reduction and plotting routines used throughout this program.

Messers D. M. Jassowski, G. Chin and A. R. Keller of the ALRC Aerophysics Laboratory provided the technical expertise in the areas of test facility design, data acquisition/instrumentation and test facility buildup upon which the success of the program depended.

TABLE OF CONTENTS

TABLE LIST

FIGURE LIST

Figure List (cont.)

I SUMMARY

The objective of this study was to determine empirically the penetration and mixing characteristics of multiple jets of ambient air injected normally into a heated uniform flow between parallel walls. The range of geometric and flow variables for this program were selected to make the experimental data relevant to the design of combustors for gas turbine engines.

Primary independent test variables were the orifice plate configuration (16 orifice plate configurations were tested) and the ratios of jet-to-mainstream momentum flux. The orifice plates contained sharp edged orifices ranging in diameter from 0.63 cm (0.25 in.) to 2.54 cm (1.0 in.) with the dimensionless orifice spacing, S/D, varied between 2 and 6. Momentum flux ratios were varied by changing mainstream temperature and velocity, and jet velocity in a prescribed manner. The mainstream flow field temperatures surveyed were 450°K (810°R), 600°K (1080°R), and 750°K (1350°R), and the mainstream velocity was varied from 15 m/sec (50 ft/sec) to 40 m/sec (155 ft/sec). Jet velocities, at the jet vena contracta, ranged from 25 m/sec (83 ft/sec) to 121 m/sec (396 ft/sec). The jet penetration and mixing characteristics were determined by total pressure and temperature surveys throughout the flow downstream of the plane of secondary injection.

The results of this study are based on experimental observations. No tasks to model the jet penetration and mixing processes were within the scope of this program. A mixing parameter, E_T, derived from observations of the experimental data, expresses the mixing effectiveness as a percent of the ideal energy exchanged between the cool jets and the hot mainstream. The correlation of E_T with the operating and design variables surveyed during this study, in graphical form, was an end product of the investigation. In addition to these E_T correlations, isometric and contour plots of a non-dimensional temperature parameter are presented for a variety of test conditions and orifice geometries. These plots show the temperature profiles in the test duct at several locations and clearly illustrate the penetration and

mixing characteristics of the secondary jets under a variety of conditions.

Based on evaluation of these data, the jet-to-mainstream momentum flux ratio is the most important operating variable influencing jet penetration and mixing. Neither the absolute momentum flux level of the two streams nor the jet-to-mainstream density ratio appeared to influence jet penetration or mixing significantly, except for the density ratio contribution to the momentum flux ratio. At a given momentum flux level and distance from the injection plane, jet penetration and mixing increased with increasing orifice diameter. However, the increase in jet penetration with increased orifice diameter was influenced strongly by the orifice spacing. Closely spaced orifices tended to inhibit penetration of the jet into the mainstream. The use of slotted orifices appears to offer no significant change in penetration when compared to circular orifices. Under some conditions double orifice rows or mixed orifice sizes in a single row yield better jet penetration and mixing compared to a single orifice row with the same total flow area. Finally, the multiple jet results of this study, when compared with single jet data, show that the interaction of adjacent jets influences the temperature and velocity centerline trajectories.

II INTRODUCTION

The Multiple Jet Study was conducted under NASA Lewis Research Center Contract NAS 3-15703. The purpose of the study was to determine experimentally the penetration and mixing characteristics of multiple jets of ambient temperature air injected perpendicularly into a bounded mainstream of hot combustion gases. Data on the penetration and mixing of jets in a crossflow has application to many problems of current interest, such as:

(1) Cooling of hot gas streams in numerous industrial and military devices.
(2) Film cooling of combustion chamber walls, turbine blades, and reentry vehicle nose cones.
(3) The aerodynamics of STOL and VTOL aircraft.
(4) The concentration and paths of pollutants downstream of industrial chimneys or downstream from discharge lines leading into rivers or streams.

The results of this investigation apply most directly to Item (1) above. In particular, the results of the Multiple Jet Study have application to combustion devices which use air dilution to cool combustion products and quench reactions. The development of valid correlations for the mixing process between cool multiple jets and a hot primary gas stream has two principal benefits: (1) Through proper design of secondary air admission ports, the combustor lengths required to achieve uniform temperature and mass flux profiles can be minimized, and (2) the decreased combustor length required for complete mixing will result in minimum residence time for production of nitrogen oxides.

Although the interaction of subsonic circular and noncircular jets injected normally into a subsonic mainstream flow has been the subject of numerous analytical and experimental studies, Ref. 1 - 5, the published works to date have dealt with single jets rather than multiple jets in a bounded cross flow as required for the cooling problem. The data of References 1 through 5 are for heated or ambient temperature jets directed upward into a mainstream flow. In addition to pressure and/or temperature measurements in the flow field,

the studies of References 1, 2 and 4 also employed visual techniques to define jet trajectories. The photographic data from Reference 6 showed the ambient temperature jet path to be essentially the same, whether the jet entered the mainstream vertically from the top or the bottom. The test conditions of the current work more closely approximates the real gas turbine combustor case than the conditions tested in the references cited above; since (1) the use of cold jets exiting into a hot primary stream is a better simulation of the combustion quenching process than studies of interactions between hot jets and a cold primary flow, and (2) the use of multiple injection ports provides a better characterization of a combustor than does single jet injection.

The current work, through the use of 3800 stagnation pressure and temperature probe measurements in the flow field at five axial stations, has resulted in detailed temperature and pressure data at each axial measurement plane. These data provide a quantitative measure of the mixing achieved. Also when these data are presented in three-dimensional plots, they provide a qualitative evaluation of the penetration and mixing. In order to process the large quantity of data from each of the 105 tests conducted during the program (over 8000 data values were measured for each test), all data reduction, analysis and flow field temperature and pressure plots were done by computer.

Sixteen orifice plates were tested at a minimum of four operating conditions each. The basic operating conditions were at a nominal mainstream to jet temperature ratio of 2.0 and nominal jet to mainstream momentum flux ratios of 6, 14, 25 and 60. On some tests other effects were evaluated; absolute momentum level was changed and several tests were conducted with mainstream to jet temperature ratios of 1.5 and 2.5. Turbulence generating grids were used on some tests and a secondary air crossflow component was introduced on some tests by the use of baffles.

Due to the large volume of data collected during this study, not all the data are shown in this report. A Comprehensive Data Report (CDR) was compiled which contains a complete reduced data listing and complete temperature and pressure plots. Copies of this document are in the possession of the NASA Project Manager.

III TECHNICAL DISCUSSION

A. TEST FACILITY DESCRIPTION

The principal test apparatus consists of an air supply system, hydrogen-fired vitiated air heater for the primary flow, primary air plenum, main air duct (10.16 cm (4 in) by 30.48 cm (12 in) by 88.9 cm (35 in) long), secondary air plenum, orifice plates (16), pressure and temperature rake with traversing system, and the instrumentation and data acquisition system. A schematic illustration of the test facility is shown in Figure 1, and a photograph showing the overall facility setup, before thermal insulation was applied, is shown in Figure 2. A portion of the main air test duct with orifice plates being installed is shown in Figure 3. The pressure probe/ thermocouple rake shown in Figure 4 was traversed at five axial locations to determine flow field mass flux and temperature distributions. The facility was designed to minimize the effects of thermal expansion of the test duct on measurement precision. Also, the facility was designed and calibration tested to produce a uniform velocity and temperature profile (within $\pm$ 2%) 5.08 cm (2.0 in) upstream of the secondary injector plane. A more detailed description of the test facility and measuring apparatus is contained in Appendix B.

Prior to conducting tests with the various orifice plates, system checkout and calibration tests were made to demonstrate system operation, measurement precision and uniformity of pressure and temperature in the test duct flow field. A discussion of these tests and a review of orifice plate test procedures is contained in Appendix C.

B. ORIFICE PLATE CONFIGURATIONS

The design features of the sixteen orifice plate configurations which were tested during the Multiple Jet Study, are shown on Table I. Each plate is identified by a configuration number which consists of one single digit number and two 2-digit numbers separated by a slash and followed by an alpha character for special identification. The first number is the aspect ratio of the orifice, (1 for circular orifices). The second number is the nondimensional orifice spacing, orifice center to center dimension, S, divided

by the orifice diameter, D; and the third number is the nondimensional orifice size, the duct height, H, divided by the orifice diameter, D. When an alpha character is appended, an "n" indicates a nominal orifice size,an "m" indicates mixed orifice sizes in a single row and "d" indicates a double orifice row plate. The 13 predrilled orifice plates (11 of these were subsequently tested) are shown in Figure 5. One of the orifice plates is shown with downstream orifice static pressure taps installed. The two turbulence generating grids which were used on selected tests also are shown in the figure.

C. DATA REDUCTION AND ANALYSIS PROCEDURES

A large quantity of data was generated from each of the 105 tests conducted during this program (8035 data values were measured during each test.) In order to process this large quantity of data all data reduction, analysis, and flow field temperature and pressure plots were done by computer. The steps involved in the data acquisition, reduction, and analysis for the Multiple Jet Program are shown schematically in Figure 6. The pressure and temperature probe signals were fed through signal conditioning equipment (i.e., amplifiers, balance and range circuits, etc.) to a digital printer and magnetic tape recorder. The printer provided a quick readout of the data for monitoring purposes whereas the magnetic tape provides permanent storage for subsequent reduction and analysis. After the test or series of tests were completed, the magnetic tape was sent from ALRC by courier to the data processing center where the magnetic tape was read into a hi-speed digital computer, upon demand from the timeshare console located at ALRC. This process was executed by inputting a data reduction program which read the tape into the Program Complex File (PCF). The output was a computer listing of the data as a function of time and a magnetic tape file of the reduced data. The computer data listing was used to check the data for inconsistencies and/or errors. The magnetic tape file was used for subsequent data analysis.

Data analysis was accomplished by inputting a data analysis computer program and a directive to read the magnetic tape data file into the PCF. The program output consisted of a computer listing of the calculated correlation

parameters and a magnetic plot tape of the selected correlations. Data plots were made by sending the plot tape to ALRC where it was processed on a microfilm printer/plotter. This machine is a high-speed electronic printer/plotter which has the capability to produce either microfilm or hard copies of the data plots. The plotter operates by projecting the plots on a cathode ray tube (CRT) and then photographing the display with either a microfilm or a hard copy camera. The machine can read the tape data at a peak rate of 20,000 bits/second and is capable of producing well over 200 plots/hour. This data system is capable of producing a complete analysis and set of data plots within three working days from receipt of the raw data tape.

1. Data Reduction Program

The objective of the data reduction program was to take the raw digital data from the test data tapes, convert the data into engineering units, and format the data to facilitate the mathematical computation which was performed with the data analysis program. To achieve this objective, the data reduction program used the various scale factors for each channel to convert from raw input to engineering unit output. Since the test data was recorded on the test tape in sequence of channel numbers and Scanivalve and thermocouple stepper switch locations, the program reformated the data to place like parameters in consecutive array positions. An interlaced array of alternating integer and real numbers was used for program output. The integer number represents the original location in the input data array and the real number represents the value of the parameter in engineering units.

An EDIT subroutine was utilized to edit the incoming data. In order for the test data reduction program to function properly, the sequence of data acquisition had to be well defined so that the various test parameters were identified correctly. Problems developed if input data had an incorrect channel number assigned or if data values were repeated or skipped. In order to eliminate these problems, the data editing subprogram prescanned the data prior to execution of the data analysis program and identified and/or corrected data sequencing anomalies.

2. Data Analysis Program

The objective of the data analysis program was to use the output from the data reduction program to calculate test run conditions (weight flow rates,velocities, Mach numbers, momentum fluxes, densities, and temperature), dimensionless temperature and pressure profiles, and correlating parameters (pattern factors and energy exchange (E_T)values). The output from the analysis program was a paper listing of the run conditions, correlating parameters, and temperature and pressure values. In addition to the paper listing, the temperature and pressure profile data were output on a magnetic drum for use as input to the computer plotting routines. When the plot program was executed, the output data was stored on magnetic tape which was then input to the microfilm printer/plotter. Details of the methods of calculation used in the data analysis program are contained in Appendix D.

D. DEFINITIONS OF DIMENSIONLESS PARAMETERS

The data resulting from tests conducted during this program were evaluated in terms of nondimensional geometry, temperature, pressure and mixing parameters.

1. Nondimensional Orifice Plate and Test Duct Geometry Parameters

a. Orifice Plate

Although the nondimensional orifice plate parameters S/D and H/D have been introduced in a previous section, some further discussion is warranted. With multiple jet injection, the spacing between adjacent orifices may be defined by either of two nondimensional parameters; (1) the orifice center to center distance, S, divided by the orifice diameter, D, or (2) orifice spacing S, divided by duct height H. For this study, the duct height was held constant.

III Technical Discussion (cont.)

b. Test Duct

The coordinate system used for the Multiple Jet Study is orthogonal, with the X axis defined as the longitudinal axis along the test duct axis, the Y axis as the vertical axis (in the direction of the orifice centerlines) and the Z axis as the horizontal axis. The coordinate system is illustrated on Figure 7. The X = 0 station is the jet injection plane, Y = 0 station is at the jet orifice exit plane, and Z = 0 is the vertical plane at the first lateral measurement station, usually the midplane between two orifices.

The downstream distances from the plane of the secondary injection may be evaluated either in terms of the downstream distance to orifice diameter ratio, X/D, or in terms of the ratio of downstream distance to duct height, X/H. If the ratio of duct height to orifice diameter is large and jet to mainstream momentum flux ratio low, opposite wall influences should be small and X/D would be expected to be the best correlating parameter. However, if the ratio of duct height to orifice diameter is small and jet to mainstream momentum flux ratio is high, then opposite wall influences probably should not be neglected and X/H as well as X/D should be considered as a correlating parameter. This is particularly evident when over penetration of the jet occurs and the correlation between penetration depth and downstream distance, X/D, deviates from the expected exponential relationship. A sample of the dimensionless temperature profile at the X/H = .25 plane is shown in the inset of Figure 7. The data was plotted over an orifice spacing of 2S, beginning at the midpoint between two orifices. The relative jet orifice sizes are shown on the figure and jet and mainstream velocity vectors are shown as V_J and U_∞, respectively. The vertical duct axis is labeled Y/H with values from 0 at the top of the duct to 1.0 at the bottom of the duct. The Z axis is unlabeled, however, its length is always 2S and twenty-one equally spaced temperature profiles are shown in the Z direction. The value of the non-dimensional temperature, θ, at a point in the Y/Z plane is indicated by the scale on the third axis at the top of the figure. (High values of θ indicate the cool region while low values of θ indicate the hot region).

2. Nondimensional Temperature

The nondimensional temperature difference in the flow field downstream of jet injection, Θ, is defined as:

$$\Theta_{x,y,z} = \frac{T_\infty - T_{x,y,z}}{T_\infty - T_J} \qquad (1)$$

where:

$\Theta_{x,y,z}$	=	Theta, nondimensional temperature difference at a point in the flow field
T_∞	=	primary flow stagnation temperature
T_J	=	jet stagnation temperature
$T_{x,y,z}$	=	stagnation temperature at a point in the flow field

Theta is a measure of the temperature suppression in the flow field compared to the maximum possible suppression. The value of theta can vary from one, when measured temperature equals the jet temperature, to zero, when the measured temperature equals the mainstream temperature.

If complete mixing of jet and mainstream flows occurs, the value of theta will be constant and $T_{x,y,z}$ will be everywhere equal to the ideal equilibrium temperature between jet and mainstream; thus,

$$\Theta_I = \frac{T_\infty - T_{EB}}{T_\infty - T_J} \qquad (2)$$

where:

Θ_I	=	ideal equilibrium theta
T_{EB}	=	stagnation temperature resulting from complete thermal energy exchange

The average value of theta, Θ_{ave}, is defined as,

$$\Theta_{ave} = \frac{T_\infty - T_{x,\,ave}}{T_\infty - T_J} \qquad (3)$$

where:

Θ_{ave}	=	average value of theta
$T_{x,ave}$	=	arithmetic average of temperatures measured in a plane at distance X from the injection plane

3. Nondimensional Pressure

The nondimensional pressure difference in the flow field downstream of jet injection, C_p, is defined as

$$C_{p_{x,y,z}} = \frac{P_{x,y,z} - P_\infty}{P_J - P_\infty} \qquad (4)$$

where:

$C_{p_{x,y,z}}$ = nondimensional pressure difference

$P_{x,y,z}$ = stagnation pressure at a point in the flow field

P_∞ = primary flow stagnation pressure

P_J = jet stagnation pressure

If the primary, jet, and downstream static pressures are equal, then C_p is the momentum flux difference ratio:

$$C_{p_{x,y,z}} \sim \frac{(\rho V^2)_{x,y,z} - (\rho V^2)_\infty}{(\rho V^2)_J - (\rho V^2)_\infty} \qquad (5)$$

where:

V = velocity

ρ = density

ρV^2 = momentum flux

4. Momentum Flux Ratio

The jet to mainstream momentum flux ratio, J,

$$J = \rho_J V_J^2 / \rho_\infty V_\infty^2$$

where:

J = momentum flux ratio

ρ_J = jet static density

ρ_∞ = mainstream static density

V_J = jet velocity at the vena contracta

V_∞ = mainstream velocity

is the most important operating variable influencing jet penetration and mixing. It is the best measure of the ability of the jet flow to penetrate the mainstream flow field.

5. Mixing Parameters

a. Temperature Distribution Efficiency (Percent Energy Exchange) (E_T)

The purpose of injecting secondary air into the primary combustor of gas turbine engines is to cool the combustion gases, through energy exchange. The degree of energy exchange which has taken place at a given station downstream of the secondary injection ports is, then, a measure of the effectiveness of the injection technique. If the primary and secondary flows are completely mixed the temperature profile across a combustion section should be flat, neglecting thermal boundary layer effects, and the temperatures should be equal to a temperature (T_{EB}) resulting from the complete exchange of thermal energy between the two streams. The thermal energy input at the injection point is:

$$E_{IN} = \dot{W}_\infty \; h^o_\infty + \dot{W}_s \; h^o{}_J \qquad (6)$$

and the thermal energy out of the system at a downstream location, assuming complete mixing and energy exchange is:

$$E_{OUT} = (\dot{W}_\infty + \dot{W}_s) \; h^o{}_{EB} \qquad (7)$$

where in Equations 6 and 7:

E_{IN}	=	thermal energy into system
E_{OUT}	=	thermal energy out of system
$\dot{W}_s$	=	secondary weight flow rate
$h^o{}_J$	=	secondary flow stagnation enthalpy
h^o_∞	=	primary flow stagnation enthalpy
$h^o{}_{EB}$	=	final stagnation enthalpy resulting from complete thermal energy exchange

Assuming an adiabatic system, the energy gained by the secondary flow should equal the energy lost by the primary flow, or for complete energy exchange:

$$\dot{W}_\infty \; h^o{}_\infty + \dot{W}_s \; h^o{}_J = (\dot{W}_\infty + \dot{W}_s) \; h^o{}_{EB} = \dot{W}_T \; h^o{}_{EB} \qquad (8)$$

Equation (8) applies if the exit enthalpy is uniform. In the real case, temperature and mass flux gradients will exist in the exit flow, and the energy balance is expressed as:

$$\dot{W}_\infty \; h^o{}_\infty + \dot{W}_s \; h^o{}_J = \sum_{i=1}^{N} \dot{W}_i \; h^o{}_i \qquad (9)$$

The incremental mass flow at any location, $\dot{W}_i$, may be considered to have originated in the free stream, the jet, or both. Thus let

$$\dot{W}_i = (\dot{W}_{si} + \dot{W}_{\infty\, i}) \qquad (10)$$

where:

$$\sum_{i=1}^{N} \dot{W}_{si} = \dot{W}_s$$

and

$$\sum_{i=1}^{N} \dot{W}_{\infty i} = \dot{W}_\infty$$

$$\sum_{i=1}^{N} \dot{W}_i = \dot{W}_T$$

Equation (9) can now be written as:

$$\sum_{i=1}^{N} W_{si} \; (h^o{}_i - h^o{}_J) + \sum_{i=1}^{N} W_{\infty\, i} \; (h^o{}_i - h^o{}_\infty) = 0 \qquad (11)$$

Using Equations(8) and (11), the percent of the potential thermal energy exchanged in the secondary stream is defined by

$$\sum_{i=1}^{N} \frac{\dot{W}_{si} \ (h^{o}_{i} - h^{o}_{J})}{\dot{W}_{s} \ (h^{o}_{EB} - h^{o}_{J})} \times 100 \qquad (12)$$

and the percent of the potential thermal energy exchanged in the primary flow is defined by:

$$\sum_{i=1}^{N} \frac{\dot{W}_{\infty i} \ (h^{o}_{i} - h^{o}_{\infty})}{\dot{W}_{\infty} \ (h^{o}_{EB} - h^{o}_{\infty})} \times 100 \qquad (13)$$

Combining Equation (12) and (13) and weighing the secondary and primary energy exchange by $\dot{W}_s/W_T$ and $\dot{W}_{\infty}/W_T$ respectively, gives

$$E_T = \sum_{i=1}^{N} \left[\frac{\dot{W}_{si} \ (h^{o}_{i} - h^{o}_{J})}{(h^{o}_{EB} - h^{o}_{J})} + \frac{\dot{W}_{\infty i} \ (h^{o}_{i} - h^{o}_{\infty})}{(h^{o}_{EB} - h^{o}_{\infty})} \right] \frac{100}{\dot{W}_T} \qquad (14)$$

where E_T is the percent energy exchanged. To simplify equation (14), the effect of specific heat variation between the primary, secondary, and mixed streams is assumed to be negligible. Also, the kinetic energy of the streams is assumed to be small. Thus, Equation (14) can be written as:

$$E_T = \sum_{i=1}^{N} \left[\frac{\dot{W}_{si} \ (T_i - T_J)}{(T_{EB} - T_J)} + \dot{W}_{\infty i} \ \frac{(T_i - T_{\infty})}{(T_{EB} - T_{\infty})} \right] \frac{100}{\dot{W}_T} \qquad (15)$$

The application of Equation (15) requires a discrimination between primary flow, $\dot{W}_{\infty i}$, and secondary flow, $\dot{W}_{si}$. This was accomplished by assuming that if the incremental temperature was less than

the energy balance temperature, the incremental flow was part of the secondary flow; i.e., if $T_i < T_{EB}$ then $\dot{W}_{si} = \dot{W}_i$ and $\dot{W}_{\infty i} = 0$. Similarly if the incremental temperature was greater than the energy balance temperature, the incremental flow was part of the primary flow; i.e., if $T_i > T_{EB}$ then $\dot{W}_{\infty i} = \dot{W}_i$ and $\dot{W}_{si} = 0$. While this is an implicit method for determining the flow sources, it results in a mixing efficiency parameter which yields realistic values when compared with the plotted temperature profiles.

b. Pattern Factor

A parameter often used to characterize the exit temperature distribution in combustors is the pattern factor defined as:

$$\delta = \frac{T_{max} - T_{ave}}{T_{ave} - T_J}$$

Since the maximum temperature which can be present in the flow is T_∞, the maximum pattern factor, δ^*, is

$$\delta^* = \frac{T_\infty - T_{ave}}{T_{ave} - T_J} = \frac{\theta_{ave}}{1 - \theta_{ave}}$$

This parameter may be calculated for each of the tests from the average theta results presented. For many of the conditions examined, this parameter is small due to small cooling flow rates, even though the mixing is very incomplete.

E. TEST RESULTS

Results from the multiple jet study are discussed in the following paragraphs. Comparisons of the two mixing parameters, the energy exchange efficiency and the pattern factor, are presented along with summaries of test run conditions and mixing data. A discussion of the influence of test operating and design parameters on jet penetration and mixing concludes the section.

1. Comparisons of Mixing Parameters

A comparison of the two mixing parameters, E_T and δ^*; can best be made by relating the parameters to the temperature distribution plots of the test data generated in this program. Values of the mixing parameters are shown on Table II based on data from tests with orifice plates 1/04/12* and 1/02/06, respectively. These conditions were chosen since they represent the range of conditions investigated; namely (1) small holes with a small momentum ratio, and (2) large holes with a large momentum ratio. A comparison of the mixing parameter values from Table II with the corresponding temperature distribution plots of Figure 8 indicates that the energy exchange parameter, E_T, better characterizes the effectiveness of the secondary injection at each measurement plane. The values of E_T were plotted as a function of X/D at several momentum ratios for each orifice plate. Each plot represents the data from an individual orifice plate and appears to be of the form

$$E_T = a\,(X/D)^n$$

where a and n are a function of J. Ultimately, it appears that an empirical equation for E_T as a function of J, (X/D), (H/D), and (S/D) or (S/H) could be derived which would express mixing efficiency as a function of the significant operating and design variables.

2. Test Data Summaries

The Multiple Jet Study test program was divided into three phases. Phase I was the initial orifice plate test series (27 tests on one orifice plate); Phase II was the preselected orifice plate test series (58 tests on 10 orifice plate configurations); and Phase III was the final orifice plate test series (20 tests on 5 configurations.) The primary objective

---

*Orifice plate configuration code:

First number	=	orifice aspect ratio
Second number	=	orifice spacing, S/D
Third number	=	duct height to orifice diameter ratio, H/D

of the Phase I tests was to determine the influence of certain operating conditions on jet mixing and penetration. The operating variables surveyed during the initial orifice plate test series were:

(1) Jet to mainstream momentum flux ratio, J
(2) Momentum flux level
(3) Jet to mainstream density ratio
(4) Turbulence level
(5) Orifice inlet (cross velocity) conditions

With the exception of the momentum flux ratio the influence of these operating parameters were found to be negligible. The Phase II testing included a further survey of the effect of jet to mainstream density ratio but did not include a survey over a range of the other non-sensitive variables. Tests at other than the nominal density ratio of 2.0 were deleted from the Phase III testing.

a. Phase I Tests - Initial Orifice Plate Test Series

All initial orifice plate series tests were conducted using orifice plate 1/02/16. The data from these tests, plus data from tests of plates 2/02/16 and 4/02/16, are summarized on Table III. These configurations had the smallest holes and the smallest orifice spacings tested.

The data presented on Table III consists of test number, orifice plate configuration data, run conditions (mainstream Mach no., momentum flux ratio, density ratio, velocity ratio, flow ratio, turbulence grid and baffle configuration, and momentum flux level) and jet/mainstream mixing data. For the initial orifice plate test series, the mixing data presented consists of the ideal theta values and the average theta values at X/H stations of .125, .250, .5 and 1.0. Except for tests 22, 24, and 28 the energy exchange efficiency, E_T values, were not calculated during the initial test series. (E_T values calculated for tests 22, 24, 26 and 77, 78, 79 and 82 are shown on Figures 21 and 15 respectively).

A comparison of the average values of theta at each of the four X/H planes shows that the average theta values are higher than the ideal theta values. This result is expected since $\bar{\theta}_{ave}$ is an arithmetic average, and, as can be been from the pressure data shown in Figure 9, the mass flux distribution is not uniform. Since high local theta values often occur with low velocities near the injection wall, the average theta values are larger than the ideal theta values.

For low momentum ratios, the rather constant average theta values indicate that mixing does not increase appreciably with downstream distance. However, for high momentum ratios, the average theta increases with downstream distance. This occurs since for these cases the jet penetration increases with downstream distance, and thus higher than average theta values occur with lower than average velocities over an increasing percentage of the duct as distance increases.

b. Phase II Tests - Preselected Orifice Plate Design

Phase II tests were conducted with the remaining ten predrilled orifice plates. Summarized test data for these tests are shown in Table IV. For the majority of these tests the energy exchange parameter, E_T, was calculated. The general trend of this data shows increasing energy exchange with increasing momentum flux ratio, orifice size and orifice spacing. Test data for orifice plate 1/03/16 was invalid due to anomalous thermocouple readings. Therefore, theta values and E_T values were not tabulated for that test series.

c. Phase III Tests - Final Orifice Plate Designs

Based on the mixing and temperature profile data generated during the initial orifice plate test series and during the preselected orifice plate test series, five design selections were made for the orifice plate configurations to be tested during Phase III. Four of these plates have the same open area as plate 1/02/08. The following is a brief summary of the basis for the designs.

(1) Plate Configuration 1/04/04

Plate 1/04/04 contains the combination of the largest diameter orifice, 2.54 cm (1.00 in), and widest orifice spacing, 10.2 cm (4.00 in), designed for the Multiple Jet Study. The design was selected as a limit study based on observations from previous Multiple Jet test data that penetration tends to increase with increasing orifice diameter and orifice spacing. The area of this plate is equal to that of 1/02/08.

(2) Plate Configuration 1/02/04

Plate 1/02/04 has the same orifice diameter as plate 1/04/04, but has 1/2 the orifice spacing and hence twice the orifice area. The orifice spacing of plate 1/02/04 is identical with the spacing on predrilled plate 1/04/08 and thus provided data for the assessment of the relative importance of S/D compared to S/H.

(3) Plate Configuration 1/03/06n

Plate 1/03/06n (n designates a nominal orifice diameter, D= 1.8 cm (.707 in)) has the same spacing, S, as plate 1/02/04, however the reduced orifice diameter results in an orifice area that is identical to the orifice area of plates 1/04/08d, 1/03/06m, 1/04/04 and 1/02/08.

(4) Plate Configuration 1/04/08d

Plate 1/04/08d (d designates a double orifice row) was chosen in order to investigate the effect on jet penetration of closely spaced multiple orifice rows. The data from tests of this plate will be compared with the data from plate 1/04/08 which previously was tested.

(5) Plate Configuration 1/03/06m

Plate 1/03/06m (m designates mixed orifice

size) was designed in order to determine if alternating large widely space orifices with smaller orifices between them will provide a combination of high jet penetration from the large jets coupled with good back filling and lateral spreading from the small jets.

The test data from the final orifice plate test series are summarized in Table V.

3. Influence of Operating and Design Parameters on Jet Penetration and Mixing

The influence of the operating parameters, momentum flux ratio, absolute momentum flux level, density ratio, turbulence level, and orifice inlet conditions are discussed in the following paragraphs. With the exception of the orifice inlet condition, these parameters are defined independently from jet/mainstream mixing considerations. The momentum flux ratio, density ratio, and flow ratio are dependent on the combustor design criteria. Thus for a given combustor, the secondary admission design parameters which may be varied to influence mainstream/jet mixing are the secondary orifice diameter, spacing, and shape. However, since the flow conditions for a given combustor determine the required orifice open area, the orifice size and spacing must be correctly coupled. The results of this study presented in the following paragraphs are based on experimental observations. No tasks to model the jet penetration and mixing processes were within the scope of this program.

a. Operating Parameters

(1) Momentum Flux Ratio

The jet to mainstream momentum flux ratio ($\rho_J V_J^2/\rho_\infty V_\infty^2$) is the single most important operating parameter influencing secondary jet penetration and mixing. The influence of momentum flux ratio on jet/mainstream interaction can be illustrated by the dimensionless

temperature profile data presented on Figure 10 and the energy exchange data of Figure 11. The data presented in Figure 10 are from tests of orifice plate 1/04/08 at a nominal density ratio of 2.0 and momentum ratios of 61.9 and 6.3. The temperature data are shown at four axial stations: 0.25, 0.50, 1.0 and 2.0 duct heights downstream from the plane of injection. The better penetration of the high momentum jet into the primary flow field is evident.

A Gaussian type vertical distribution of the temperature parameter about its maximum value is evident at the first measuring plane. The temperature centerline at the first station for the J = 61.9 case is at a penetration depth, Y/H, of approximately 0.6, while for the J = 6.3 case, the temperature centerline is at a Y/H of approximately 0.25. The energy exchange efficiencies, E_T, for J = 61.9 and J = 6.3 are 66% and 45% respectively, at X/H = 0.25 (Figure 11). The temperature profile data at the X/H = 0.5 plane shows the jet penetration depth has not increased significantly for either the J = 61.9 case or the J = 6.3 case. However, the amount of mixing has increased by 13%, from 66% to 79%, for J = 61.9, while the percent mixing has increased only 5%, from 45% to 50%, for J = 6.2. At the higher momentum, Figure 10 shows that the entire primary flow field has been influenced by the secondary injection at X/H = 0.5, while with the lower jet momentum, over two-thirds of the primary flow field is still unaffected by the secondary injection. The data of Figure 10 indicate that, for both the low and high momentum flux ratios, temperature centerline penetration depth does not increase significantly with increasing X/H beyond X/H = 0.25 (X/D = 2). However, a flattening of the vertical temperature profile occurs with increasing X/H for both momentum flux ratios. Apparently the criterion for effective jet/mainstream mixing is jet penetration to approximately 1/2 the duct height within approximately two jet diameters downstream, and the establishing of a symmetrical vertical temperature distribution profile at this point. If these conditions are met, then the spreading of the temperature profile, which is noted on all tests, will result in the flattened temperature distribution at downstream stations. Also, the data of Figure 10 indicates that if a flat temperature profile is desired, over penetration of the jets into the mainstream is preferable to under penetration.

Similar trends can be inferred from the contour plots of $1 - \frac{\theta}{\theta_{ave}}$ which are shown in Figure 12 for the same tests and conditions shown in Figure 10. These plots show the differences in temperature gradients within the jets and difference in jet boundaries for th high and low momentum flux ratios.

(2) Absolute Momentum Level

The absolute momentum flux level does not significantly influence jet penetration or jet/mainstream mixing over the range tested. The similarity of the temperature difference ratio, θ, profiles at X/H = 0.25 and 1.0 for mainstream velocities of 25 and 50 m/sec at J = 6.1 and at mainstream velocities of 16 and 23 m/sec at J = 58 for orifice plate 1/02/16 can be seen from the data presented in Figure 13.

(3) Density Ratio

The jet to mainstream density ratio does not appear to influence jet penetration or mixing significantly over a range from 1.6 to 2.6, except for the density ratio contribution to the momentum flux ratio. The similarity of the dimensionless temperature profile curves for density ratios of 1.6, 2.1 and 2.6 is shown in Figure 14. The data in Figure 14 were from orifice plate 1/02/08 at a nominal momentum flux ratio of 25. Profiles are shown at axial stations corresponding to 0.50, 1.0 and 2.0 duct heights downstream from the injection plane. The energy exchange efficiency data shown in Figures 11, 15, 16 and 17 also indicate that momentum flux ratio, rather than an independent density ratio, is the most significant operating variable controlling jet/mainstream mixing.

(4) Turbulence Level (Use of Turbulence Generating Grids)

Although no direct measurements of flow field turbulence intensity were made, a comparison has been made of the effect

on jet penetration and mixing resulting from use of turbulence generating grids. Two grid designs were used: 0.795 cm (0.313 in) diameter rods with 2.54 cm (1.0 in) spacing and 0.41 cm (0.162 in) diameter rods with 1.27 cm (0.5 in.) spacing. Both grids were mounted 10.4 cm (4 in) upstream of the jet injection plane. The highest level of turbulence would be expected with the larger grid cross rods. The use of this turbulence generating grid tends to reduce the maximum value of θ slightly, compared to tests without the grid, but the jet penetration depth was not altered significantly. A comparison of θ values with and without turbulence grids can be made by inspection of Figure 18.

b. Design Parameters

The difference in temperature distribution obtained by varying orifice diameter and spacing so as to maintain a constant orifice area are shown in Figure 19. Temperature profile data at X/H = 1 for momentum ratios of 6 and 60 are shown for plates 1/02/08, 1/03/06n and 1/04/04 which all have jet area to cross-stream area ratios of 0.049. The lack of similarity in the profiles is evident, indicating that for a given operating condition considerable variations in the downstream temperature distributions can be effected by changes in orifice diameter and spacing.

(1) Effect of Varying Orifice Diameter at Constant S/D

For a constant S/D and constant momentum flux ratio, secondary jet penetration into the mainstream at any given downstream distance, X/H, increases with increasing orifice diameter. This trend is evident from an examination of Figure 20 which shows the dimensionless temperature profiles at a station one duct height downstream of the injection plane for tests with nominal momentum flux ratios of 14 and 25 and a nominal temperature ratio of 2. The data are presented for orifice plate configurations with S/D = 2, and with duct height to orifice diameter ratios of 16, 12, 8, 6 and 4, moving left to right across the figure at each momentum flux level. The date of Figure 20 are presented at a constant distance downstream of the

injection plane of X/H = 1. If the data had been presented at equivalent downstream distance to orifice diameter ratios, X/D, the better penetration of the large orifices would be even more significant.

The effect of orifice diameter on jet/mainstream energy exchange, E_T, at several momentum flux ratios and downstream distances can best be illustrated by the E_T data of Figures 21, 22, 16, 23 and 24. The data on these figures are for duct height to diameter ratios of 16, 12, 8, 6 and 4, respectively, all with an S/D of 2. These data show the increase in efficiency as orifice diameter increases. Also the data from these figures indicate that the exponential nature of the E_T versus X/D relationship is valid except with large orifices at high momentum flux ratios. For large orifices and high momentum flux ratios, overpenetration of the jets occurs and causes this deviation from a constant exponential dependency of E_T on X/D.

(2) Effect of Varying Orifice Diameter at Constant S/H

If the ratio of orifice spacing to duct height, S/H, and the momentum and density ratios are held constant, the result of increasing orifice diameter is to increase the orifice area and hence increase the jet to mainstream flow ratio. Temperature profiles at X/H = 1 for orifice plates 1/04/08 and 1/03/06n (S/H = .5) for momentum ratios from 6 to 60 are shown in Figure 25. The similarity of the temperature distribution for the two plates is evident. The result of increasing orifice diameter at constant S/H is to shift the temperature distribution to higher theta values consistent with the larger cooling air flow without altering the shape of the distributions. The similarity of the energy exchange coefficients for the two configurations can be seen from the data presented in Figures 11 and 26.

This is perhaps the most significant result of present investigation since it suggests that for a given momentum ratio there exists an optimum value of S/H. Thus the orifice size can then be selected to provide the desired jet to mainstream mass flow split.

From Figures 27 and 28 it appears that the optimum value of S/H for momentum flux ratios near 60 is 0.5, while for lower momentum flux ratios S/H must be increased to maintain optimum jet penetration.

(3) Effect of Varying Spacing at Constant Orifice Diameter

For a given jet diameter and momentum ratio, mixing tends to increase with increased orifice spacing over the range tested. An increase in spacing at constant orifice diameter causes S/D and S/H to increase. The limiting cases appear to be the rapid formation of a two-dimensional air curtain which inhibits mixing at small S/D, and the formation of lateral non-uniformities at large S/D. The data of Figure 27 show dimensionless temperature profiles at X/H = 0.25 and 1.0 for plates with H/D = 8 at a nominal momentum ratio of 60. S/D values for these tests increase from 2 to 6 from left to right, corresponding to increasing S/H from .25 to .75. The penetration of the jet temperature centerline increases slightly with increasing spacing at X/H = 0.25, however the major effect of increased spacing is the shape of temperature profiles at downstream stations. For small spacings the jets merge rapidly forming a two-dimensional blockage with the result that cooling is never achieved in the vicinity of the opposite wall. For larger spacings however, penetration continues to increase with downstream distance. Both lateral and transverse mixing occur with relatively uniform temperature distributions achieved at the downstream locations.

The data of Figure 28 for S/D's of 2, 3, 4 and 6 at momentum ratios of 6 and 26 show a very uniform lateral temperature distribution for small S/D. In addition, at small S/D a temperature "plateau" is seen from the top of the duct to a penetration point where the values of θ begin to decrease. As S/D is increased, a more definite maximum θ point is observed and the "plateau" effect is diminished. Referring to the data of Figure 27, at X/H = 0.25, the large orifice spacings, while producing nonuniform lateral temperature distributions, do result in both vertical and lateral symmetry of the temperature profiles. By the X/H = 1 station, however, lateral

spreading of the jets has taken place and results in a uniform lateral temperature profile. Also, at large S/D, the symmetrical Gaussian type vertical distribution of temperature has decayed in a symmetrical manner to yield a fairly uniform vertical temperature distribution.

The decay of the unsymmetrical vertical distribution of the closely spaced jets results in a nonuniform vertical temperature profile at the downstream location. In addition to the temp--rature profile data presented in Figures 27 and 28, the energy exchange efficiency data of Figures 16, 29, 11 and 30 from orifice plates 1/02/08, 1/03/08, 1/04/08 and 1/06/08, respectively, show a trend of increasing mixing efficiency with increasing S/D. These data also indicate that the optimum value of S/D is dependent on the momentum flux ratio. Mixing efficiency data for plates 1/02/12 and 1/04/12 (S/D's = 2 and 4, respectively; H/D = 12) presented in Figures 22 and 17 also show an increase in mixing with increased S/D.

(4) Orifice Shape

Slotted orifices with aspect ratios of 2 and 4 with the major axis of the slots parallel to the mainstream flow appear to offer no significant change in jet penetration or mixing compared to circular orifices with the same area and orifice spacing. The data of Figure 31 show typical temperature profiles at X/H = 1.0 and temperature contours at X/H = 0.125 for the circular and aspect ratio 2 and 4 configurations at a nominal momentum ratio of 25. The insignificant effect of aspect ratio on penetration is contradictory to the finding of Reference 7. A curious feature of the data is the inflection point in the temperature profiles for the slotted orifices along the top wall of the test duct. Examination of the temperature contour plots at X/H = 0.125 may indicate the reason for the inflection point and low temperatures along the top duct wall (Figure 31). The temperature contours for the circular orifice show the eliptical shape of two distinct jets. The contour plots for the aspect ratio 2 and aspect ratio 4 configurations indicate a nearly uniform lateral temperature distribution. The contour plots perhaps

indicate that the jet major cross-section axis has turned 90° (major axis perpendicular to the mainstream flow) and the jet has been deflected nearly parallel to the mainstream.

(5) Injection Orifice Cross Flow (Use of Baffles)

The effect of a cross flow component on the upstream side of the secondary injection orifice was evaluated using baffles in the secondary plenum for several tests on orifice plate 1/02/16. The ratio of orifice cross flow to orifice axial velocity at the maximum cross flow condition was 0.13. At this condition, no significant change was noted in either the orifice discharge coefficient or the θ profiles, compared to the no cross flow case.

(6) Double Orifice Rows

During the final orifice plate test series, one double row orifice plate, plate 1/04/08d, was tested. Temperature profile data for this plate is shown at X/H = 1 and nominal momentum flux ratios of 6 and 60 (Figure 32). Also shown in Figure 32 are profile data for the following comparable configurations:

(a) Plate 1/04/08 - A single row plate of the same diameter and lateral spacing as 1/04/08d but with one-half the total flow area.

(b) Plate 1/04/04 - A single row plate of the same total flow area and S/D as plate 1/04/08d but with fewer orifices of larger diameter.

(c) Plate 1/03/06n - A single row plate of the same total orifice area and S/H as plate 1/04/08d but with fewer orifices of larger diameter.

For orifice plate 1/04/08d two rows of 1.27 cm (0.5 in.) orifices were spaced two orifice diameters apart in the streamwise direction and the X = 0 point was taken as the plane through the center of the orifices in the upstream row. Comparison of the data for plate 1/04/08d with the data presented for plate 1/04/08 shows a significant increase in jet penetration with the double row configuration at both the low and the high momentum flux ratios. At the high momentum flux ratios the jets from plate 1/04/08d have overpenetrated and the temperature distribution is not as uniform as for plate 1/04/08. For X/D less than 8, the mixing efficiencies for 1/04/08d (Figure 33) are less than for 1/04/08 (Figure 11). However the increase in E_T with distance is greater for the double row than for the single row, thus for X/D greater than 8 the mixing efficiency for plate 1/04/08d is greater than for 1/04/08.

A comparison of the data from plate 1/04/08d with data from plate 1/04/04 shows the temperature profile of the former to be more uniform than the profile from plate 1/04/04. The large orifices of plate 1/04/04 provide much better penetration than does the double row of smaller orifices but at the expense of increased lateral non-uniformity and more severe overpenetration at high momentum ratios.

When the data from plate 1/04/08d are compared with data from plate 1/03/06n, the latter configuration appears to yield a more uniform lateral temperature profile and slightly better penetration at the low momentum flux ratios. At the high momentum flux ratio, the two plates yield very similar temperature profiles.

(7) Single Row of Mixed Orifice Size

In addition to the double orifice row plate tested during the final orifice plate test series, a single orifice row plate with mixed orifice sizes was also tested. Temperature profile data from tests of this plate, plate 1/03/06m, are shown in Figure 34 at nominal momentum flux ratios of 14 and 60 at an X/H of 1.0. The orifice configuration used on plate 1/03/06m was a single row of orifices with alternating diameters

of 2.39 cm (0.94 in.) and 0.838 cm (0.33 in.) with adjacent holes spaced 5.08 cm (2 in.) apart. The profile data were taken from the center of a small orifice to the center of a small orifice across two large orifices. In addition to the data from plate 1/03/06m, temperature profile data are presented in Figure 34 for two comparable configurations: (1) plate 1/03/06n, which has the same total flow area and S/H (S/H = .5) as plate 1/03/06m but with a single row of 1.78 cm (0.7 in.) diameter orifices, and (2) plate 1/04/04, which has the same total flow area as plate 1/03/06m but which has an S/H of 1.0 and orifice diameters of 2.54 cm (1.0 in.). Plates 1/03/06n and 1/04/04 provide the limiting cases for the mixed size geometry. That is, if the hole sizes in 1/03/06m were to approach equality, plate 1/03/06n would be the result. At the other limit, plate 1/04/04 would be formed if the small holes in 1/03/06m were made infinitely small with the orifice area held constant.

The data presented in Figure 34 indicate that alternating orifice sizes in a single row increases jet penetration compared to a row of constant diameter orifices of the same total area and hole spacing. This increased penetration is from the jets issuing from the large orifices; as expected the jets from the small orifices do not penetrate far into the mainstream. The mixed orifice size configuration 1/03/06m, causes a more nonuniform lateral temperature profile than does configuration 1/03/06n. The energy exchange efficiency data presented in Figures 26 and 35 for the constant orifice size plate and the mixed orifice size plate, respectively, show energy exchange efficiency for the mixed orifice size configuration to be less dependent on momentum flux ratio than is a constant orifice size configuration. (For the mixed orifice size plate the larger of the two orifice diameters was selected as the base for the X/D parameter)

The temperature profiles for the mixed orifice size plate may also be compared to those from the other limiting case, 1/04/04. This comparison shows that the two configurations have similar lateral temperature profiles but that the constant orifice diameter plate penetrates further at the low momentum. This greater penetration is most

likely due to the larger orifice diameters of plate 1/04/04. At high momentum flux ratio, the two configurations yield similar temperature profiles. The mixing efficiency data from plate 1/04/04 (Figure 36) when compared to the data from plate 1/03/06m (Figure 35) show the two plates to yield similar mixing efficiencies at equal momentum flux ratios at X/D's greater than 4. The mixed orifice size configuration shows less dependence of E_T or X/D.

4. Comparison of Multiple Jet Study Data Trends with Single Jet Data

a. Temperature Centerline

A comparison of the equation for the temperature centerline location for a single jet, based on the analysis of Reference 8, with multiple jet data is shown in Figure 37. The analysis of Reference 8 was for hot jets entering a cold mainstream while the current data is for cold jets entering a hot mainstream. The multiple jet data presented on the figure are from orifice plates 1/02/16 and 1/06/08. These two configurations represent the most closely spaced orifice pattern tested and the most widely spaced pattern tested (based on S/D), respectively. The multiple jet data for both configurations show less increase in penetration distance with increasing downstream distance than would be predicted based on the single jet analysis. Furthermore, the multiple jet data indicate that, beyond an X/D of approximately 10, there is no increase in jet temperature centerline penetration. This data comparison indicates that the exponents on both the X/D and J terms of the correlating equation for single jets used in Reference 8 are different for multiple jet injection. Therefore, the single jet correlation should not be used to predict temperature centerline trajectories of multiple jet configurations.

b. Velocity Centerline

A comparison of the velocity centerline equation from the analysis of Reference 8 with the multiple jet data from plates 1/02/16 and 1/06/08 is presented in Figure 38. These data show closer agreement between the single and multiple jet data than did the temperature

centerline data presented previously. An adjustment of the exponents used for X/D and J for the single jet data correlation and incorporation of a geometric parameter such as S/D or S/H should yield a reasonable multiple jet correlation equation for velocity centerline. The penetration of the velocity centerline apparently does not reach a maximum within ten X/D's downstream from the injection point as did the temperature centerline.

IV CONCLUSIONS

A. MIXING PARAMETERS

1. An energy exchange parameter defined during this program adequately characterizes the mixing effectiveness over a range of test operating and design conditions.

2. An empirical correlation equation as a function of dimensionless geometric and operating parameters could be developed from the data obtained during the Multiple Jet Study program.

B. OPERATING PARAMETERS

1. The jet to mainstream momentum flux ratio is the single most important operating variable influencing jet penetration and mixing.

2. The absolute momentum flux level does not influence jet penetration or mixing significantly.

3. The jet to mainstream density ratio does not appear to influence jet penetration or mixing significantly, except through its contribution to the momentum flux ratio.

4. The effect of turbulence level on jet penetration and mixing was insignificant within the range of turbulence examined.

B. DESIGN PARAMETERS

1. At a given momentum flux ratio and at a fixed distance from the injection plane, jet penetration and mixing increases with increasing orifice diameter.

2. The spacing between orifices has a significant effect on lateral spreading of the jets, jet penetration, and jet mixing. Closely spaced orifices (spacing to diameter ratio, S/D, of 2) inhibit jet penetration and cause nonuniform downstream temperature profiles.

IV Conclusions (cont.)

3. If the ratio of center-to-center orifice spacing to duct height and the momentum flux ratio are held constant,and orifice diameter varied,the resultant temperature profiles are similar in shape but offset from one another by the differences in ideal $\bar{\theta}$. This suggests that for a given momentum flux ratio there exists an S/H such that nearly uniform temperature distributions are achieved. The hole size may then be chosen based on the desired jet mass flow rate.

4. Slotted orifices (aspect ratios of 2 and 4, major axis in the direction of primary flow) appear to produce no significant change in jet penetration or mixing compared to circular orifices of equal area.

5. When baffles were used to channel the secondary injection flow and create a cross flow component, no significant effect on jet penetration or mixing was observed.

6. Double orifice rows spaced two orifice diameters apart and having twice the total jet flow area of a single row result in better penetration than a single orifice row of the same diameter. Double orifice rows provide more uniform mixing than a single row of the same total flow area and same S/D; however, jet penetration into the mainstream is greater with the single row of large orifices. When the double orifice row is compared to a single row of equal flow area and S/H, the single row data appear to yield a more uniform lateral temperature profile and slightly better penetration.

7. Alternating orifice sizes in a single row increases jet penetration when compared with a row of constant diameter orifices of the same flow area and spacing. However, mixed orifice sizes may cause non-uniform lateral temperature distributions. If the mixed orifice size data are compared to date from a row of constant diameter orifices of the same flow area but twice the orifice spacing, the jet penetration with the constant diameter orifice plate is better than the jet penetration from the large orifices of the mixed diameter configuration.

REFERENCES

1. Kamotani, Yasuhiro; and Greber, Isaac: Experiments on a Turbulent Jet in a Cross Flow, Report FTAS/TR-71-62, Case Western Reserve Univ. (NASA CR 72893), June 1971.

2. Keffer, J. F., and Baines, W. D.: The Round Turbulent Jet in a Cross-Wind. J. Fluid Mech., Vol.15, Pt 4, April 1965, pp. 481-496.

3. Callaghan, E. E., and Ruggeri, R. S.: Investigation of the Penetration of an Air Jet Directed Perpendicularly to an Air Stream. NASA TN 1615, 1948

4. Ramsey, J. W., and Goldstein, R. J.,: Interaction of a Heated Jet with a Reflecting Stream. Report HTL-TR-92, Minnesota Univ. (NASA CR 72513), April 1970

5. Ruggeri, R. S., Callaghan, E. E., and Bowden, D. T.,: Penetration of Air Jets Issuing from Circular, Square and Elliptical Orifices Directed Perpendicularly to an Air Stream. NACA TN 2019, 1950.

6. Margason, R. J.,: The Path of a Jet Directed at Large Angles to a Subsonic Free Stream. NASA TN D-4919, 1968

7. Barnett, H. C., Hibbard, R. R.: Basic Considerations in the Combustion of Hydrocarbon Fuels with Air. NACA Report 1300, 1959

8. Holdeman, J. D.: Correlation for Temperature Profiles in the Plane of Symmetry Downstream of a Jet Injected Normal to a Crossflow. NASA-TND-6966.

APPENDIX A

SYMBOLS

A	flow area
a	a constant
C_p	pressure coefficient, $\frac{P - P_J}{P_\infty - P_J}$
C_D	orifice discharge coefficient
D	orifice diameter
d	double orifice row
E_{in}	energy into system
E_{out}	energy leaving system
E_T	mixing efficiency, (See Equation 15)
g	gravitational constant
H	duct height
h^o	stagnation enthalpy
i	index
J	momentum flux ratio $(\rho V^2)_J/(\rho V^2)$
m	mixed orifice size
N	number of orifices
n	nominal
P	Stagnation pressure
S	orifice spacing
T	temperature
V	velocity
$\dot{W}$	weight flow rate
x	x direction, parallel to duct axis
y	y direction, parallel to orifice centerline

z	z direction, normal to duct axis

Subscripts

J	jet property
i	ideal
ave	average
EB	energy balance
s	secondary

Greek

θ	temperature difference ratio, $\frac{T_\infty - T_{xyz}}{T_\infty - T_J}$
∞	free-stream condition
δ^*	pattern factor, $\frac{\theta_{ave}}{1 - \theta_{ave}}$

APPENDIX B

A. DETAILED TEST FACILITY DESCRIPTION

The principal test apparatus consists of an air supply system, hydrogen-fired vitiated air heater for the primary flow, primary air plenum, main air duct (test section), secondary air plenum, orifice plates (16), pressure and temperature rake with traversing system, and the instrumentation and data acquisition system. A schematic illustration of the test facility was shown in Figure 1, and a photograph showing the overall facility setup before thermal insulation was applied was shown in Figure 2. The facility was designed to minimize the effects of thermal expansion of the test duct on measurement precision. Also, the facility was designed and calibration tested to produce a uniform velocity and temperature profile (with $\pm$ 2%) 5.08 cm (2.0 in.) upstream of the secondary injection plane.

1. Air Supply System

Air is supplied to the mainstream plenum and secondary jet plenum from a blowdown air system which consists of a 75 HP compressor which continuously pumps a 1000 cu ft storage tank to a maximum pressure of 600 psig (air storage capacity of approximately 3000 lbm). The air is filtered and dried to remove dust, oil and moisture. A tempering heat exchanger on the tank outlet warms the air to compensate for real gas effects in order to maintain a constant temperature Air flow rate to the mainstream duct and the secondary plenum is controlled by individual remotely operated regulator valves upstream of individual ASME long-radius metering nozzles. Total system steady-state flow rate capability as a function of test duration is shown by the curve of Figure 39.

2. Air Heating System

A hydrogen air burner is used to heat the primary air flow to the required temperatures of 450° K (810° R), 600° K (1080° R), and 750° K (1350° R). The burner has the capability to heat 5 lbm/sec of air up to temperatures of 830° K. One of the operational advantages of the air heater is the ability to provide very accurate, stable temperature control.

The air heater system consists of an air inlet section to diffuse the air upstream of the multiple orifice concentric ring hydrogen injector, a combustion section,

and a mixing section. The combustor contained stainless steel baffles to promote large-scale mixing and is terminated by an abrupt contraction to further enhance mixing. The mixing section contains a jet breaker and screens to eliminate temperature stratification and to aid in the generation of a more uniform velocity profile in a short length. The system is ignited by an automotive spark plug and provision is made for automatic fuel shutoff if ignition is not achieved within 2 seconds of fuel flow initiation. Instrumentation is provided to monitor combustion temperature and pressure continuously in the heater. Temperature was controlled by adjusting hydrogen flow rate.

3. Main Air Plenum

The main air plenum consists of a 60.7 cm (24 in.) diameter, 92 cm (36 in.) long circular cylinder of .157 (.062 in.) wall thickness with .315 cm (.125 in.) flat end plates, all of 304 stainless steel. The upstream end plate is bolted to the cylinder to allow access. Screens are employed in the cylinder to ensure a uniform flow profile. The cylinder has thermocouples on the exterior surface in order to monitor transient thermal response.

In order to reduce the heat losses to the plenum walls, .005 cm (0.002 in.) thick stainless steel foil is spot welded to the inside plenum wall. An air gap between the foil and the wall was provided by first tack welding .075 cm (0.030 in.) stainless steel wire to the wall in a spiral configuration and then welding the foil to the wire.

4. Main Air Duct (Test Section)

The test section is a 10.17 cm (4.0 in.) high by 30.48 cm (12 in.) wide duct 88.9 cm (35.0 in.) long and incorporates a contoured entrance section beginning at a contraction ratio of 5.3 (with respect to duct area). A boundary layer trip is placed on the top duct wall at the location corresponding to a minimum Reynolds number, based on length, of 10^5. A trip is also located on the duct bottom wall 2.54 cm downstream of the top wall trip; both trips are approximately 0.25 cm high (corresponding to the boundary layer displacement thickness). The section is fabricated from .157 cm (.062 in.) 304 stainless steel sheet. Wall static pressure taps are installed in the test section at required stations on all four walls. Thermocouples are placed on the outside of the duct walls to measure duct wall temperature.

Portions of the test duct walls are heated electrically in order to reduce transient heat losses. The heater consisted of nichrome wire strips placed along the outside wall of the test section and insulated electrically with asbestos mats. A photograph of a portion of the test duct prior to adding the nichrome wire was shown in Figure 3. The test duct Reynolds number as a function of primary flow velocity and temperature is shown in Figure 40. Predicted boundary layer development within the test duct is shown in Figure 41.

5. Secondary Air Plenum

The secondary plenum is rectangular in cross section 30.5 cm (12 in.) by 15.2 cm (6 in.) at the main air duct interface (maximum velocity approximately 2.4 m/sec (8 ft/sec). The secondary plenum is bolted to the top of the test section with the orifice plate forming the floor of the plenum. The interface between test duct, orifice plate, and secondary plenum is sealed with asbestos-silicon gaskets and is designed so that any leakage of primary or secondary air is to the atmospher rather than between primary and secondary circuits. Pressure tubes extend through the downstream wall of the plenum from the orifice plate static pressure taps to the pressure transducer. Rubber seals are used to prevent leakage where the pressure tubes pass through the plenum wall. A jet breaker with screens is placed at the plenum inlet to aid in producing a uniform velocity profile. Secondary air flow is introduced to the plenum through a 5.1 cm (2 in.) fitting (maximum velocity = 70.2 m/sec (230 ft/sec). Two steps on three side walls of the plenum provide a ledge for placing baffles at heights of 2.54 cm (1.0 in.) and 1.27 cm (0.5 in.) from the plenum floor. The baffles were used on selected tests to provide a cross velocity component in the orifice flow.

6. Orifice Plates and Turbulence Grids

The design features of the sixteen orifice plate configurations were shown in Table I. Each orifice plate has six flush static pressure taps surrounding the orifice. Also, static taps at the x = -5.1 cm (-2 in.) and x = 2.5 cm (1 in.) stations are provided in the orifice plate. The orifice plates are made from 0.198 cm (0.078 in.) thick 304 stainless steel sheet and are secured between the test duct and secondary plenum bottom flanges.

During selected tests, turbulence inducing grids were inserted into the test duct 10.2 cm (4 in.) upstream of the jet injection plane. Two grid designs were used; both were of stainless steel and one had 2.54 cm (1.0 in.) spacing with 0.79 cm (5/16 in.) diameter cross rods and the other had 1.27 cm (0.5 in.) spacing with 0.411 cm (0.162 in.) diameter cross rods. The grids were secured within the test duct by spot welding the cross rods to the test duct wall.

A photograph of 13 predrilled orifice plates (11 of these were subsequently tested) and the two turbulence inducing grids was shown in Figure 5. One of the orifice plates is shown with pressure tap instrumentation installed.

7. Rake and Traverse System

a. Rake and Probes

Twenty temperature and pressure probes are used to measure free-stream stagnation conditions in the test duct. The probes are welded to a support bar and are aligned in a vertical plane. The center-to-center distance between probes is 0.475 cm (0.187 in.) and the probes extend to within 0.500 cm (0.197 in.) of the top and bottom duct surfaces. A photograph of the probe design was shown in Figure 4.

Since the direction of the velocity vector is not known, a total pressure tube with a flat inlet is used to measure duct stagnation pressure. This probe configuration has essentially 100% total pressure recovery up to flow angles of approximately $\pm$ 11°. The velocity inferred from the pressure probe measurements was assumed to be the velocity component parallel to the duct axis. Each probe element consists of a 0.149 cm (0.059 in.) diameter full-hard stainless steel total pressure probe with a 0.107 cm (0.042 in.) inside diameter. The rake also incorporates a 0.102 cm (0.040 in.) diameter chromel-alumel, Inconel-sheathed thermocouple spaced about 0.22 cm (0.09 in.) from the total pressure element in the plane of the probes. The junction of the thermocouple is not sheathed in order to minimize errors due to heat conduction to the junction along the sheath. The whole assembly is resistance welded to the rake support assembly. Since no high temperature brazing is required, the steel probe tubes retain their hardness and, therefore, stiffness and dimensional rigidity. All materials and construction techniques used in the probe fabrication were suitable for extended operation at 755° K (900° F) in air.

The rake support assembly is built of 1.27 cm (0.5 in.) diameter tubing to provide the rigidity necessary for accurate location of the measuring position. To eliminate distortion from uneven heating, the probe support is water cooled except for a 15 cm (6 in.) thermal isolation section.

The thermocouples terminate on a rigid support connected to the aft end of the probe, at which point heavy gage thermocouple wire is connected permanently. The 20 pressure tubes terminate in Scanivalve tabulations, brazed into a cooled copper disc, at which point conventional plastic tubing connections are connected.

b. Traverse Mechanism

(1) Mechanical System

The pressure/temperature rake is mounted rigidly to the traversing table. The table consists of a heavy gage platform which slides on 1.9 cm (0.75 in.) diameter horizontal shafts in the direction of the main duct flow. X station stops are solenoid detents which are controlled automatically by the data system. X direction power is supplied by a cable, pulley, and weight system. The traverse in the normal direction is achieved by a SLO-SYN stepping motor linked to a pretensioned timing chain and idler sprocket which drives the probe mounting platform. The mounting platform is made from heavy gage aluminum. The rake support stand is bolted to the mounting platform and provision is made for X, Y, and Z axis adjustments.

(2) Electrical System

The SLO-SYN stepping motor combines high torque which accurately determined angular step sizes. The maximum stepping rate is 200 steps per second with a maximum torque of 130 in. oz. The motor rotation increment is $1.8° \pm 0.09°$ (noncumulative). This is converted to the probe Z traverse by a precision sprocket-timing chain drive which is in constant preload to eliminate hysteresis. The gear ratio is such that one motor step corresponds to a rake step of 0.025 cm (0.010 in.) with an error of $\pm$ 0.000127 cm (0.0005 in.). Since the stepper motor error is noncumulative, the rake can be precisely located in 0.0127 cm (0.005 in.) increments throughout most of the channel span.

For all cases of interest, the desired step size is greater than 0.0127 cm, so the steps are made by a series of pulses to the motor. An electro-mechanical

pulse generator controls the location of the probe by timing the number of pulses. The generator consists of a perforated tape reader which scans a paper tape perforated with a set of commands which yields the desired number of steps between Z stations. In addition, the system provides command signals which provide synchronization of the data acquisition system with probe step rate. Finally, the system provides a signal which identifies probe location on the Z and X axes.

A separate command paper tape is made for each orifice plate assembly. A simple computer program is used to prepunch onto each tape the commands which define the measuring station locations for each orifice plate referenced to the centerline of the duct. The tape also provides the X-traverse signal at the end of each Z traverse.

8. Instrumentation and Data Acquisition

Test data are recorded using an analog-to-digital data acquisition system with a sampling rate of up to 50 channels per second. Digital data are immediately available in printed form on paper and also are recorded on incremental magnetic tape for subsequent computer reduction. In addition, system parameters such as inlet temperature and flow rate are displayed continusously in digital form and also recorded on high-accuracy, adjustable-range potentiometric records for use by the experimentor in adjusting and controlling operating conditions.

9. Flow Facility Support and System Insulation

The test duct is supported rigidly in the plane of jet injection to assure that the injection plane remains fixed when the system dimensions change due to thermal expansion of the material. All other points in the system are supported along one Y plane only and are free to expand or contract about the plane in the X, Y, and Z directions. All incoming air and H_2 lines are flex lines and the traverse table is fixed rigidly to the test section at the plane of jet injection on ly. The entire hot air system is wrapped with approximately 3 in. of fiberglass batting in order to reduce heat losses.

APPENDIX C

A. FLOW SYSTEM CHECKOUT, CALIBRATION AND TEST PROCEDURE

1. Checkout and Calibration Tests

Prior to conducting tests of the various orifice plate configurations, system calibration tests and checkout tests were conducted. The primary objectives of these calibration/checkout tests were:

(a) To verify that the hydrogen-air heater operation was free from surges and that the temperature control was operating effectively.

(b) To verify that adequate motor torque and rake positioning repeatability could be achieved.

(c) To verify that the duct free-stream stagnation pressure and temperature were within $\pm$ 2% of the average values at a distance from the duct walls greater than 1.27cm (0.5 in.) at a plane 5.1 cm (2 in.) upstream of the jet injection point.

(d) To verify that the system flow control, traversing mechanism and instrumentation were functioning adequately.

a. Hydrogen-Air Heater Checkout

Tests were made with the air and H_2 supply mated to the main plenum but without the rectangular test section mated to the main plenum. The tests were conducted at the three test temperatures and with the maximum, nominal, and minimum air flow rates. Fast response pressure transducers and thermocouples were monitored during the test to evaluate system performance. If a start surge overpressure occurred or if ignition did not occur, test procedures were modified and the system was retested as necessary.

b. Traverse Mechanism Checkout

Prior to installing the probe traversing mechanism in the test duct, the system was tested for station alignment precision and total traverse time. The alignment of the probe axis is estimated to be within 2° of the test duct axis. The lateral station positioning, Z/S, was within 1% of the desired rake locations and the total time to complete one traverse was approximately 90 seconds.

c. Test Duct Stagnation Condition Evaluation and Probe Checkout

After the main air system had been tested to ensure smooth operation, the test duct was connected to the main plenum and tests made to determine if stagnation pressure and temperature are constant across the test within the allowable limits (± 2% at distances over 1.27 cm from duct walls). Tests were conducted at nominal mainstream flow rates at temperatures of 450° K (350° F), 600° K (620° F), and 750° K (890° F) and at maximum flow rates at 600° K (620° F), with the secondary plenum orifice plate blanked off. Modifications were made to the original combustor configuration (the addition of screens and baffles) until the desired pressure and temperature profiles were achieved.

In addition to an evaluation of the duct temperature and pressure profiles, these tests: (1) served as an evaluation of probe operation in the hot gas environment, (2) allowed a leak check to be made of the secondary plenum with blank orifice plate, and (3) allowed further test data instrumentation checkout.

2. Test Procedure

The following test procedures were used for the Multiple Jet Study tests:

a. Pretest

(1) Main air and secondary air metering nozzles were selected and installed.

(2) Tank charged to 600 psig.

(3) Orifice plate selected and installed in secondary plenum and pressure tape connections made.

(4) If secondary plenum baffle insert was used, it was installed and secondary plenum sealing surfaces tightened.

(5) Perforated paper control tape for the particular orifice plate was loaded into the tape reader and locate buttons pushed.

(6) The rake was checked and manually aligned as necessary.

(7) READY button was pressed to allow the control system to position rake to beginning of first traverse.

(8) The digital system was readied by inputting the appropriate run number and configuration number.

b. Start Transient

The main air supply was turned on at moderate flow rate, the igniter energized, and a low flow rate of hydrogen (~10% steady-state flow) introduced. If ignition did not occur within approximately two seconds as indicated by a high response thermocouple in the combustor, hydrogen flow was automatically terminated and the system purged with main flow air for approximately 60 seconds. Hydrogen and air flow rates were set to a more favorable ratio for ignition and the process repeated. When ignition occurred, the air and hydrogen flow rates were brought simultaneously up to the planned values and the hydrogen flow was trimmed to give the desired plenum test temperature. Based on wall thermocouple readings, the system thermal steady state was reached and the test data acquisition began.

c. Test Data Acquisition

After the facility reached steady-state operation, the rake traverse was initiated. Except for monitoring and control of test conditions, the remainder of the test sequence continued automatically under the control of the tape reader. The number of stations sampled was identical for all orifices plates tested. The only variable was the Z spacing which was varied dependent on the particular orifice spacings. In all cases, the total Z span was equal to twice the orifice spacing. Twenty-one Z stations were sampled at the first three axial locations and 11 Z stations were sampled at the fourth X station and 21 Z locations were sampled at the fifth X station, for a total of 95 X, Z points. For all plates with $H/D < 16$, the axial stations were at $X/H = 0.25, .5, 1.0, 1.5$, and 2.0. For tests with small orifices ($H/D = 16$), an $X = 1.27$ cm (0.5 in.) station was substituted for the $X = 20.3$ cm (8.0 in.) station. The Z stations were symmetrically spaced about the midpoint between the two centermost orifices.

At the beginning and the midpoint of each traverse, all channels were scanned in order to provide run number, time, system parameters, and rake parameter measurements. After the first complete data scan, the rake, under the control of the prepunched tapes, was traversed to the next Z station and the thermocouple stepper and Scanivalve No. 2 were monitored to record the rake temperatures and pressures. Approximately 4 seconds were required at each station for steady state to be reached and data to be taken. The rake then stepped to the next Z station and the process

repeated. At the completion of data acquisition from the last Z station, the rake, under the control of the paper tape, was stepped back to the next X station and was ready for the Z traverse in the reverse direction to the first traverse.

The process of data acquisition outlined for the first X location was repeated until all X, Z points had been sampled, at which time the hydrogen flow to the heater was terminated, the air flow reduced, and the rake manually returned to the starting position in preparation for the next test.

APPENDIX D

A. DATA ANALYSIS PROGRAM

1. Objective

The objective of the data analysis program is to use the output from the data reduction program to calculate test run conditions (weight flow rates, velocities, Mach numbers, momentum fluxes, densities, and temperature), dimensionless temperature and pressure profiles, and correlating parameters (pattern factors, temperature deviation ratios, and energy exchange, E_T, values). The output from the analysis program is a paper listing of the run conditions, correlating parameters, and temperature and pressure values. In addition to the paper listing, the temperature and pressure profile data are output on a magnetic drum for use as input to the computer plotting routines. When the plot program is executed, the output data are stored on magnetic tape which is then input to the microfilm printer/plotter.

2. Methods of Calculation

a. Mainstream Conditions

The weight flow rate in the test duct upstream of the secondary injection orifices is calculated from the main venturi pressure drop, flow coefficient, and temperature data. The velocity in the test duct upstream of the secondary injection orifices is calculated using the continuity equation with the gas density based on the ideal equation of state and corrected to static conditions. The mainstream stagnation temperature is measured directly with a thermocouple in the main air plenum. Mainstream Mach number is calculated from the mainstream stagnation temperature and mainstream velocity. The mainstream pressure ratios, used for static density calculations, are measured from total pressure measurements in the main air plenum and static pressure measurements in the test duct 5.1 cm upstream of the secondary injection plane. Momentum flux in the mainstream is the product of the static density and the square of the mainstream velocity.

b. Jet Conditions

The jet weight flow rate is calculated from the secondary air venturi pressure drop, flow coefficient, and temperature. The jet velocity is the velocity at the

jet vena contracta and is calculated from the jet pressure ratio (measured wall static pressure adjacent to orifice and measured secondary stagnation pressure), gas constant, isentropic exponent, and measured secondary flow stagnation temperature. The jet static density is calculated from the ideal equation of state and the jet pressure ratio. Momentum flux of the jet is the product of the jet static density and the square of the vena contracta velocity. Orifice discharge coefficients are calculated from the ratio of measured secondary flow, divided by the number of secondary orifices, to the ideal isentropic flow through the orifice, based on the measured pressure ratio.

c. Jet to Mainstream Conditions

The momentum flux ratio, density ratio, velocity ratio, and flow rate ratio are the jet values of the parameter divided by the mainstream values. The temperature ratio is the mainstream temperature divided by the jet temperature.

d. Flow Field Conditions

Dimensionless temperature difference ratios, Θ (free-stream temperature minus temperature at a point divided by free-stream minus jet temperature), are calculated for each rake temperature measurement. Also, dimensionless pressure difference ratios, C_p (pressure measured at a point minus primary flow pressure divided by secondary stagnation pressure minus primary stagnation pressure), are calculated for each rake pressure measurement. The maximum values of Θ and C_p in the center plane of each orifice are listed along with the vertical location of the maximum value at each axial measurement station.

The average values of Θ, C_p, and temperature are listed at each axial station. Also, at each axial station, mixing correlation parameters are listed. These parameters are (1) the pattern factor (the free-stream temperature minus the average temperature at station X divided by the average temperature at X minus the jet temperature), (2) the temperature deviation ratio (the average temperature minus the ideal mixed temperature divided by the free-stream temperature minus the ideal mixed temperature), and (3) E_T (the percent of the maximum possible energy exchange between jet and free-stream). A sample program listing is contained in Table VI.

TABLE I

ORIFICE PLATE CONFIGURATIONS

	Orifice Configurations*	Orifice Diameter D, cm (in)	Orifice Spacing S, cm (in)	Number of Orifices N	Orifice Spacing to Duct Height S/H	Ratio of Total Orifice Area to Duct Area, %
1.	1/02/06	1.69(.67)	3.39(1.33)	9	.333	6.5
2.	1/02/08	1.27(.50)	2.54(1.00)	12	.250	4.9
3.	1/02/12	0.84(.33)	1.69(.67)	18	.167	3.3
4.	1/03/08	1.27(.50)	3.81(1.50)	8	.375	3.3
5.	1/02/16	0.64(.25)	1.27(.50)	24	.125	2.5
6.	1/04/08	1.27(.50)	5.08(2.0)	6	.500	2.5
7.	1/03/16	0.64(.25)	1.91(.75)	16	.187	1.6
8.	1/04/12	0.84(.33)	3.39(1.33)	9	.333	1.6
9.	1/06/08	1.27(.50)	7.62(3.00)	4	.750	1.6
10.	2/02/16**	0.64(.25)	1.27(.50)	24	.125	2.5
11.	4/02/16**	0.64(.25)	1.27(.50)	24	.125	2.5
12.	1/04/04	2.54(1.00)	10.16(4.00)	3	1.000	4.9
13.	1/02/04	2.54(1.00)	5.08(2.00)	6	.500	9.8
14.	1/04/08d	1.27(.50)	5.08(2.0)	12	.500	4.9
15.	1/03/06n	1.80(.71)	5.08(2.0)	6	.500	4.9
16.	1/03/06m	***	5.08(2.0)	6	.500	4.9

* Orifice Code

1st Number = Orifice Aspect Ratio

2nd Number = Nondimensional Orifice Spacing, S/D

3rd Number = Nondimensional Orifice Size, H/D, where H is the Test Duct Height

** Non-circular Orifices

*** Mixed Orifice Sizes - Small Orifice Diameter 0.84 cm

Large Orifice Diameter 2.40 cm

TABLE II

COMPARISON OF MULTIPLE JET STUDY
MIXING PARAMETERS

Test Number	Orifice Plate Configuration	Area Ratio, $A_{orifice}/A_{duct}$	Momentum Flux Ratio, J	Downstream Distance, X/H	% Energy[1] Exchanged, E_T	Pattern[1] Factor, δ^*
51	1/04/12	.016	6.5	.250	30.4	.051
↓	↓	↓	↓	.500	43.1	.056
				1.00	42.3	.053
51	1/04/12	.016	6.5	2.00	53.7	.058
85	1/02/06	.065	62.5	.250	58.5	.406
↓	↓	↓	↓	.500	76.7	.411
				1.00	88.9	.408
85	1/02/06	.065	62.5	2.00	89.2	.445

(1) See pages 15 and 16 for parameter definitions

TABLE III

TEST DATA SUMMARY FOR ORIFICE PLATES 1/02/16, 4/02/16 and 2/02/16

Test No.	Orifice Plate No.	Orifice Dia. cm (in)	Orifice S/D	Orifice S/H	Orifice H/D	No. Orifices	% Flow Area (A_J/A_T)	Main-Stream Mach No	Momen. Ratio J	Density Ratio P_J/P_∞	Vel. Ratio V_J/V_∞	Flow Ratio $\dot{W}_J/\dot{W}_\infty$	Ideal Theta	X/H	Table of Average Thetas .125 θ_{ave}	.250 θ_{ave}	.500 θ_{ave}	1.00 θ_{ave}	Test Conditions
1	1/02/16	.635 (25)	2.0	.125	16	24	2.46	.048	6*	2.1*	1.76*	.06*	—		Test data not reduced				Nominal
2								.048	14.01	2.12	2.57	.09	.0855		.1150	.1164	-	.1323	Nominal
3									25.76	2.14	3.47	.12	.1101		.1355	.1441	.1597	.1726	Nominal
4									57.43	2.15	5.16	.18	.1588		.1887	.2045	.2329	.2567	Nominal
5									6.43	2.08	1.76	.06	.0572		.1099	.0997	.0951	.0944	Large Dia. Grid
6									14.59	2.12	2.62	.09	.0855		.1148	.1177	.1219	.1233	Large Dia. Grid
7								.048*	25*	2.1*	3.5*	.12*	—		Test Data not reduced				Large Dia. Grid
8								.046	61.20	2.10	5.40	.18	.1588		.1704	.1866	.2139	.2352	Large Dia. Grid
9								.048	5.68	2.12	1.66	.06	.0572		.0744	.0785	.0774	.0770	Small Dia. Grid
10								.048*	14*	2.12*	2.6*	.09*	—		Test data not reduced				Small Dia. Grid
11								.048	24.81	2.16	3.39	.12	.1101		.1217	.1324	.1432	.1549	Small Dia. Grid
12									55.78	2.19	5.05	.18	.1588		.1710	.1897	.2217	.2453	Small Dia. Grid
13									6.23	2.16	1.70	.06	.0572		.0844	.0838	.0844	.0840	Small Height Baffle
14									14.33	2.18	2.57	.09	.0855		.1096	.1136	.1202	.1239	Small Height Baffle
15									23.61	2.20	3.28	.12	.110		.1244	.1282	.1401	.1552	Small Height Baffle
16									52.36	2.23	4.84	.18	.1588		.1611	.1745	.2016	.2264	Small Height Baffle
17									6.28	2.15	1.71	.06	.0572		.0869	.0862	.0920	.0906	Large Height Baffle
18									14.31	2.17	2.57	.09	.0855		.1137	.1170	.1279	.1302	Large Height Baffle
19									25.13	2.19	3.39	.12	.110		.1162	.1326	.1450	.1593	Large Height Baffle
20									55.75	2.22	5.01	.18	.1588		.1633	.1758	.2068	.2309	Large Height Baffle
21								.064*	14*	2.12*	2.56*	.09*	-		Test data not reduced				-
22								.049	23.79	2.74	2.95	.13	.1179		.1388	.1509	.1629	.1743	High Density Ratio
23								.048	5.91	1.58	1.93	.05	-		.0745	.0713	.0794	.0818	Low Density Ratio
24								.049	6.03	2.65	1.51	.07	-		.0918	.0932	.0948	.0968	High Density Ratio
25								.048	23.37	1.61	3.81	.10	.0945		.1375	.1484	.1530	.1680	Low Density Ratio
26								.032	59.12	2.20	5.18	.18	.1588		.1743	.1902	.2279	.2463	Low Momentum Level
27								.096	6.11	2.18	1.67	.06	.0572		.0953	.0938	.0960	.0937	High Momentum Level
28	4/02/16	.625 (25)	2	.125	16	24	2.45	.032	5.92	2.13	1.67	.06	.0572		.1029	.0951	.0954	.0879	Nominal
29									14.89	2.15	2.63	.09	.0855		.1192	.1237	.1258	.0238	Nominal
30									27.45	2.18	3.55	.12	.1101		.1611	.1667	.1696	.1737	Nominal
31									63.37	2.20	5.36	.18	.1588		.2077	.2065	.2102	.2219	Nominal
32								.036	27.90	1.61	4.16	.10	.0945		.1229	.1261	.1283	.1288	Low Density Ratio
33								.031	26.26	2.72	3.11	.13	.1179		.1512	.1577	.1627	.0730	High Density Ratio

TABLE III (cont.)

TEST DATA SUMMARY FOR ORIFICE PLATES 1/02/16, 4/02/16 and 2/02/16

Test No.	Orifice Plate No.	Orifice Dia. cm. (in)	Orifice S/D	Orifice S/H	Orifice h/D	No. Orifices	% Flow Area (A_J/A_T)	Main-Stream Mach No	Momen. Ratio J	Density Ratio ρ_J/ρ_∞	Vel. Ratio V_J/V_∞	Flow Ratio $\dot{W}_J/\dot{W}_\infty$	Ideal Theta	X/H	Table of Average Thetas .125 θ_{ave}	.250 θ_{ave}	.500 θ_{ave}	1.00 θ_{ave}	Test Conditions
77	2/02/16	.635 (.25)	2.0	.125	16	24	2.45	.033	6.31	2.15	1.71	.06	.0573		.0847	.0868	.0886	.0681	Nominal
78	↓	↓	↓	↓	↓	↓	↓	.033	15.33	2.18	2.65	.09	.0858		.1111	.1160	.1287	.1267	Nominal
79								.032	28.46	2.20	3.59	.15	.1110		.1361	.1436	.1521	.1608	Nominal
80								.032	28*	1.61*	4.1*	.10*	Test data not reduced						
81								.032*	28*	2.72*	3.1*	.13*	Test data not reduced						
82								.029	29.53	2.74	3.28	.13	.1226		.1438	.1499	.1607	.1664	High Density Ratio

* Indicates nominal values

TABLE IV

TEST DATA SUMMARY FOR PRESELECTED ORIFICE PLATE TEST SERIES

Test No.	Orifice Plate No.	Orifice Dia. cm (in)	Orifice S/D	Orifice S/H	Orifice H/D	No. Orifices	% Flow Area	Main-Stream Mach No	Momen. Ratio	Density Ratio	Vel. Ratio	Flow Ratio	Ideal Theta	X/H	.250	.500	1.00	2.00	.250	.500	1.00	2.00
															Table of Average Thetas				Table of ET Values			
34	1/06/08	1.27(.50)	6	1.750	8	4	1.64	.033	7.13	2.13	1.83	.04	.0415		.0447	.0418	.0409	.0458	25.1	27.0	38.2	65.1
35									14.13	2.17	2.17	.06	.0571		.0631	.0624	.0618	.0665	41.9	48.9	62.2	84.5
36									26.36	2.19	3.47	.08	.0746		.0862	.0800	.0851	.0895	59.2	62.3	80.2	90.0
37								.038	60.03	1.66	6.01	.10	.0939		.0918	.0929	.0938	.1036	82.5	63.2	70.8	87.6
38								.030	27.56	2.71	3.19	.09	.0828		.0819	.0854	.0835	.0869	47.8	60.4	73.3	86.1
39	1/03/16	.635(.25)	3	.187	16	16	1.64	.033	6.46	2.14	1.74	.04	.0415		Invalid thermocouple data							
40									13.08	2.16	2.46	.06	.0567		Invalid thermocouple data							
41									23.53	2.20	3.27	.07	.0738		Invalid thermocouple data							
42									62.04	2.22	5.28	.12	.1130		Invalid thermocouple data							
43								.038	24.95	1.62	3.92	.07	.0630		Invalid thermocouple data							
44								.030	25.38	2.69	3.07	.08	.0819		Invalid thermocouple data							
45	1/02/12	.846(.333)	2	.167	12	18	3.27	.033	5.46	2.15	1.59	.08	.0753		Invalid thermocouple data							
46									13.80	2.19	2.51	.12	.1124		.1308	.1361	.1451	.1370	30.5	38.4	46.6	49.6
47									24.47	2.21	3.31	.15	.1416		.1487	.1599	.1729	.1715	31.7	40.4	49.3	56.1
48									57.31	2.26	5.04	.24	.2023		.2005	.2166	.2438	.2637	44.0	52.7	64.7	72.0
49								.037	28.57	1.65	4.16	.14	.1277		.1577	.1674	.1766	.1778	ET Values not Comp.			
50								.030	25.30	2.76	3.03	.17	.1542		.1611	.1724	.1841	.1884	ET Values not Comp.			
51	1/04/12	.846(.333)	4	.333	12	9	1.64	.033	6.48	2.13	1.75	.04	.0416		.0483	.0527	.0503	.0544	30.4	43.1	42.3	53.7
52									12.30	2.18	2.38	.06	.0569		.0665	.0706	.0692	.0731	39.3	49.6	53.0	62.4
53									23.35	2.20	3.26	.08	.0743		.0837	.0890	.0885	.0871	48.5	58.9	65.4	69.2
54									60.34	2.24	5.19	.12	.1126		.1111	.1159	.1205	.1209	56.9	69.3	82.6	88.7
55								.037	24.49	1.63	3.88	.07	.0631		.0815	.0849	.0862	.0848	52.2	60.9	67.9	73.2
56								.030	24.7	2.73	3.01	.09	.0824		.0822	.0835	.0920	.0923	41.5	50.8	63.8	69.7
57	1/02/08	1.27 .50	2.0	.250	8	12	4.9	.032	5.94	2.19	1.65	.12	.1112		.1271	.1297	.1314	.1291	28.5	36.9	43.0	48.6
58									13.80	2.22	2.49	.18	.1595		.1597	.1637	.1724	.1762	ET Values not comp.			
59									25.38	2.24	3.36	.23	.2010		.1880	.2006	.2130	.2209	ET Values not comp.			
60									25.24	1.64	3.92	.20	.1698		.1665	.1830	.1919	.1996	32.8	48.9	58.3	68.7
83								.037	59.63	2.26	5.14	.36	.2762		.2460	.2518	.2700	.3106	ET Values not comp.			
61								.029	25.43	2.78	3.02	.26	.2158		.2018	.2127	.2260	.2332	37.8	50.9	60.1	70.3

TABLE IV (cont.)

TEST DATA SUMMARY FOR PRESELECTED ORIFICE PLATE TEST SERIES

Test No.	Orifice Plate No.	Orifice Dia. cm (in)	Orifice S/D	Orifice S/H	Orifice H/D	No. Orifices	% Flow Area	Main-Stream Mach No	Momen. Ratio	Density Ratio	Vel. Ratio	Flow Ratio	Ideal Theta	X/H	.250	.500	1.00	2.00	.250	.500	1.00	2.00
															Table of Average Thetas				Table of ET Values			
62	1/03/08	1.27 (.50)	3.0	.375	8	8	3.27	.033	5.69	2.14	1.63	.08	.0754		.0943	.0923	.0933	.0910	39.8	44.6	51.2	55.5
63	↓	↓	↓	↓	↓	↓	↓	-	-	-	-	-	-		Test data not reduced							
64	↓	↓	↓	↓	↓	↓	↓	↓	25.94	2.23	3.41	.15	.1421		.1717	.1666	.1662	.1622	ET Values not comp.			
65	↓	↓	↓	↓	↓	↓	↓	.037	26.71	2.76	3.11	.17	-		.2009	.1686	.1595	.1527	ET Values not comp.			
66	↓	↓	↓	↓	↓	↓	↓	.030	30.09	1.65	4.27	.14	.1545		.1380	.1500	.1542	.1603	43.0	59.0	72.7	80.8
67	1/04/08	1.27 (.50)	4.0	.5	8	6	2.45	.032	6.28	2.10	1.73	.06	.058		.0773	.0757	.0698	.0711	44.9	49.7	56.3	65.7
68	↓	↓	↓	↓	↓	↓	↓	↓	14.43	2.14	2.60	.09	.0841		.0902	.0888	.0899	.0936	44.4	54.4	56.3	65.7
69	↓	↓	↓	↓	↓	↓	↓	↓	26.92	2.17	3.53	.11	.1087		.1186	.1173	.1176	.1200	55.2	66.5	80.1	91.7
84	↓	↓	↓	↓	↓	↓	↓	.032	61.91	2.22	5.28	.17	.1576		.1498	.1536	.1538	.1530	66.2	78.5	87.7	91.0
70	↓	↓	↓	↓	↓	↓	↓	.037	26.84	1.62	4.07	.10	.0918		.1084	.1051	.1091	.1094	ET Values not Comp.			
71	↓	↓	↓	↓	↓	↓	↓	.029	28.48	2.68	3.26	.13	.1207		.1115	.1172	.1201	.1239	49.1	64.3	79.0	90.7
72	1/02/06	1.7 (.667)	2.0	.333	6	9	6.54	.032	6.14	2.16	1.68	.16	.1440		.1518	.1597	.1599	-	25.4	34.7	44.4	-
73	↓	↓	↓	↓	↓	↓	↓	↓	15.21	2.20	2.63	.24	.2053		.1991	.2099	.2130	.2122	34.6	47.0	60.7	70.3
74	↓	↓	↓	↓	↓	↓	↓	↓	26.49	2.23	3.45	.31	.2510		.2338	.2457	.2523	.2522	41.2	56.7	71.3	81.3
85	↓	↓	↓	↓	↓	↓	↓	↓	62.48	2.23	5.29	.47	.3390		.2889	.2915	.2896	.3079	58.5	76.7	88.9	89.2
75	↓	↓	↓	↓	↓	↓	↓	.036	25.81	1.59	4.03	.26	.2095		.2216	.3032	.2320	.2345	39.9	-	71.5	80.9
76	↓	↓	↓	↓	↓	↓	↓	.029	27.45	2.75	3.16	.35	.2704		.2353	.2489	.2521	.2616	ET Values not Comp.			

TABLE V

TEST DATA SUMMARY FOR FINAL ORIFICE PLATE TEST SERIES

Test No.	Orifice Plate No.	Orifice Diameter, cm (in.)	Orifice S/D	Orifice S/H	Orifice H/D	No. of Orifices	% Flow Area	Main-stream Mach No.	Momentum Ratio	Density Ratio	Velocity Ratio	Flow Ratio	Ideal Theta	X/H = .25	.50	1.0	2.0	.25	.50	1.0	2.0
														Table of Average Theta Values				Table of K_T Values			
86	1/04/04	2.54 (1.00)	4.0	1.0	4	3	4.9	.032	6.06	2.14	1.68	.12	.1114	.1169	.1216	.1159	.1150	29.8	49.0	51.7	72.2
87									14.65	2.17	2.69	.18	.1602	.1516	.1473	.1537	.1491	38.9	47.7	67.6	79.2
88									27.20	2.20	3.52	.23	.2014	--	.1833	.1749	.1862	NA	56.5	63.5	78.2
89									63.23	2.22	5.34	.35	.2774	.2616	.2492	.2473	.2559	50.0	58.6	65.3	83.5
90	1/04/08d	1.27 (.50)	8.0	.5	8	12	4.9	.032	6.04	2.16	1.67	.12	.1114	.1060	.1144	.1172	.1165	25.3	36.1	57.4	70.7
91								.032	14.37	2.19	2.56	.18	.1518	.1384	.1476	.1623	.1593	29.3	47.3	74.5	87.1
92								.033	26.35	2.22	3.45	.23	.2008	.1658	.1786	.1912	.1881	34.0	57.6	83.8	92.2
93								.033	59.84	2.25	5.16	.35	.2768	.2368	.2534	.2442	.2470	53.0	77.2	82.3	84.9
94	1/03/06n	1.80 (.707)	2.8	.5	6	6	4.9	.033	5.87	2.16	1.65	.12	.1097	.1192	.1167	.1180	.1223	33.8	42.4	53.7	65.1
95								.033	13.89	2.19	2.52	.18	.1582	.1552	.1641	.1623	.1637	41.0	57.3	72.1	81.4
96								.032	26.62	2.20	3.58	.23	.2011	.1726	.1862	.1791	.1910	45.6	62.6	77.8	90.4
97								.032	60.59	2.23	5.21	.36	.2772	.2511	.2514	.2423	.2413	69.2	82.7	88.5	88.3
98	1/03/06m	*	3.0	.5	6	6	4.9	NA	NA	NA	NA	NA	--	--	--	--	--	--	--	--	--
99								.032	14.24	2.19	2.55	.18	.1545	.1587	.1600	.1575	.1510	45.8	57.8	74.9	83.7
100									26.57	2.19	3.48	.23	.2005	.1765	.1811	.1748	.1843	47.8	63.7	77.0	78.0
101									61.28	2.21	5.27	.35	.2762	.2552	.2350	.2304	.2371	64.7	64.4	69.5	77.7
102	1/02/04	2.54 (1.00)	2.0	.5	4	6	9.8	.032	5.80	2.20	1.63	.23	.1998	.1883	.2036	.2088	.2085	27.6	28.6	51.6	60.6
103									13.32	2.21	2.45	.35	.2759	.2547	.2750	.2801	.2802	40.0	55.5	71.7	86.2
104									24.61	2.22	3.33	.46	.3354	.2897	.3125	.3156	.3102	49.3	68.1	85.3	91.9
105									39.39	2.22	4.21	.60	.3975	.3289	.3461	.3357	.3469	59.6	79.8	93.0	92.1

*Mixed orifice size .84 cm (.33-in.) and 2.40 cm (.943-in.)

TEST DATA FOR MULTIPLE JET PROGRAM

TEST NUMBER 96. RUN NUMBER 135 ORIFICE PLATE NO. 1/03/06A

******* PLANNED TEST CONDITIONS *******

MOMENTUM RATIO=	32.000
TEMPERATURE RATIO=	2.000
MAINSTREAM VELOCITY=	50.000
JET VELOCITY=	200.000
MAINSTREAM TEMP=	1080.000

******* SYSTEM PARAMETERS *******

AVERAGE MAINSTREAM FLOWRATE=	.279341+00KG/SEC	.615846+00LBM/SEC
AVERAGE SECONDARY FLOWRATE=	.655209-01KG/SEC	.144450+00LBM/SEC
AVERAGE HYDROGEN FLOWRATE=	.689771-03KG/SEC	.152069-02LBM/SEC
AVERAGE MAINSTREAM TEMPATURE=	598.2128DEG K	1076.7830DEG R
AVERAGE SECONDARY TEMPERATURE=	281.6437DEG K	506.9586DEG R
AVERAGE HYDROGEN-AIR RATIO=	.0025	
AVERAGE WATER MOLE FRACTION=	.0544	
AVERAGE MAINSTREAM GAS CONSTANT=	296.53JOUL/KG K	55.11FT-LBF/LBM-R
AVERAGE MAINSTREAM GAMMA=	1.3985	
AVERAGE ENERGY BALANCE TEMP=	534.5472DEG K	962.1851DEG R

	START		END	
	DEG K	DEG R	DEG K	DEG R
EXTENSION SECTION WALL TEMP=	618.83	1113.89	573.75	1032.76
TEST DUCT WALL TEMP,X/H=-.75,TOP	558.20	1004.76	568.20	1022.76
TEST DUCT WALL TEMP,X/H=-.75,SIDE	548.05	986.50	556.34	1001.41
TEST DUCT WALL TEMP,X/H=-.75,BOTTOM	529.07	952.32	534.94	962.90
TEST DUCT WALL TEMP,X/H=0.25,BOTTOM	535.50	963.90	554.58	998.24
TEST DUCT WALL TEMP,X/H=1.00,BOTTOM	528.37	951.06	551.72	993.10
SECONDARY PLENUM WALL TEMP,Y/H=.25	315.55	567.99	317.16	570.89
HEATER COMBUSTION TEMPERATURE	602.04	1083.67	602.38	1084.28

SAMPLE TEST DATA ANALYSIS OUTPUT TABLE VI

******* MAINSTREAM CONDITIONS AT X/H=-0.5 *******

TEST NUMBER 96. RUN NUMBER 135 ORIFICE PLATE NO. 1/08/06a

TIME SEC	STAG PRESS PSIA	STATIC PRESS PSIA	STAG TEMP R	WEIGHT FLOW LBM/SEC	MACH NO	STATIC DENSITY LB/FT3	VELOCITY FT/SEC	MOMENTUM FLUX
354.30	14.6661	14.6551	1078.80	.6160+00	.0323	.3550-01	52.06	.9621+02
435.10	14.6661	14.6552	1081.71	.6152+00	.0323	.3541-01	52.13	.9621+02
526.30	14.6661	14.6552	1073.10	.6182+00	.0324	.3569-01	51.97	.9637+02
606.60	14.6663	14.6555	1078.58	.6152+00	.0323	.3551-01	51.98	.9592+02
697.90	14.6658	14.6549	1075.89	.6173+00	.0324	.3560-01	52.03	.9636+02
777.90	14.6663	14.6552	1075.06	.6159+00	.0323	.3562-01	51.86	.9582+02
868.90	14.6651	14.6550	1075.63	.6144+00	.0322	.3560-01	51.77	.9543+02
948.50	14.6573	14.7944	1075.10	.6166+00	.0321	.3586-01	51.59	.9542+02
968.20	14.6661	14.6552	1074.76	.6155+00	.0323	.3563-01	51.81	.9567+02
1048.10	14.6661	14.6552	1079.37	.6148+00	.0323	.3548-01	51.98	.9586+02
AVERAGE=	14.6651	14.6691	1076.78	.6158+00	.0323	.3559-01	51.92	.9593+02

***** JET CONDITIONS *****

Table VI (cont.)

TEST NUMBER 96. RUN NUMBER 135 ORIFICE PLATE NO. @@@@@@@@@@

TIME SEC	STAG PRESS PSIA	STATIC PRESS PSIA	STAG TEMP R	WEIGHT FLOW LBM/SEC	MACH NO	STATIC DENSITY LB/FT3	VELOCITY FT/SEC	MOMENTUM FLUX	CDJET	CD1	CD2	CD3	CD4	CD5	CD6
354.30	14.9102	14.6325	507.26	.1444+00	.1636	.7835-01	180.55	.2554+04	.624	.651	.646	.611	.614	.616	.612
435.10	14.9107	14.6330	507.08	.1446+00	.1636	.7838-01	180.55	.2555+04	.625	.651	.651	.612	.617	.615	.609
526.30	14.9086	14.6328	506.90	.1447+00	.1631	.7841-01	179.88	.2537+04	.627	.654	.654	.615	.620	.617	.611
606.60	14.9107	14.6332	506.99	.1443+00	.1636	.7840-01	180.45	.2553+04	.624	.650	.649	.610	.616	.614	.608
697.90	14.9098	14.6318	506.94	.1447+00	.1637	.7840-01	180.60	.2557+04	.625	.647	.648	.613	.616	.617	.613
777.90	14.9074	14.6337	506.72	.1443+00	.1624	.7844-01	179.16	.2518+04	.628	.654	.653	.616	.619	.619	.612
868.90	14.9086	14.6325	506.76	.1446+00	.1632	.7843-01	179.97	.2540+04	.626	.653	.653	.614	.618	.617	.610
948.50	14.9103	14.6230	507.08	.1444+00	.1665	.7834-01	183.67	.2643+04	.614	.639	.639	.601	.606	.605	.598
968.20	14.9096	14.6329	507.03	.1444+00	.1633	.7839-01	180.23	.2546+04	.625	.651	.651	.612	.617	.616	.609
1048.10	14.9081	14.6329	506.99	.1442+00	.1629	.7839-01	179.70	.2532+04	.626	.652	.652	.613	.617	.616	.610
AVERAGE=	14.9094	14.6318	506.96	.1444+00	.1636	.7839-01	180.47	.2553+04	.624						

***** JET TO MAINSTREAM CONDITIONS *****

TEST NUMBER 96. RUN NUMBER 135 ORIFICE PLATE NO. 1/03/06n

TIME	MOMENTUM RATIO	DENSITY RATIO	VELOCITY RATIO	TEMP RATIO	FLOW RATIO
354.30	26.55	2.21	3.47	2.13	.2344
435.10	26.56	2.21	3.46	2.13	.2351
526.30	26.33	2.20	3.46	2.12	.2340
606.60	26.61	2.21	3.47	2.13	.2345
697.90	26.54	2.20	3.47	2.12	.2343
777.90	26.28	2.20	3.45	2.12	.2344
868.90	26.62	2.20	3.48	2.12	.2353
948.50	27.70	2.18	3.56	2.12	.2343
968.20	26.62	2.20	3.48	2.12	.2346
1048.10	26.41	2.21	3.46	2.13	.2346
AVERAGE=	26.62	2.20	3.48	2.12	.23

**** AVERAGE VALUES OF THETA AND CP, VALUES OF MIXING PARAMETER, ET, AND MAX PATTERN FACTOR ****

X/H	AVE THETA	AVE CP	ET	PATTERN FACTOR	TEMP DEVIATION RATIO	AVE TEMP DEG R	AVE TEMP DEG K
.25	.1726	-.0163	45.61	.2086	.1416	978.41	543.56
.50	.1862	-.0140	62.63	.2287	.0744	970.71	539.28
1.00	.1791	-.0129	77.80	.2182	.1094	974.72	541.51
1.50	.1926	-.0150	87.39	.2385	.0424	967.04	537.25
2.00	.1910	-.0122	90.35	.2360	.0504	967.96	537.76

Table VI (cont.)

*** ET=100.(SUM(WDOT(I)(T(I)<T(EB))-T(EB))/(T(JET)-T(EB))+SUM(WDOT(I)(T(I)>T(EB))-T(EB))/(T(FS)-T(EB))/WDOT(TOTAL)
TEMP DEVIATION RATIO=(TAVE(X)-T(ENERGY BALANCE)/(T(FREE STREAM)-T(ENERGY BALANCE))
*** PATTERN FACTOR=(T(FREE STREAM)-TAVE(X))/(TAVE(X)-T(JET))

*** TABLE OF MAXIMUM THETA VALUES IN ORIFICE CENTER PLANES ***

LEFT SIDE X/H	Y/H	Z/S	THETA MAX	RIGHT SIDE X/H	Y/H	Z/S	THETA MAX
.25	.45	.50	.503	.25	.50	1.50	.511
.50	.59	.50	.381	.50	.59	1.50	.384
1.00	.59	.50	.281	1.00	.59	1.50	.285
1.50	.03	.00	.000	1.50	.55	1.50	.244
2.00	.45	.50	.227	2.00	.55	1.50	.221

*** TABLE OF MAXIMUM CP VALUES IN ORIFICE CENTER PLANE ***

LEFT SIDE X/H	Y/H	Z/S	CP MAX	RIGHT SIDE X/H	Y/H	Z/S	CP MAX
.25	.50	.50	.067	.25	.55	1.50	.093
.50	.64	.50	.082	.50	.64	1.50	.085
1.00	.78	.50	.050	1.00	.78	1.50	.054
1.50	.03	.00	.000	1.50	.83	1.50	.036
2.00	.83	.50	.030	2.00	.88	1.50	.036

*** TABLE OF THETA VALUES ***

TEST NUMBER 96. RUN NUMBER 135 ORIFICE PLATE NO. 1/103/061

Table VI (cont.)

X/H .2500

Z/S=		.0000	.1000	.2000	.3000	.4000	.5000	.6000	.7000	.8000	.9000	1.0000
Y/H	Y/D											
.034	.191	.0163	.0158	.0199	.0199	.0417	.0477	.0458	.0277	.0222	.0177	.0219
.080	.455	.0110	.0188	.0447	.0447	.0950	.0760	.0699	.0604	.0385	.0126	.0107
.127	.720	.0640	.1009	.1759	.1759	.1725	.1196	.1342	.1858	.1611	.0828	.0418
.174	.984	.1490	.2046	.2787	.2787	.1951	.1407	.1813	.2598	.2783	.1825	.0975
.221	1.249	.2091	.2681	.3284	.3284	.2087	.1705	.2164	.3026	.3478	.2748	.1505
.267	1.513	.2252	.3024	.3557	.3557	.2305	.2002	.2347	.3167	.3820	.3079	.1797
.314	1.778	.2307	.3232	.3835	.3835	.2681	.2367	.2657	.3517	.4142	.3254	.1829
.361	2.042	.2271	.3262	.4158	.4158	.3387	.3148	.3432	.4163	.4326	.3317	.1742
.408	2.307	.1993	.3099	.4315	.4315	.4314	.4197	.4386	.4692	.4365	.2970	.1511
.454	2.571	.1557	.2603	.4214	.4214	.4975	.5035	.5050	.4876	.4046	.2340	.1028
.501	2.836	.1079	.1913	.3666	.3666	.5000	.5018	.4877	.4502	.3463	.1739	.0714
.548	3.100	.0449	.1101	.2746	.2746	.4480	.4551	.4253	.3719	.2392	.0987	.0413
.595	3.365	.0198	.0527	.1691	.1691	.3395	.3524	.3217	.2614	.1467	.0546	.0255
.641	3.629	.0061	.0152	.0689	.0689	.1855	.2019	.1721	.1284	.0617	.0204	.0160
.688	3.894	.0014	.0013	.0180	.0180	.0696	.0726	.0586	.0357	.0116	.0049	.0126
.735	4.158	.0038	-.0002	.0008	.0008	.0126	.0142	.0061	.0033	-.0022	-.0016	.0081
.782	4.423	-.0014	.0027	.0140	.0140	.0059	.0033	.0036	-.0000	-.0035	-.0002	.0097
.828	4.687	.0060	.0055	.0064	.0064	.0049	.0045	.0051	.0034	.0032	.0038	.0132
.875	4.952	.0251	.0176	.0184	.0184	.0187	.0179	.0184	.0176	.0184	.0181	.0257
.922	5.216	.0287	.0267	.0282	.0282	.0270	.0260	.0267	.0259	.0267	.0263	.0325

X/H .2500

Z/S=		1.0000	1.1000	1.2000	1.3000	1.4000	1.5000	1.6000	1.7000	1.8000	1.9000	2.0000
Y/H	Y/D											
.034	.191	.0219	.0261	.0318	.0392	.0537	.0625	.0520	.0400	.0265	.0226	.0227
.080	.455	.0107	.0183	.0448	.0644	.0774	.0770	.0922	.1005	.0777	.0412	.0245
.127	.720	.0418	.0644	.1497	.1766	.1735	.1290	.1585	.2015	.2005	.1446	.0845
.174	.984	.0975	.1543	.2743	.2966	.2286	.1578	.1858	.2443	.2827	.2283	.1583
.221	1.249	.1505	.2427	.3590	.3541	.2659	.1916	.1997	.2636	.3160	.2954	.2143
.267	1.513	.1797	.2868	.3974	.3696	.2879	.2235	.2224	.2789	.3453	.3156	.2288
.314	1.778	.1829	.3148	.4302	.3984	.3073	.2531	.2542	.3089	.3761	.3365	.2356
.361	2.042	.1742	.3109	.4420	.4502	.3744	.3229	.3259	.3809	.4105	.3483	.2312
.408	2.307	.1511	.2911	.4483	.4920	.4596	.4353	.4202	.4490	.4286	.3356	.2053
.454	2.571	.1028	.2384	.4237	.5034	.5154	.5087	.5023	.4860	.4172	.2777	.1641
.501	2.836	.0714	.1641	.3462	.4607	.5005	.5111	.4997	.4678	.3809	.2318	.1180
.548	3.100	.0413	.0990	.2332	.3821	.4389	.4657	.4567	.4015	.2844	.1504	.0685
.595	3.365	.0255	.0523	.1365	.2568	.3360	.3735	.3628	.2993	.1944	.0915	.0421
.641	3.629	.0160	.0231	.0611	.1178	.1888	.2163	.2102	.1516	.0974	.0464	.0259
.688	3.894	.0126	.0158	.0280	.0458	.0748	.0842	.0889	.0586	.0396	.0237	.0195
.735	4.158	.0081	.0145	.0165	.0169	.0226	.0293	.0264	.0191	.0169	.0168	.0193
.782	4.423	.0097	.0168	.0177	.0152	.0153	.0160	.0160	.0147	.0175	.0211	.0222
.828	4.687	.0132	.0197	.0220	.0187	.0168	.0159	.0166	.0173	.0212	.0247	.0268
.875	4.952	.0257	.0295	.0309	.0293	.0289	.0290	.0312	.0323	.0353	.0371	.0387
.922	5.216	.0325	.0358	.0367	.0361	.0358	.0369	.0394	.0406	.0424	.0444	.0474

*** TABLE OF THETA VALUES ***

TEST NUMBER 96. RUN NUMBER 135 ORIFICE PLATE NO. 1/03/064

X/H 1.0000

Z/S=		.0000	.1000	.2000	.3000	.4000	.5000	.6000	.7000	.8000	.9000	1.0000
Y/H	Y/D											
.034	.191	.2090	.1364	.1365	.1303	.1314	.1274	.1292	.1229	.1312	.1283	.1356
.080	.455	.2399	.1523	.1533	.1431	.1424	.1390	.1455	.1418	.1494	.1485	.1518
.127	.720	.2631	.1657	.1647	.1569	.1604	.1588	.1622	.1626	.1643	.1709	.1690
.174	.984	.2726	.1817	.1774	.1739	.1705	.1723	.1758	.1797	.1834	.1892	.1883
.221	1.249	.2806	.1968	.1943	.1924	.1857	.1895	.1881	.1913	.2030	.2064	.2083
.267	1.513	.2824	.2162	.2174	.2093	.2023	.2083	.2071	.2119	.2195	.2256	.2253
.314	1.778	.2689	.2322	.2338	.2257	.2180	.2229	.2228	.2263	.2339	.2358	.2362
.361	2.042	.2544	.2488	.2434	.2399	.2381	.2412	.2398	.2408	.2474	.2448	.2468
.408	2.307	.2323	.2518	.2499	.2508	.2520	.2526	.2542	.2525	.2545	.2479	.2449
.454	2.571	.1934	.2549	.2535	.2544	.2622	.2652	.2628	.2601	.2556	.2446	.2428
.501	2.836	.1621	.2515	.2536	.2661	.2711	.2781	.2723	.2652	.2552	.2364	.2302
.548	3.100	.1245	.2329	.2467	.2636	.2772	.2808	.2784	.2681	.2454	.2218	.2150
.595	3.365	.0747	.2147	.2374	.2544	.2718	.2812	.2794	.2671	.2360	.2065	.1889
.641	3.629	.0384	.1979	.2182	.2483	.2677	.2810	.2750	.2549	.2256	.1920	.1745
.688	3.894	.0196	.1710	.1948	.2280	.2569	.2646	.2612	.2389	.2058	.1618	.1407
.735	4.158	.0113	.1385	.1686	.1999	.2311	.2411	.2347	.2103	.1729	.1306	.1098
.782	4.423	.0206	.1108	.1400	.1749	.1988	.2109	.2027	.1805	.1396	.1031	.0869
.828	4.687	.0304	.0895	.1143	.1475	.1784	.1759	.1661	.1520	.1161	.0798	.0709
.875	4.952	-.0500	.0681	.0860	.1110	.1340	.1337	.1298	.1148	.0889	.0619	.0586
.922	5.216	-.0009	.0647	.0689	.0915	.1056	.1060	.0984	.0902	.0781	.0604	.0532

Table VI (cont.)

X/H 1.0000

Z/S=		1.0000	1.1000	1.2000	1.3000	1.4000	1.5000	1.6000	1.7000	1.8000	1.9000	2.0000
Y/H	Y/D											
.034	.191	.1356	.1298	.1273	.1280	.1285	.1291	.1272	.1278	.1366	.1393	.1462
.080	.455	.1518	.1529	.1473	.1456	.1431	.1443	.1403	.1431	.1472	.1514	.1562
.127	.720	.1690	.1710	.1645	.1632	.1614	.1631	.1570	.1580	.1610	.1649	.1691
.174	.984	.1883	.1868	.1832	.1778	.1788	.1754	.1743	.1726	.1786	.1757	.1826
.221	1.249	.2083	.2082	.2033	.1954	.1916	.1873	.1851	.1864	.1933	.1905	.1986
.267	1.513	.2253	.2250	.2227	.2154	.2105	.2090	.2023	.2048	.2085	.2117	.2154
.314	1.778	.2362	.2379	.2345	.2292	.2293	.2238	.2178	.2182	.2243	.2245	.2264
.361	2.042	.2468	.2468	.2450	.2434	.2492	.2409	.2344	.2344	.2417	.2360	.2374
.408	2.307	.2449	.2504	.2499	.2489	.2576	.2510	.2521	.2441	.2474	.2438	.2418
.454	2.571	.2428	.2470	.2547	.2598	.2658	.2634	.2637	.2561	.2515	.2437	.2429
.501	2.836	.2302	.2369	.2518	.2663	.2776	.2773	.2698	.2613	.2519	.2388	.2380
.548	3.100	.2150	.2220	.2455	.2644	.2819	.2828	.2779	.2659	.2428	.2284	.2233
.595	3.365	.1889	.2027	.2328	.2592	.2803	.2849	.2810	.2616	.2367	.2114	.2042
.641	3.629	.1745	.1825	.2187	.2534	.2747	.2845	.2795	.2582	.2263	.1938	.1834
.688	3.894	.1407	.1682	.2006	.2447	.2632	.2741	.2666	.2423	.2041	.1691	.1579
.735	4.158	.1098	.1334	.1752	.2145	.2341	.2518	.2410	.2205	.1765	.1354	.1323
.782	4.423	.0869	.1094	.1449	.1872	.2133	.2281	.2096	.1960	.1522	.1154	.1075
.828	4.687	.0709	.0866	.1269	.1568	.1802	.1954	.1829	.1593	.1222	.0963	.0866
.875	4.952	.0586	.0700	.0924	.1172	.1360	.1447	.1392	.1185	.0989	.0795	.0781
.922	5.216	.0532	.0593	.0767	.0946	.1031	.1096	.1097	.0963	.0891	.0759	.0730

*** TABLE OF CP VALUES ***

TEST NUMBER 96. RUN NUMBER 135 ORIFICE PLATE NO. 1/03/064

X/H .2500

Z/S=		.0000	.1000	.2000	.3000	.4000	.5000	.6000	.7000	.8000	.9000	1.0000
Y/H	Y/D											
.034	.191	.0035	.0032	-.0064	-.0064	-.0638	-.0754	-.0600	-.0286	-.0105	-.0016	.0048
.080	.455	.0013	-.0017	-.0225	-.0225	-.0865	-.1017	-.0822	-.0418	-.0187	-.0017	.0054
.127	.720	-.0096	-.0146	-.0441	-.0441	-.1283	-.1414	-.1180	-.0738	-.0362	-.0178	-.0011
.174	.984	-.0201	-.0258	-.0745	-.0745	-.1605	-.1717	-.1504	-.1068	-.0710	-.0270	-.0129
.221	1.249	-.0194	-.0230	-.0961	-.0961	-.1755	-.1802	-.1723	-.1321	-.0821	-.0176	-.0169
.267	1.513	-.0091	-.0030	-.0750	-.0750	-.1765	-.1753	-.1764	-.1428	-.0699	-.0044	-.0133
.314	1.778	.0013	.0125	-.0456	-.0456	-.1702	-.1698	-.1708	-.1361	-.0314	.0142	-.0059
.361	2.042	.0102	.0314	-.0077	-.0077	-.1516	-.1578	-.1558	-.0949	.0176	.0206	.0014
.408	2.307	.0120	.0350	.0430	.0430	-.1061	-.1148	-.0920	-.0126	.0510	.0318	.0063
.454	2.571	.0098	.0339	.0680	.0680	.0180	.0341	.0131	.0652	.0574	.0265	.0072
.501	2.836	.0092	.0233	.0600	.0600	.0990	.0675	.0798	.0879	.0477	.0178	.0078
.548	3.100	.0090	.0163	.0391	.0391	.0966	.0462	.0738	.0614	.0309	.0122	.0080
.595	3.365	.0091	.0119	.0226	.0226	.0584	.0259	.0470	.0360	.0180	.0097	.0077
.641	3.629	.0089	.0098	.0147	.0147	.0328	.0156	.0262	.0216	.0115	.0088	.0080
.688	3.894	.0087	.0085	.0101	.0101	.0185	.0100	.0160	.0131	.0080	.0074	.0088
.735	4.158	.0083	.0079	.0083	.0083	.0122	.0084	.0111	.0095	.0074	.0067	.0093
.782	4.423	.0079	.0076	.0076	.0076	.0087	.0059	.0083	.0071	.0064	.0063	.0091
.828	4.687	.0064	.0058	.0065	.0065	.0064	.0001	.0060	.0056	.0052	.0040	.0075
.875	4.952	.0024	.0020	.0012	.0012	.0016	-.0061	.0013	.0002	.0006	-.0002	.0024
.922	5.216	-.0036	-.0050	-.0041	-.0041	-.0051	-.0249	-.0058	-.0061	-.0080	-.0068	-.0046

Table VI (cont.)

X/H .2500

Z/S=		1.0000	1.1000	1.2000	1.3000	1.4000	1.5000	1.6000	1.7000	1.8000	1.9000	2.0000
Y/H	Y/D											
.034	.191	.0048	-.0005	-.0081	-.0245	-.0471	-.0799	-.0652	-.0393	-.0111	.0010	.0048
.080	.455	.0054	.0009	-.0114	-.0461	-.0683	-.0983	-.0899	-.0728	-.0222	-.0058	.0010
.127	.720	-.0011	-.0079	-.0231	-.0811	-.1146	-.1359	-.1312	-.1076	-.0561	-.0206	-.0088
.174	.984	-.0129	-.0141	-.0453	-.1223	-.1548	-.1672	-.1591	-.1417	-.0887	-.0248	-.0220
.221	1.249	-.0169	-.0130	-.0512	-.1376	-.1729	-.1756	-.1725	-.1568	-.1056	-.0182	-.0191
.267	1.513	-.0133	.0000	-.0321	-.1497	-.1779	-.1712	-.1705	-.1616	-.0914	-.0055	-.0098
.314	1.778	-.0059	.0128	.0015	-.1468	-.1734	-.1657	-.1646	-.1538	-.0621	.0166	-.0007
.361	2.042	.0014	.0220	.0460	-.0909	-.1550	-.1572	-.1570	-.1277	-.0220	.0304	.0051
.408	2.307	.0063	.0223	.0717	-.0102	-.0872	-.1212	-.1081	-.0617	.0316	.0371	.0062
.454	2.571	.0072	.0198	.0800	.0659	.0122	-.0202	.0009	.0245	.0649	.0321	.0058
.501	2.836	.0078	.0153	.0569	.0810	.0801	.0796	.0747	.0723	.0555	.0222	.0062
.548	3.100	.0080	.0112	.0351	.0591	.0774	.0927	.0753	.0579	.0375	.0166	.0063
.595	3.365	.0077	.0105	.0203	.0340	.0494	.0603	.0478	.0341	.0222	.0121	.0059
.641	3.629	.0080	.0087	.0136	.0197	.0290	.0348	.0280	.0196	.0142	.0096	.0068
.688	3.894	.0088	.0081	.0097	.0132	.0177	.0207	.0167	.0124	.0101	.0087	.0069
.735	4.158	.0093	.0076	.0087	.0095	.0125	.0135	.0115	.0085	.0084	.0088	.0064
.782	4.423	.0091	.0073	.0078	.0080	.0091	.0097	.0081	.0065	.0068	.0080	.0062
.828	4.687	.0075	.0044	.0052	.0063	.0067	.0062	.0065	.0038	.0056	.0063	.0050
.875	4.952	.0024	-.0003	.0007	.0006	.0025	.0017	-.0001	-.0009	-.0004	.0009	-.0004
.922	5.216	-.0046	-.0068	-.0067	-.0067	-.0048	-.0060	-.0071	-.0072	-.0078	-.0055	-.0070

*** TABLE OF CP VALUES

TEST NUMBER 96. RUN NUMBER 135 ORIFICE PLATE NO. 1/03/06

X/H 1.0000

Z/S=		.0000	.1000	.2000	.3000	.4000	.5000	.6000	.7000	.8000	.9000	1.0000
Y/H	Y/D											
.034	.191	-.0722	-.0459	-.0371	-.0371	-.0416	-.0409	-.0324	-.0307	-.0283	-.0342	-.0167
.080	.455	-.0647	-.0503	-.0454	-.0454	-.0425	-.0410	-.0363	-.0324	-.0296	-.0398	-.0294
.127	.720	-.0543	-.0550	-.0542	-.0542	-.0457	-.0464	-.0423	-.0393	-.0375	-.0488	-.0403
.174	.984	-.0411	-.0555	-.0590	-.0590	-.0482	-.0530	-.0537	-.0488	-.0450	-.0527	-.0478
.221	1.249	-.0286	-.0572	-.0603	-.0603	-.0535	-.0575	-.0603	-.0547	-.0495	-.0527	-.0493
.267	1.513	-.0123	-.0597	-.0604	-.0604	-.0590	-.0575	-.0591	-.0568	-.0474	-.0502	-.0476
.314	1.778	.0050	-.0601	-.0543	-.0543	-.0585	-.0623	-.0578	-.0571	-.0487	-.0453	-.0406
.361	2.042	.0183	-.0529	-.0500	-.0500	-.0569	-.0619	-.0567	-.0532	-.0466	-.0396	-.0331
.408	2.307	.0210	-.0391	-.0462	-.0462	-.0520	-.0566	-.0559	-.0468	-.0368	-.0265	-.0198
.454	2.571	.0241	-.0243	-.0351	-.0351	-.0441	-.0483	-.0524	-.0347	-.0244	-.0182	-.0113
.501	2.836	.0225	-.0097	-.0169	-.0169	-.0322	-.0382	-.0434	-.0211	-.0135	-.0014	-.0009
.548	3.100	.0165	.0046	-.0009	-.0009	-.0179	-.0204	-.0254	-.0091	-.0005	.0113	.0125
.595	3.365	.0112	.0147	.0144	.0144	.0041	.0011	-.0063	.0100	.0157	.0205	.0184
.641	3.629	.0077	.0268	.0223	.0223	.0206	.0231	.0159	.0274	.0260	.0248	.0242
.688	3.894	.0060	.0290	.0271	.0271	.0390	.0424	.0361	.0407	.0323	.0282	.0274
.735	4.158	.0045	.0245	.0280	.0280	.0504	.0500	.0515	.0464	.0346	.0255	.0230
.782	4.423	.0008	.0215	.0264	.0264	.0491	.0505	.0502	.0388	.0331	.0214	.0169
.828	4.687	-.0057	.0153	.0174	.0174	.0391	.0426	.0403	.0280	.0247	.0146	.0115
.875	4.952	-.0251	.0092	.0097	.0097	.0276	.0306	.0279	.0167	.0123	.0053	.0040
.922	5.216	-.0348	-.0000	.0006	.0006	.0127	.0171	.0122	.0052	.0011	-.0025	-.0024

Table VI (cont.)

X/H 1.0000

Z/S=		1.0000	1.1000	1.2000	1.3000	1.4000	1.5000	1.6000	1.7000	1.8000	1.9000	2.0000
Y/H	Y/D											
.034	.191	-.0167	-.0187	-.0203	-.0265	-.0345	-.0331	-.0380	-.0410	-.0386	-.0344	-.0419
.080	.455	-.0294	-.0285	-.0285	-.0319	-.0390	-.0367	-.0410	-.0464	-.0410	-.0422	-.0436
.127	.720	-.0403	-.0382	-.0380	-.0389	-.0444	-.0428	-.0476	-.0491	-.0481	-.0520	-.0510
.174	.984	-.0478	-.0429	-.0443	-.0449	-.0483	-.0495	-.0540	-.0548	-.0554	-.0572	-.0526
.221	1.249	-.0493	-.0464	-.0491	-.0469	-.0518	-.0560	-.0566	-.0581	-.0601	-.0593	-.0567
.267	1.513	-.0476	-.0452	-.0522	-.0471	-.0552	-.0577	-.0584	-.0578	-.0587	-.0594	-.0582
.314	1.778	-.0406	-.0380	-.0467	-.0495	-.0541	-.0598	-.0596	-.0583	-.0557	-.0538	-.0547
.361	2.042	-.0331	-.0355	-.0435	-.0486	-.0538	-.0583	-.0594	-.0589	-.0528	-.0471	-.0451
.408	2.307	-.0198	-.0259	-.0360	-.0454	-.0507	-.0537	-.0564	-.0530	-.0446	-.0381	-.0353
.454	2.571	-.0113	-.0132	-.0247	-.0415	-.0452	-.0518	-.0501	-.0461	-.0351	-.0211	-.0215
.501	2.836	-.0009	-.0022	-.0136	-.0317	-.0387	-.0412	-.0378	-.0339	-.0174	-.0068	-.0075
.548	3.100	.0125	.0094	-.0020	-.0171	-.0200	-.0275	-.0249	-.0161	-.0015	.0066	.0050
.595	3.365	.0184	.0206	.0121	.0069	.0031	-.0030	-.0034	.0029	.0119	.0175	.0153
.641	3.629	.0242	.0272	.0244	.0293	.0244	.0187	.0247	.0201	.0226	.0242	.0193
.688	3.894	.0274	.0265	.0327	.0412	.0414	.0387	.0417	.0383	.0308	.0268	.0222
.735	4.158	.0230	.0249	.0346	.0446	.0499	.0535	.0501	.0418	.0358	.0263	.0188
.782	4.423	.0169	.0205	.0329	.0408	.0502	.0538	.0510	.0421	.0287	.0242	.0150
.828	4.687	.0115	.0149	.0261	.0349	.0426	.0456	.0487	.0356	.0213	.0177	.0091
.875	4.952	.0040	.0067	.0181	.0241	.0318	.0327	.0338	.0222	.0117	.0067	.0022
.922	5.216	-.0024	-.0018	.0068	.0119	.0170	.0166	.0155	.0095	.0025	-.0031	-.0059

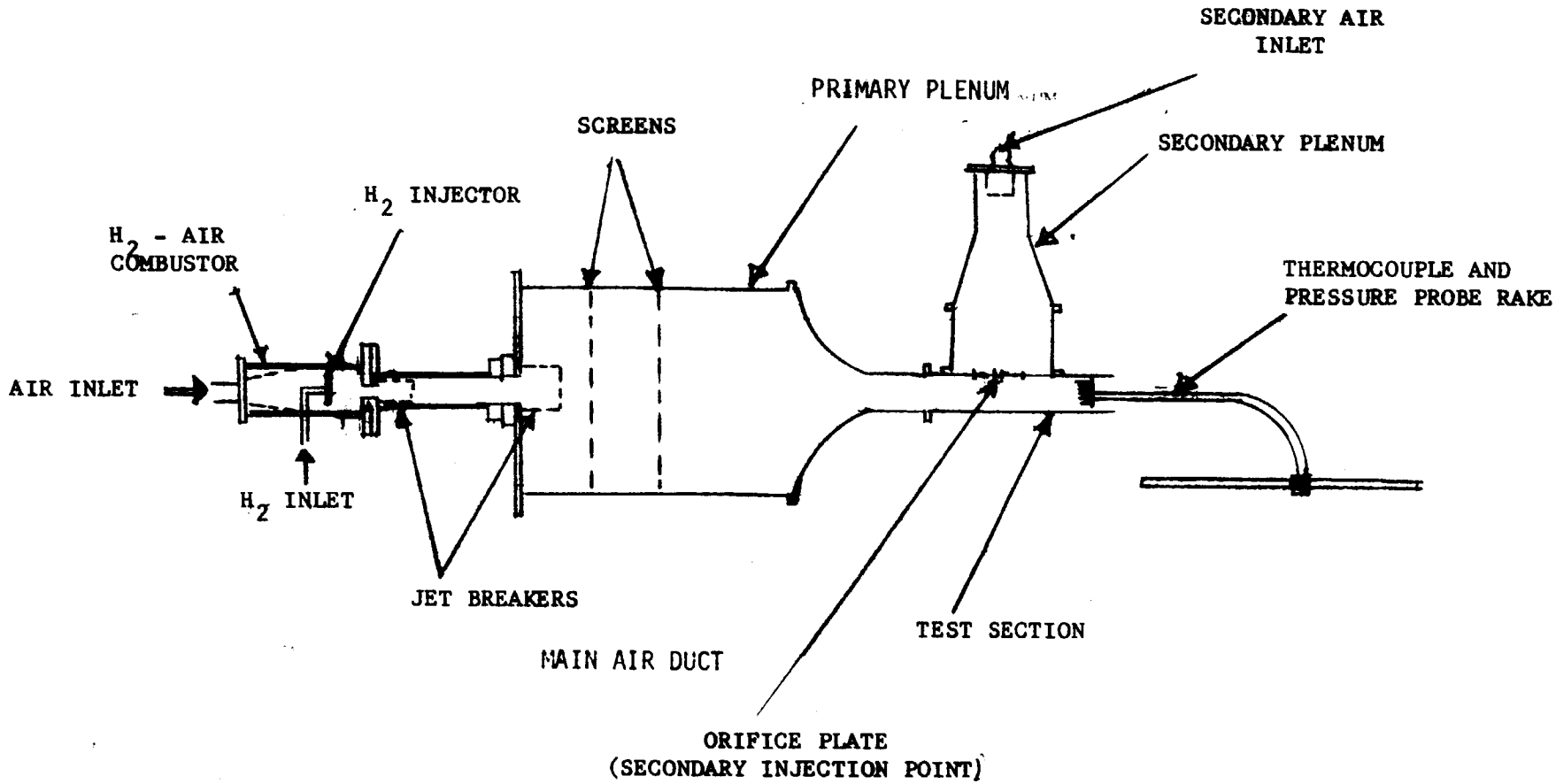

FIGURE 1. MULTIPLE JET TEST APPARATUS

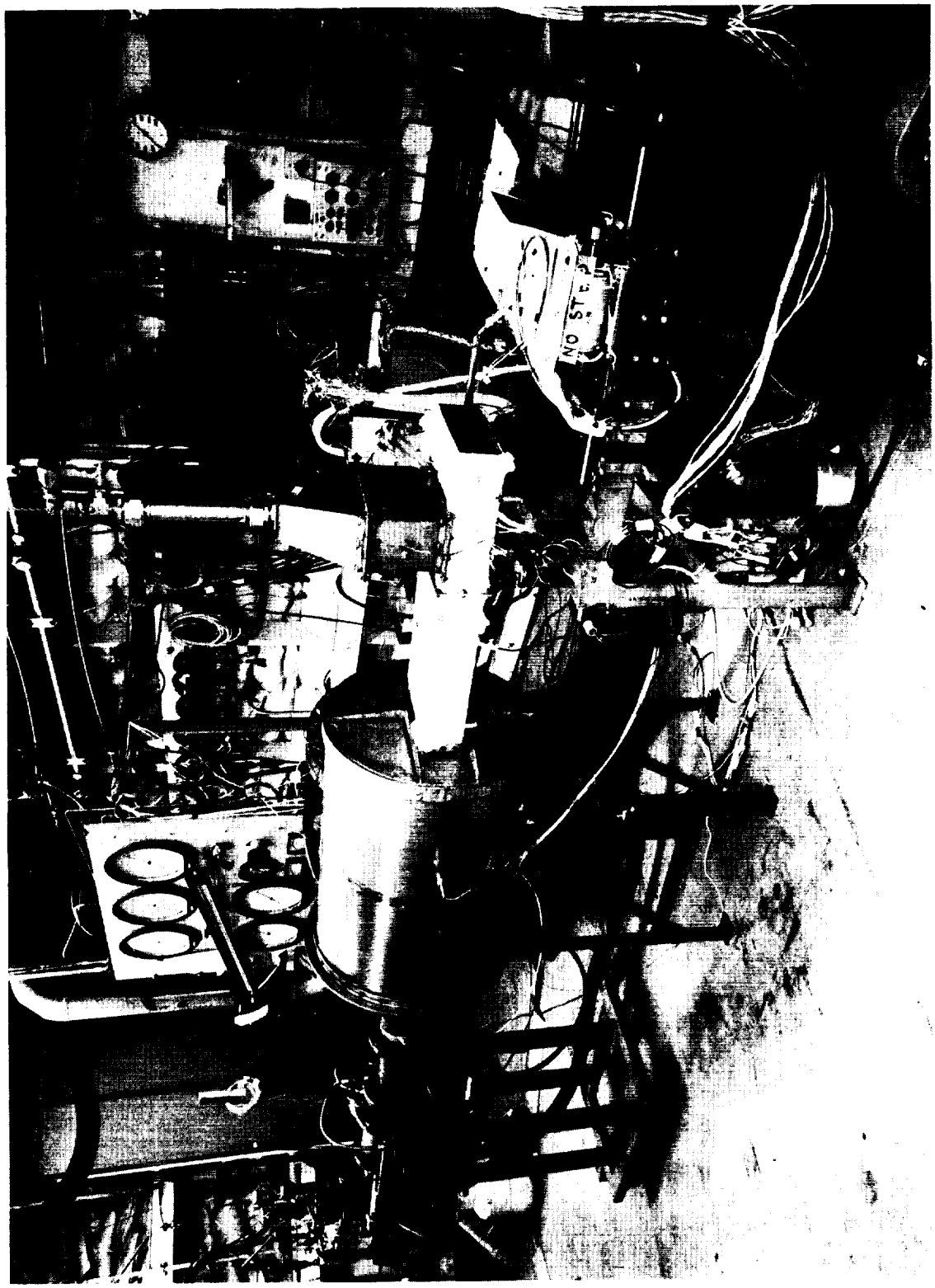

FIGURE 2. MULTIPLE JET STUDY TEST FACILITY

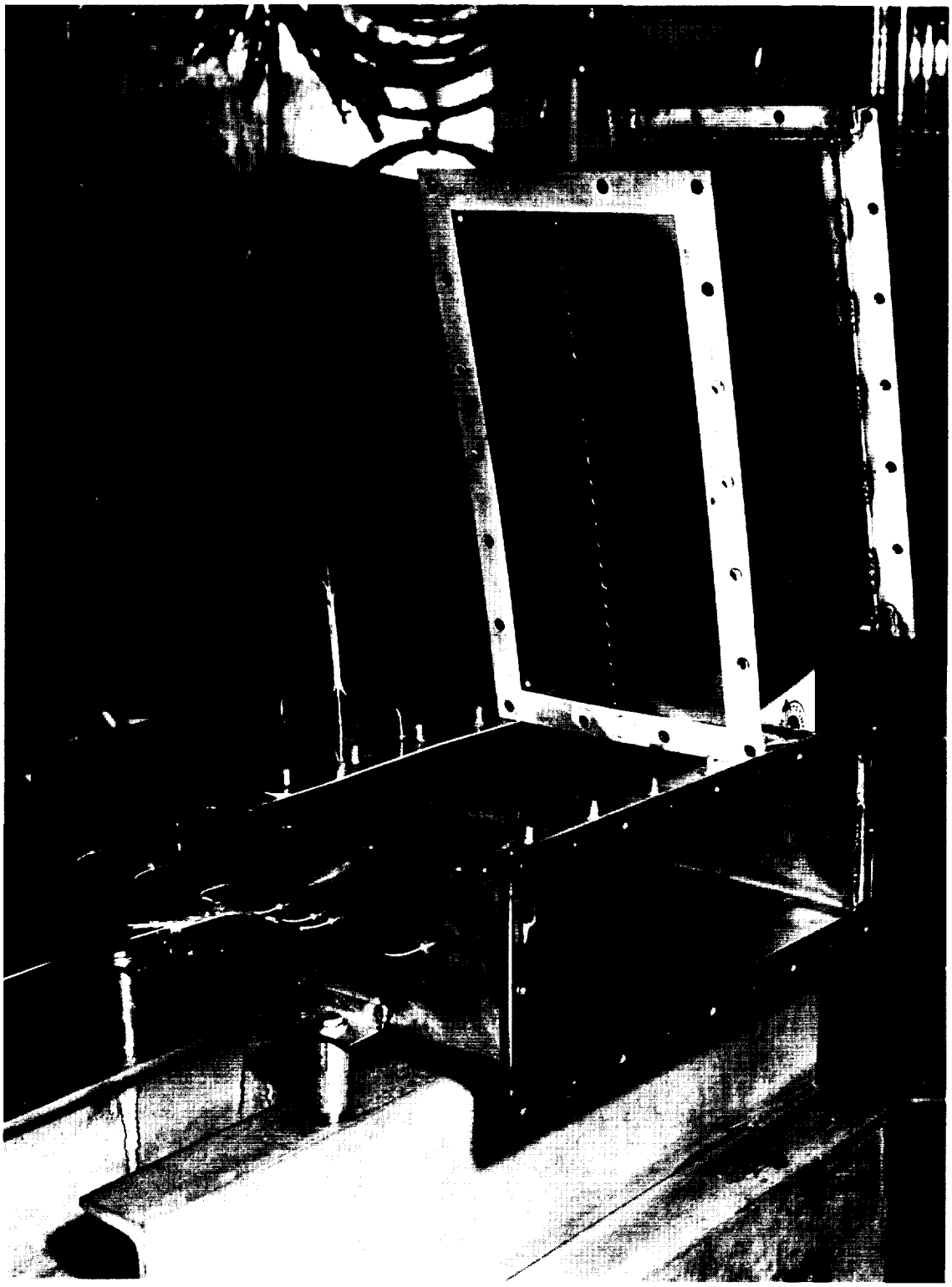

FIGURE 3. MULTIPLE JET STUDY TEST DUCT

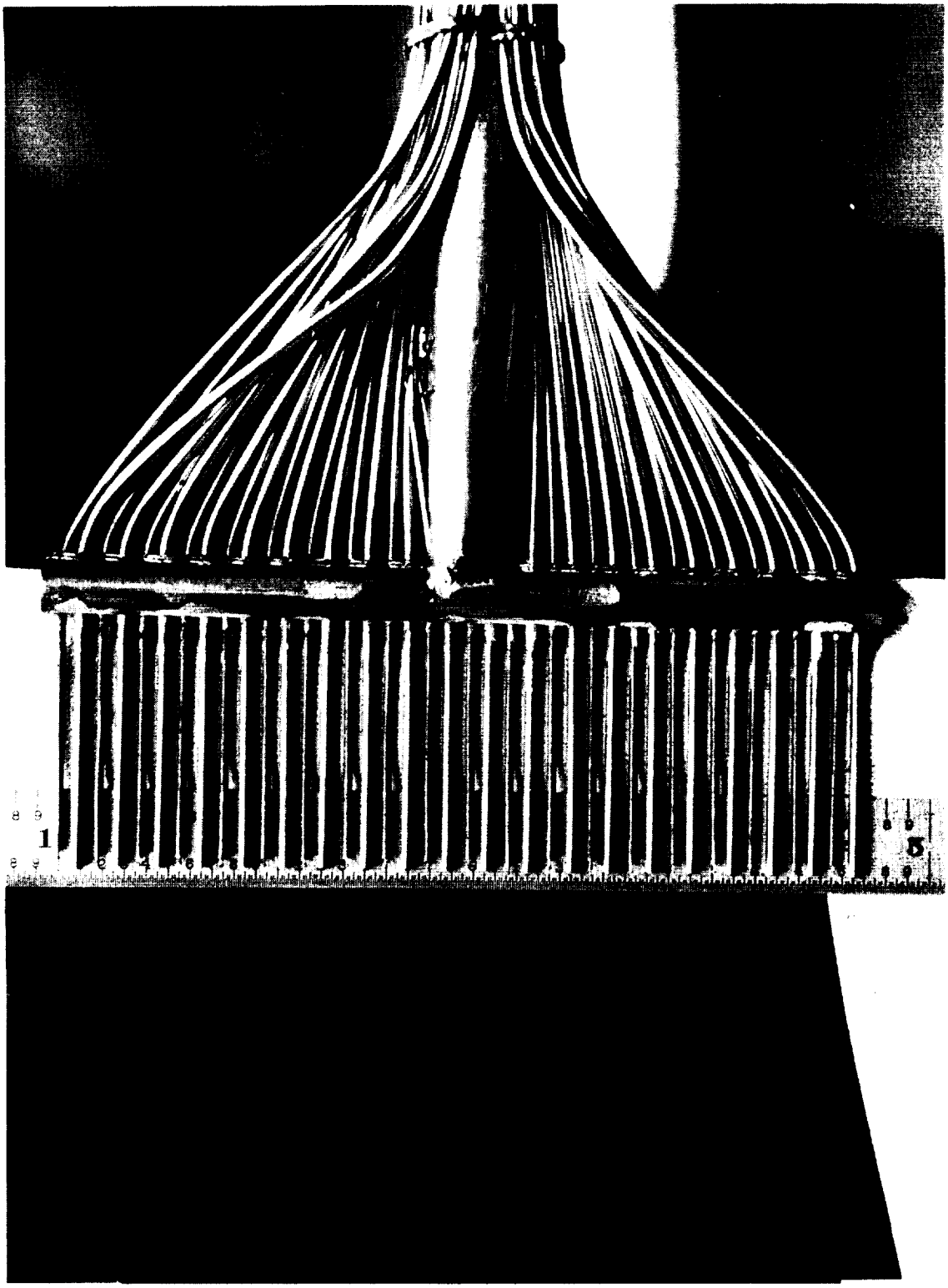

FIGURE 4. MULTIPLE JET STUDY INSTRUMENTATION RAKE

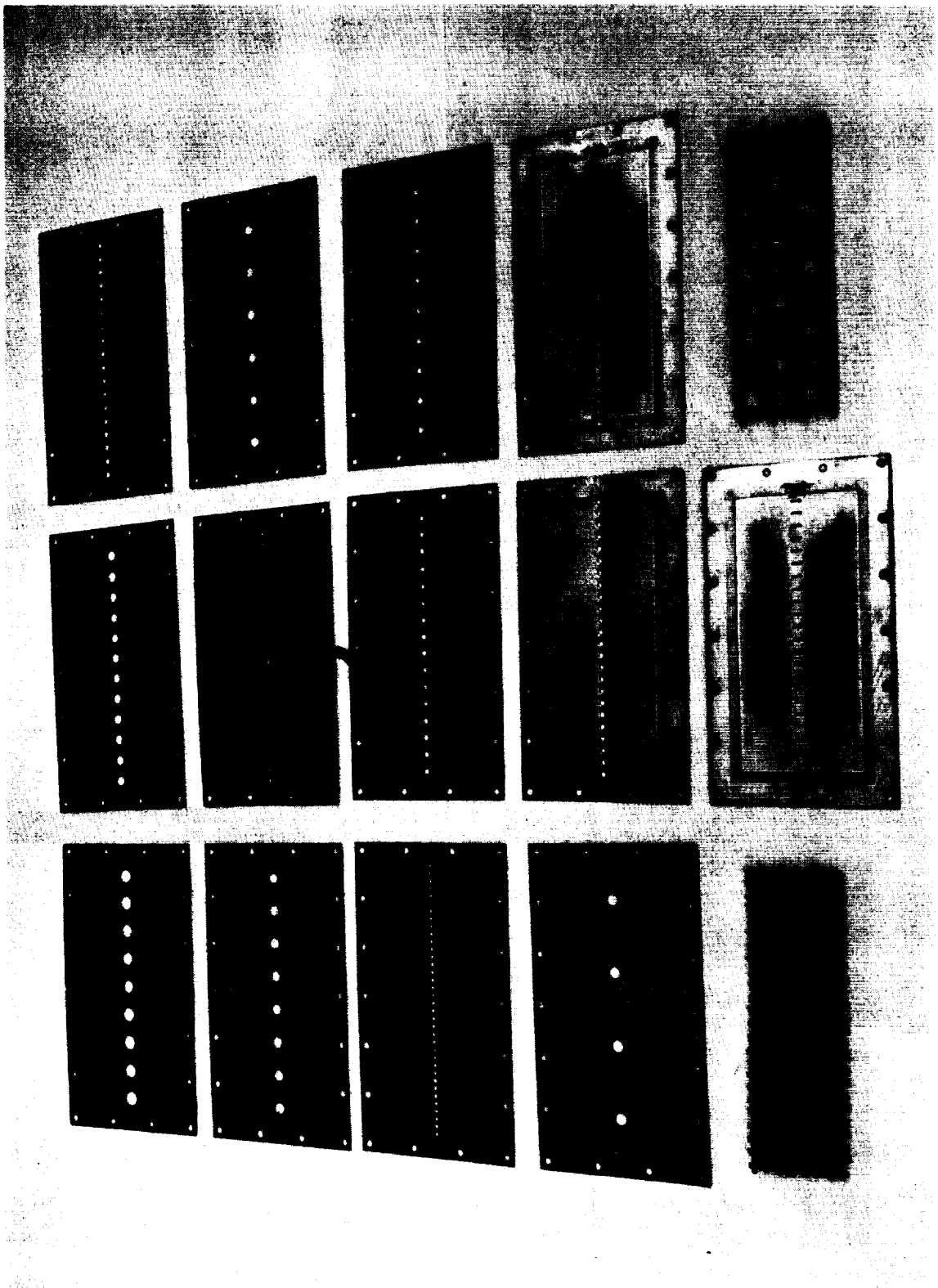

Figure 5 MULTIPLE JET STUDY ORIFICE PLATES AND TURBULENCE GRID

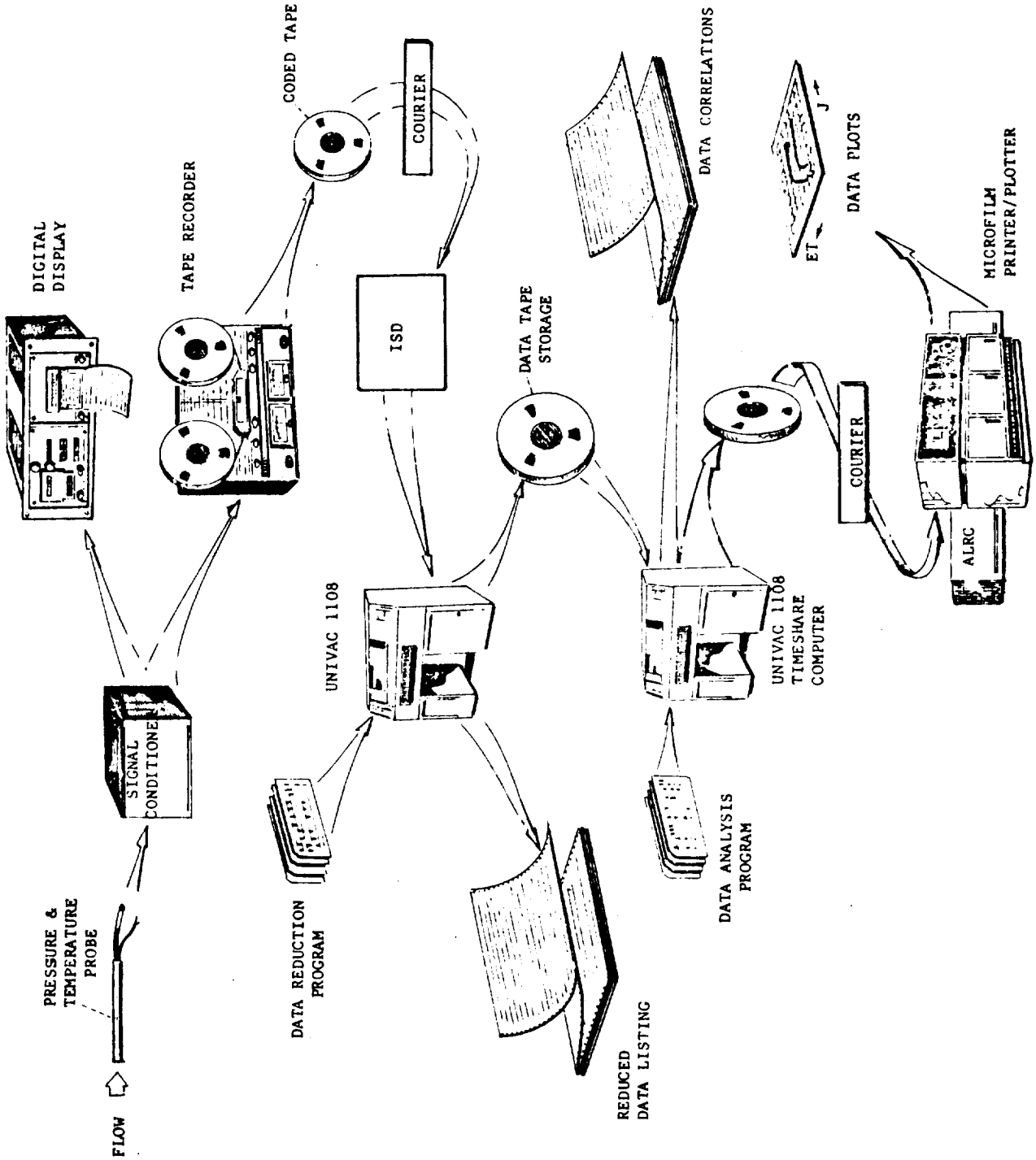

FIGURE 6. COMPUTERIZED DATA ACQUISITION, REDUCTION, AND ANALYSIS SYSTEM

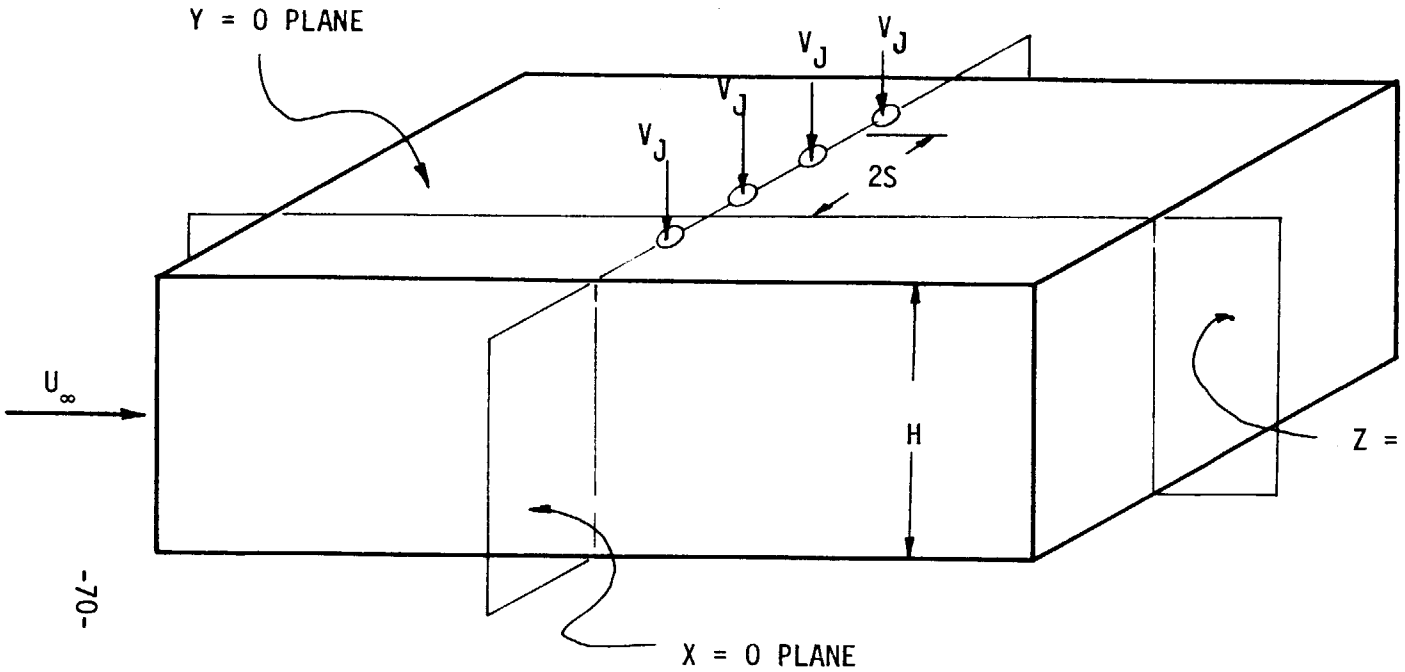

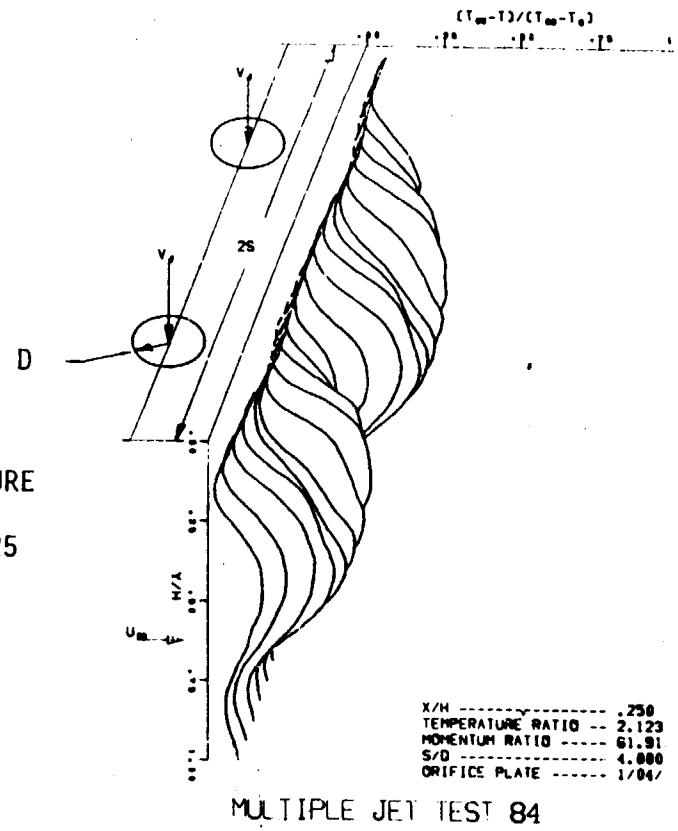

SAMPLE TEMPERATURE
PROFILE PLOT
@ PLANE X/H = .25

FIGURE 7. MULTIPLE JET STUDY COORDINATE SYSTEM

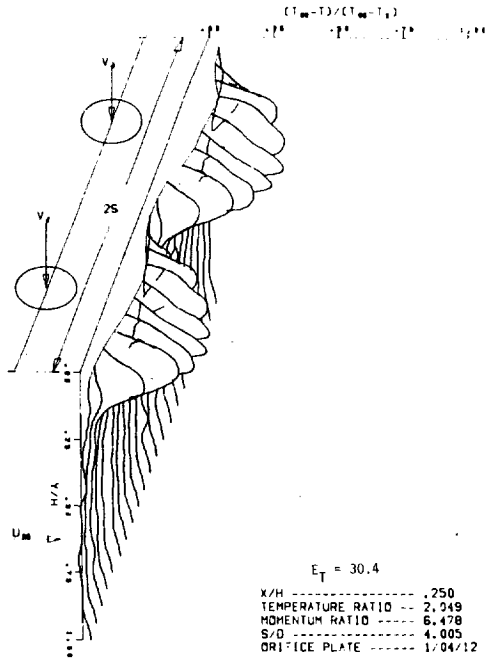

MULTIPLE JET TEST 51

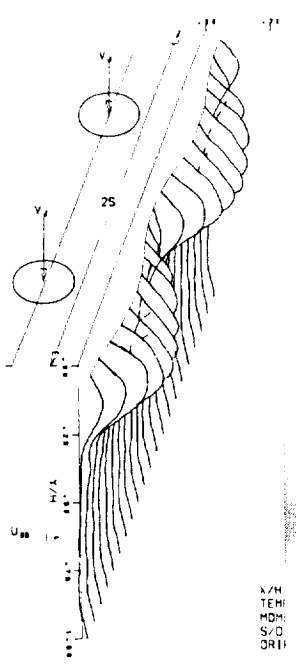

MULTIPLE JET T

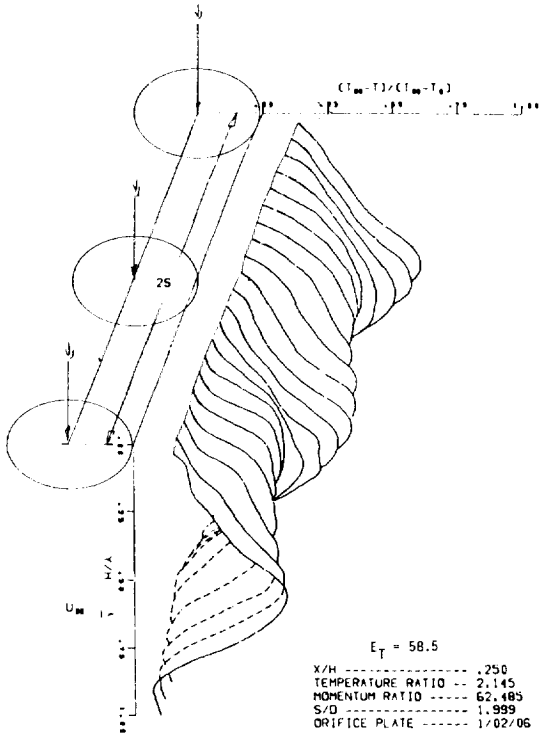

MULTIPLE JET TEST 85

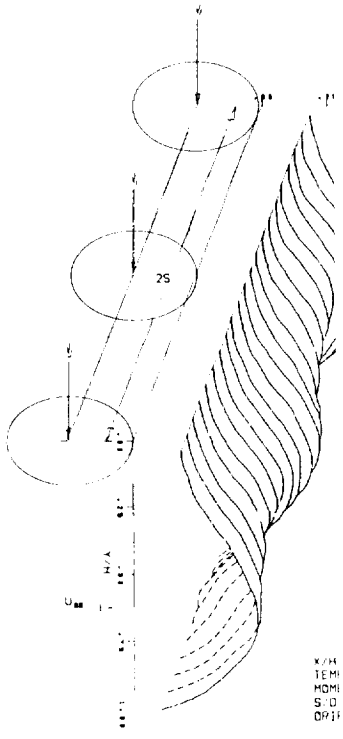

MULTIPLE JET T

FIGUR

FOLDOUT FRAME 1

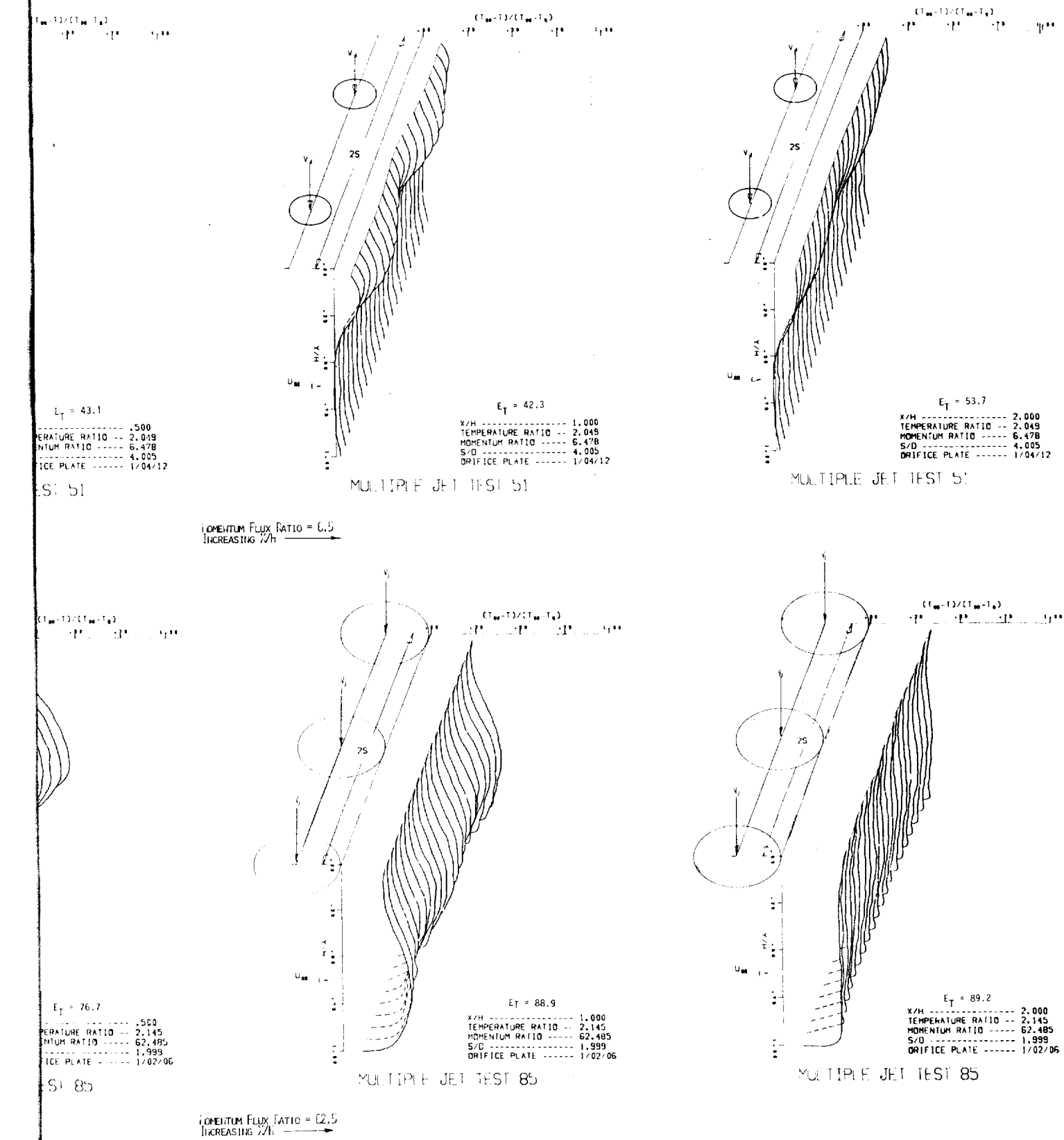

FIGURE 8

E 8. COMPARISON OF MIXING EFFICIENCIES AND TEMPERATURE PROFILES

FOLDOUT FRAME 2

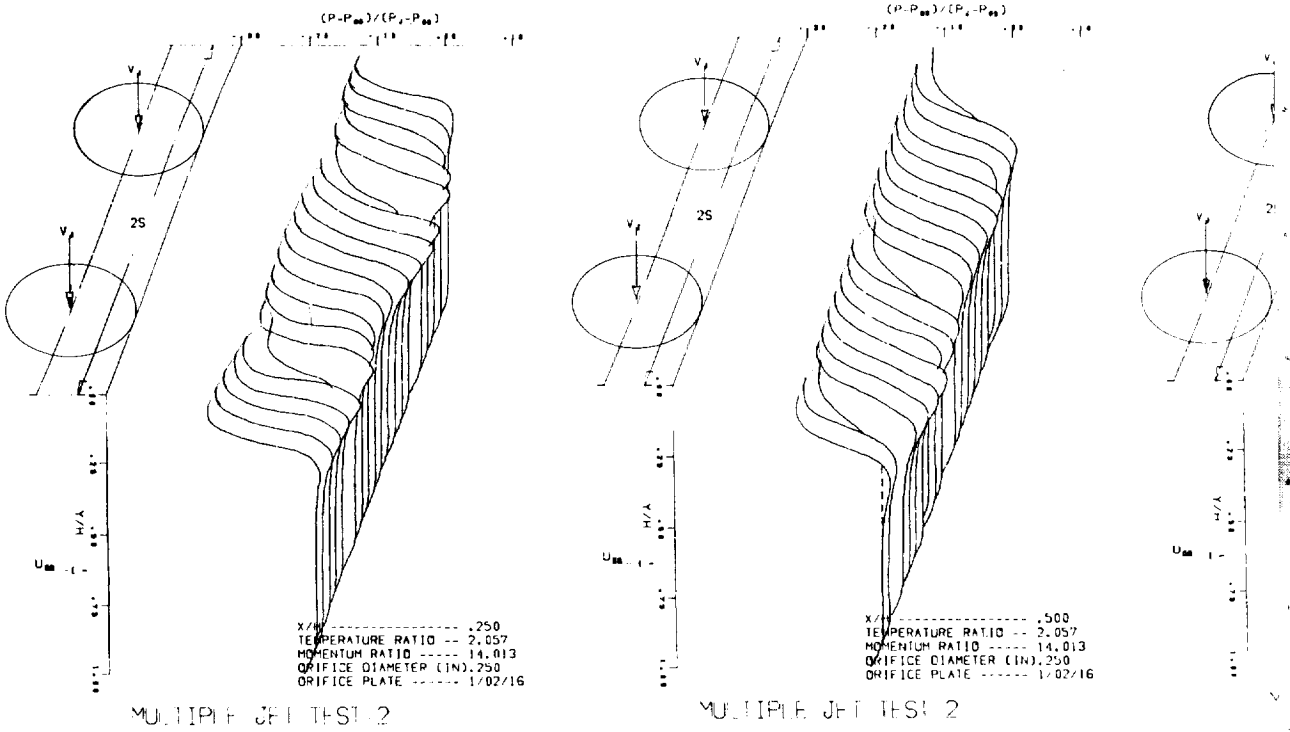

DIMENSIONLESS PRESSURE PROFILES FOR MOMENTUM FLUX RATIO = 14

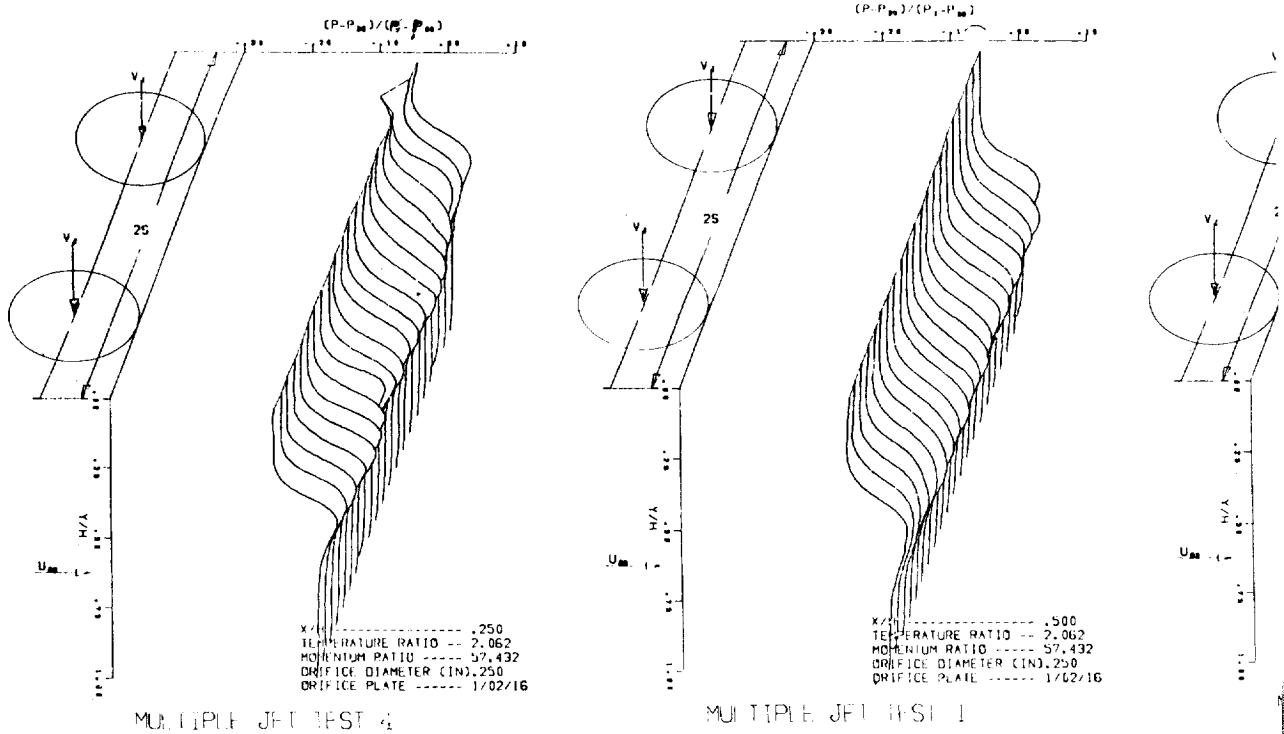

DIMENSIONLESS PRESSURE PROFILES FOR MOMENTUM FLUX RATIO = 57

FIGURE 9. COMPARISON OF PRESSURE DISTRI

FOLDOUT FRAME 1

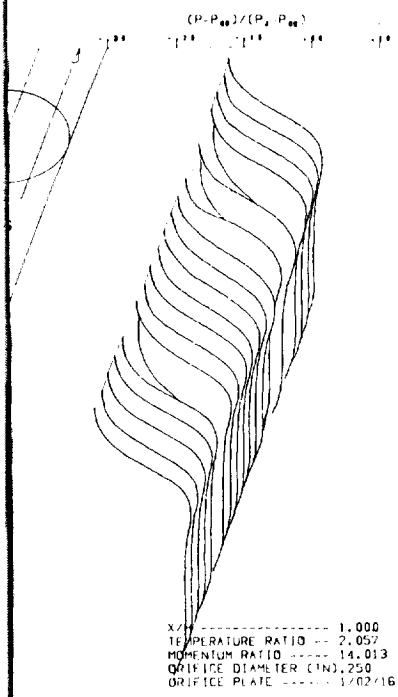

ULTIPLE JET TEST 2

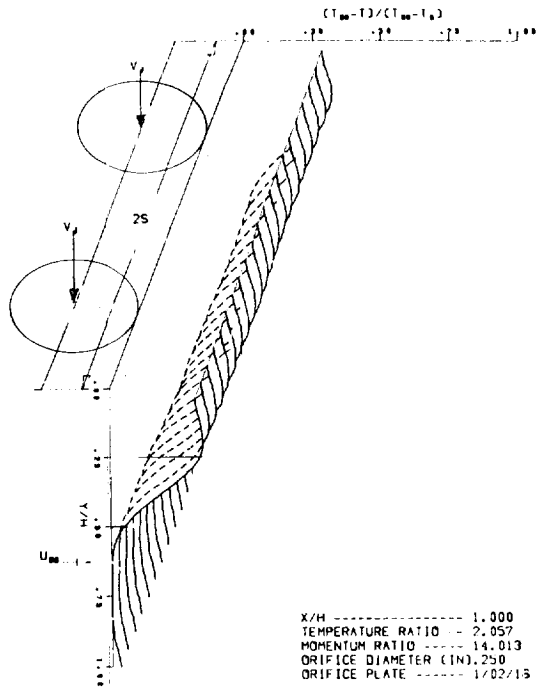

MULTIPLE JET TEST 2

DIMENSIONLESS TEMPERATURE PROFILES FOR MOMENTUM FLUX RATIO = 14

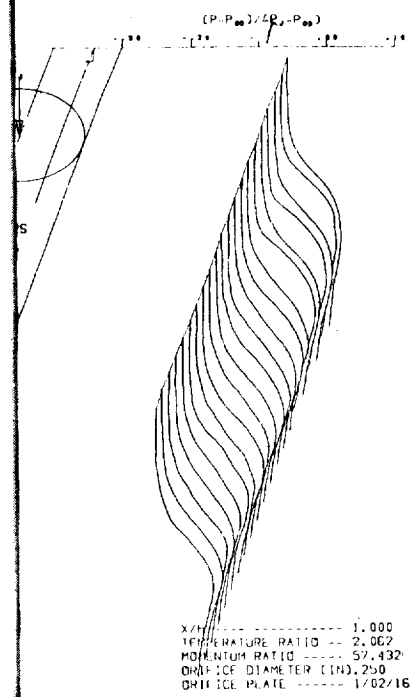

ULTIPLE JET TEST 4

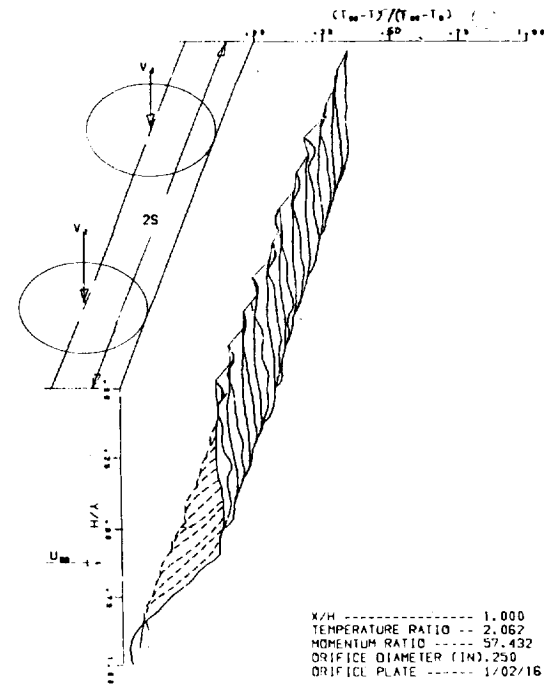

MULTIPLE JET TEST 4

DIMENSIONLESS TEMPERATURE PROFILES FOR MOMENTUM FLUX RATIO = 57

BUTION AT J = 14 AND J = 57

Figure 9

FOLDOUT FRAME 2

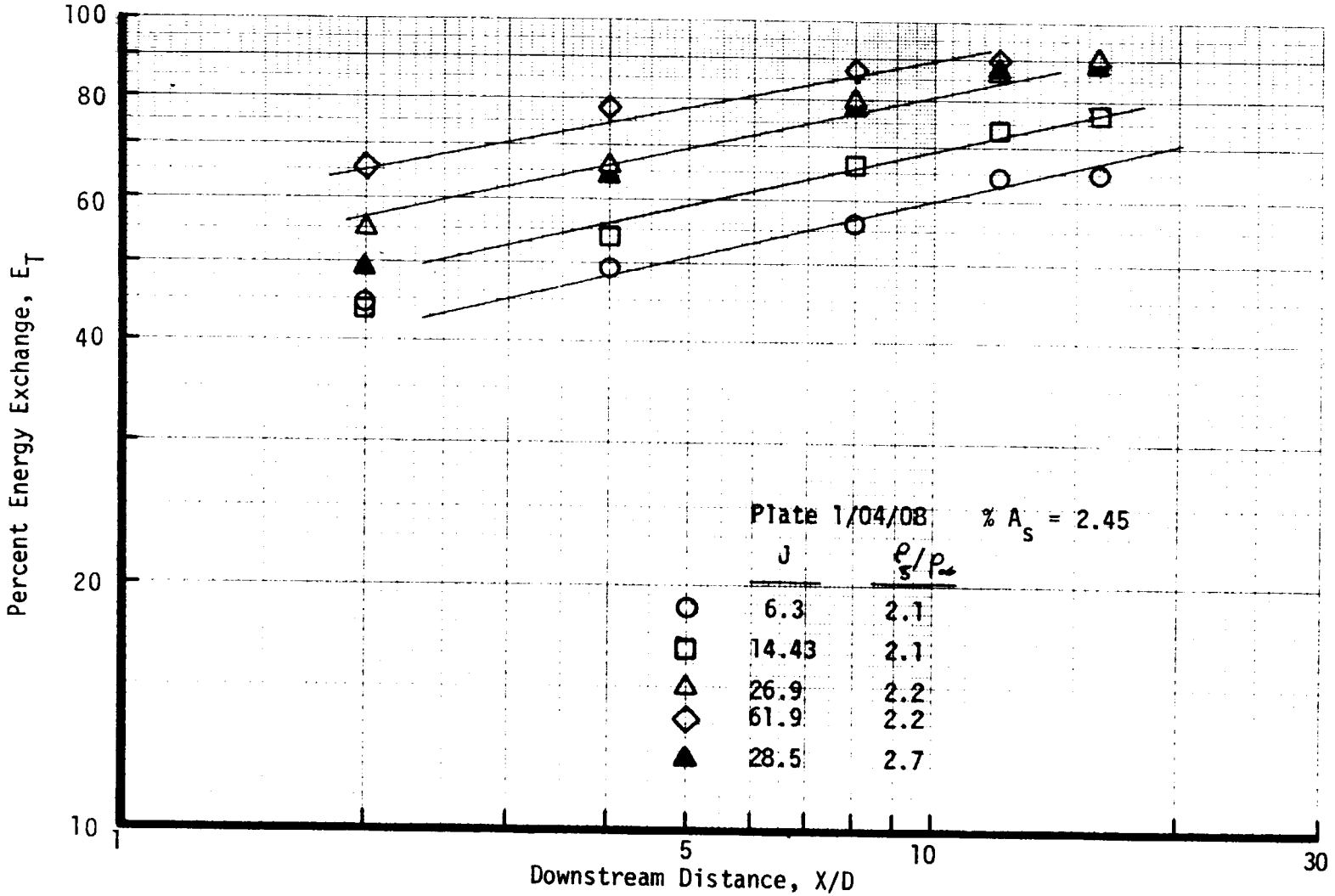

FIGURE 11. EFFECT OF X/D ON ENERGY EXCHANGE EFFICIENCY, ORIFICE PLATE 1/04/08

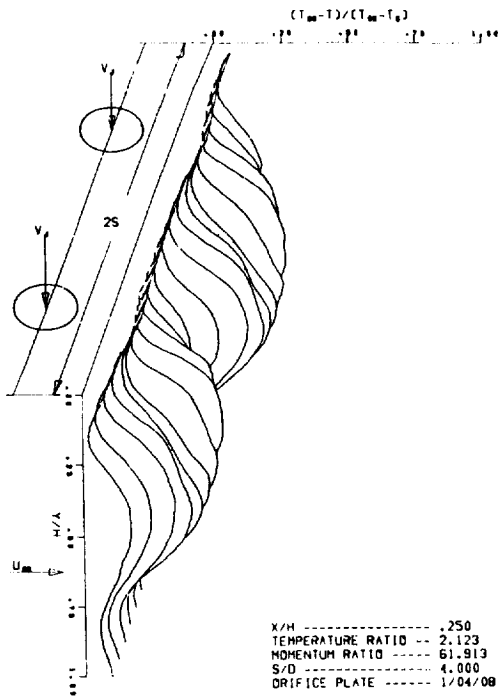

MULTIPLE JET TEST 84

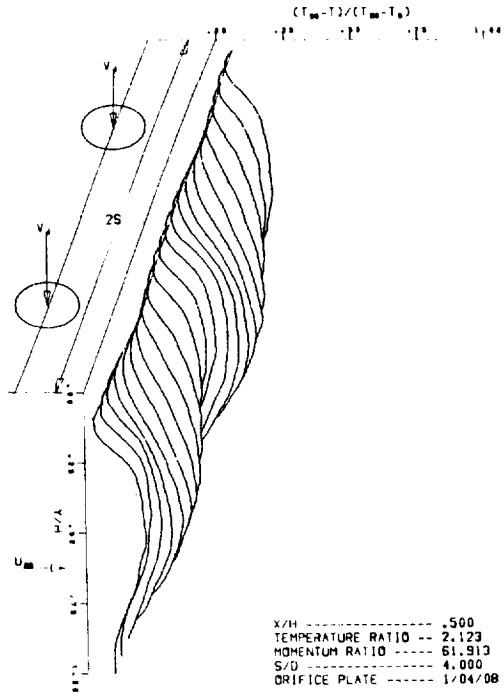

MULTIPLE JET TEST 84

DIMENSIONLESS TEMPERATURE PROFILES FC
INCREASI

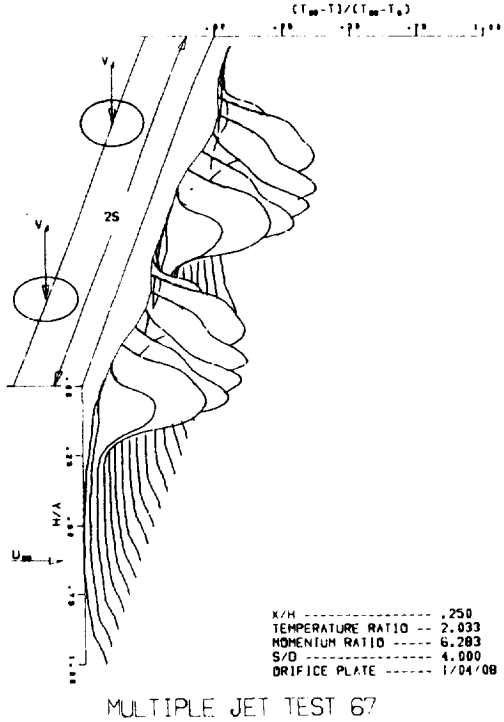

MULTIPLE JET TEST 67

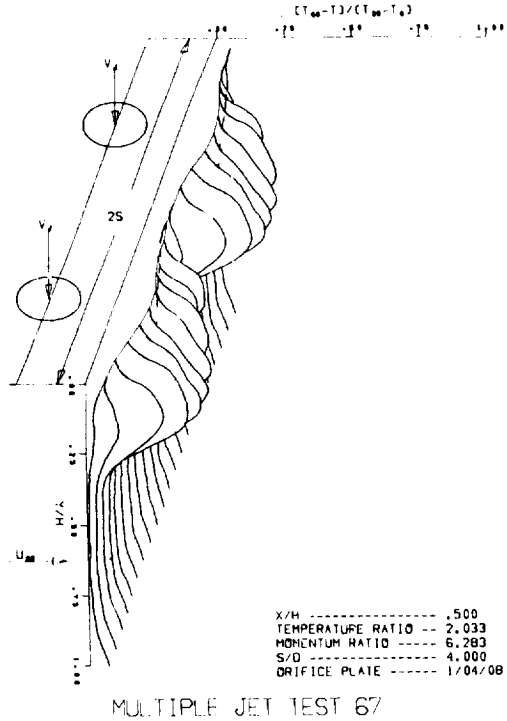

MULTIPLE JET TEST 67

DIMENSIONLESS TEMPERATURE PR

FIGURE 10. EFFECT OF MOMENTUM

FOLDOUT FRAME

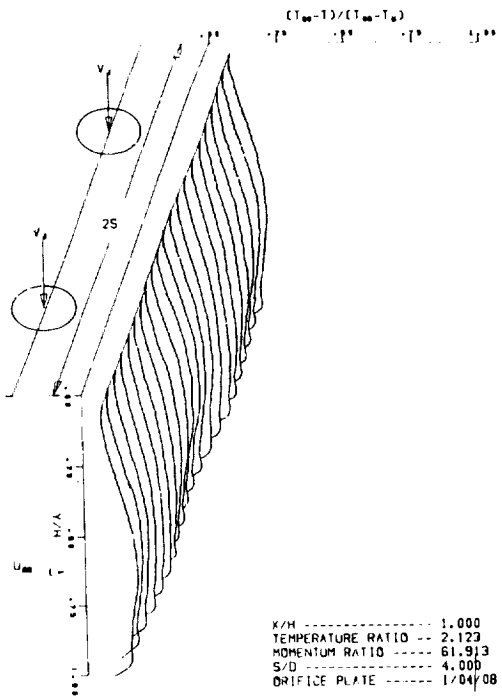

MULTIPLE JET TEST 84

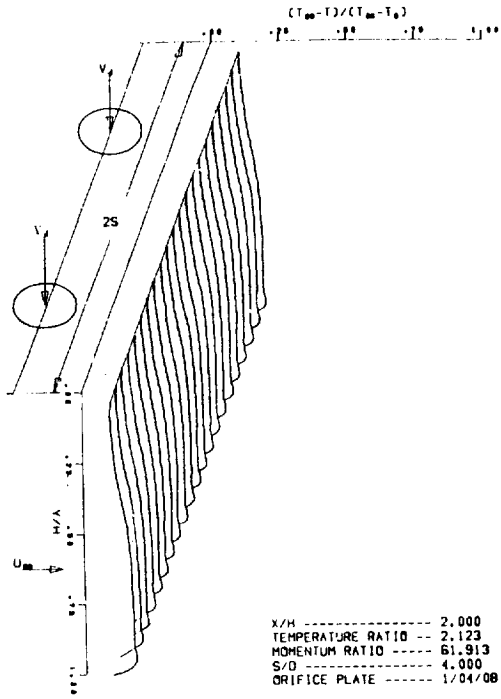

MULTIPLE JET TEST 84

R NOMINAL MOMENTUM FLUX RATIO = 62
NG X/H ⟶

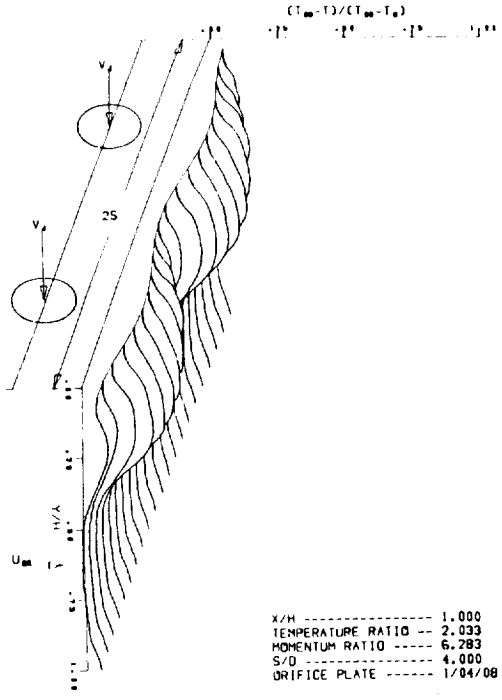

MULTIPLE JET TEST 67

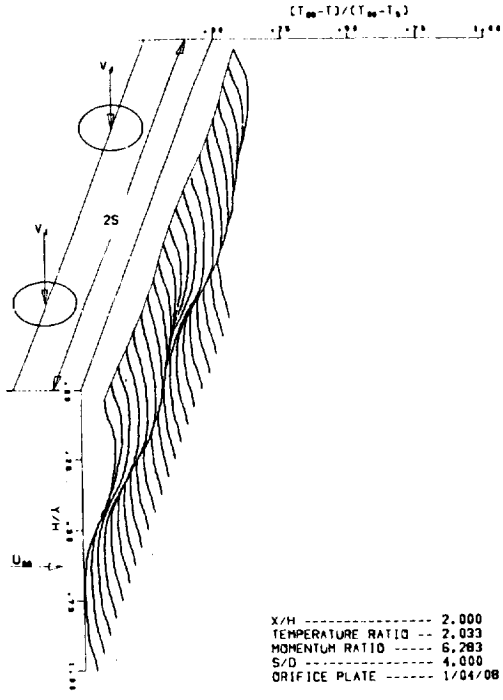

MULTIPLE JET TEST 67

OFILES FOR NOMINAL MOMENTUM FLUX RATIO = 6.2
INCREASING X/H ⟶

FLUX RATIO ON TEMPERATURE PROFILE

Figure 10

FOLDOUT FRAME 2

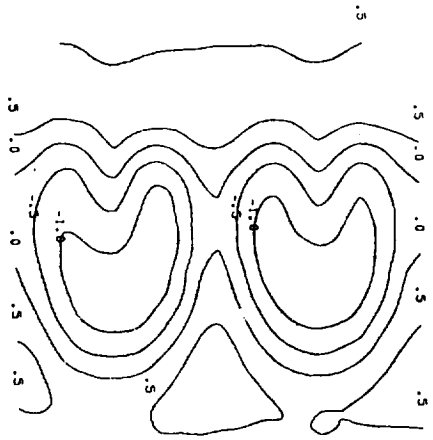

$1.-\theta/\theta_{AVG}$

INTERVAL = .5

X/H ---------- .250
TEMPERATURE RATIO -- 2.123
MOMENTUM RATIO ----- 61.913
S/D ---------- 4.000
ORIFICE PLATE ------ 1/04/08

MULTIPLE JET TEST 84

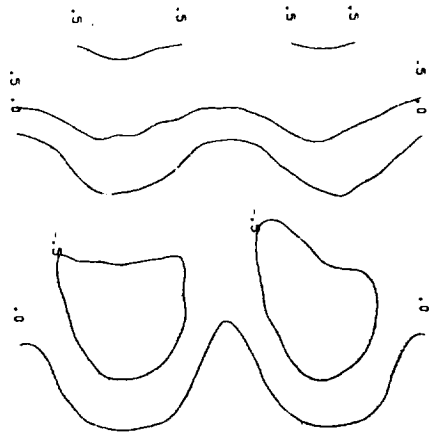

$1.-\theta/\theta_{AVG}$

INTERVAL = .5

X/H ---------- .500
TEMPERATURE RATIO -- 2.123
MOMENTUM RATIO ----- 61.913
S/D ---------- 4.000
ORIFICE PLATE ------ 1/04/08

MULTIPLE JET TEST 84

DIMENSIONLESS TEMPERATURE CONTOURS FOR INCREASIN

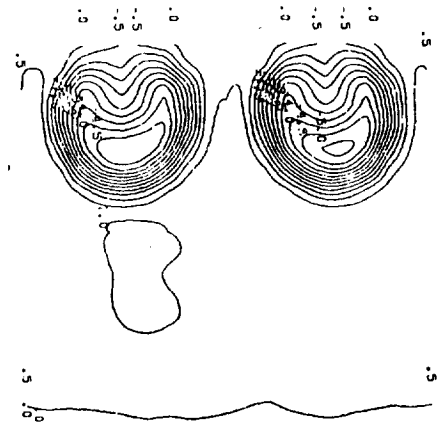

$1.-\theta/\theta_{AVG}$

INTERVAL = .5

X/H ---------- .250
TEMPERATURE RATIO -- 2.033
MOMENTUM RATIO ----- 6.283
S/D ---------- 4.000
ORIFICE PLATE ------ 1/04/08

MULTIPLE JET TEST 67

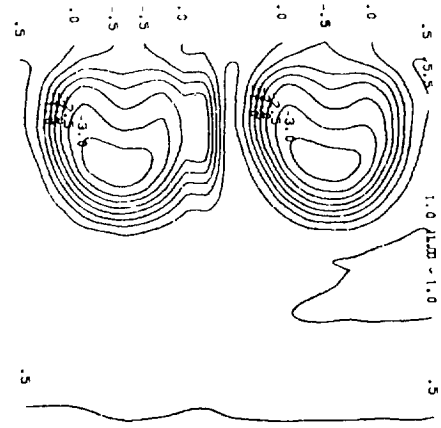

$1.-\theta/\theta_{AVG}$

INTERVAL = .5

X/H ---------- .500
TEMPERATURE RATIO -- 2.033
MOMENTUM RATIO ----- 6.283
S/D ---------- 4.000
ORIFICE PLATE ------ 1/04/08

MULTIPLE JET TEST 67

DIMENSIONLESS TEMPERATURE CONTOURS INCREA

FIGURE 12. EFFECT OF MOMENTUM FI

FOLDOUT FRAME 1

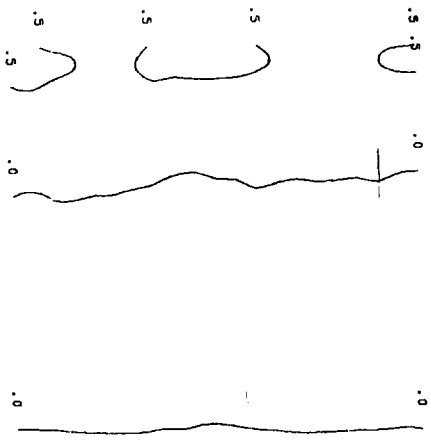

$1.-\theta/\theta_{AVG}$

INTERVAL = .5

X/H ---------- 1.000
TEMPERATURE RATIO -- 2.123
MOMENTUM RATIO ----- 61.913
S/D ---------- 4.000
ORIFICE PLATE ------ 1/04/08

MULTIPLE JET TEST 84

NOMINAL MOMENTUM FLUX RATIO = C2
G X/H

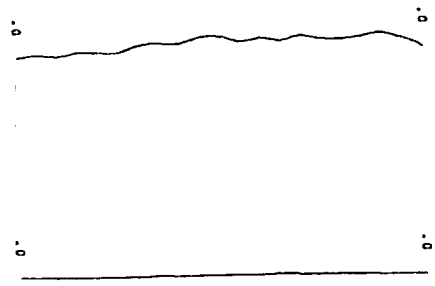

$1.-\theta/\theta_{AVG}$

INTERVAL = .5

X/H ---------- 2.000
TEMPERATURE RATIO -- 2.123
MOMENTUM RATIO ----- 61.913
S/D ---------- 4.000
ORIFICE PLATE ------ 1/04/08

MULTIPLE JET TEST 84

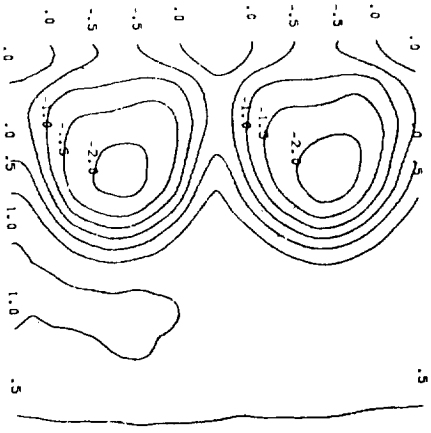

$1.-\theta/\theta_{AVG}$

INTERVAL = .5

X/H ---------- 1.000
TEMPERATURE RATIO -- 2.033
MOMENTUM RATIO ----- 6.283
S/D ---------- 4.000
ORIFICE PLATE ------ 1/04/08

MULTIPLE JET TEST 67

FOR NOMINAL MOMENTUM FLUX RATIO = C.2
SING X/H

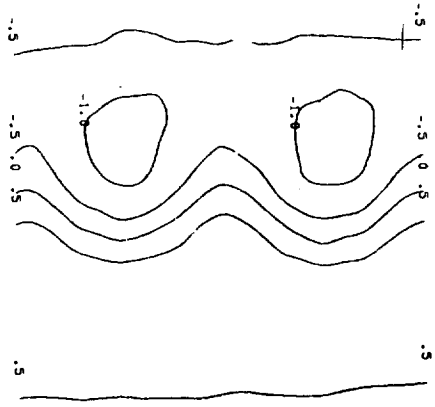

$1.-\theta/\theta_{AVG}$

INTERVAL = .5

X/H ---------- 2.000
TEMPERATURE RATIO -- 2.033
MOMENTUM RATIO ----- 6.283
S/D ---------- 4.000
ORIFICE PLATE ------ 1/04/08

MULTIPLE JET TEST 67

LUX RATIO ON TEMPERATURE CONTOURS

Figure 12

FOLDOUT FRAME 2

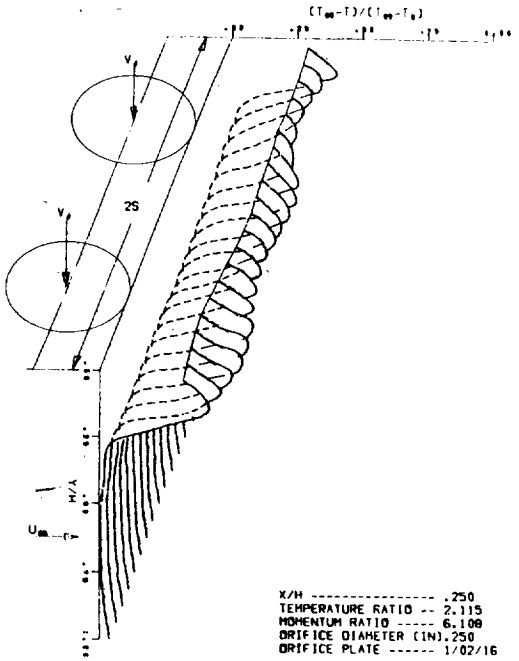

MULTIPLE JET TEST 27

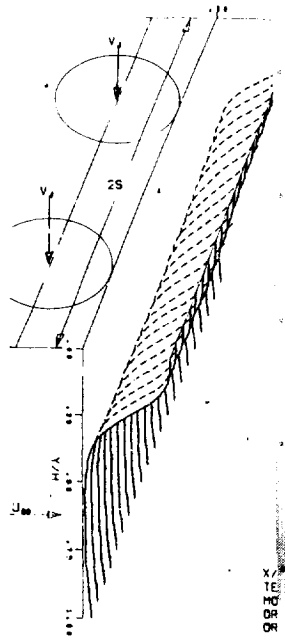

MULTIPLE JET

MAINSTREAM VELOCITY = 50 m/SEC (165 FT/SEC)
NOMINAL MOMENTUM FLUX RATIO = 6

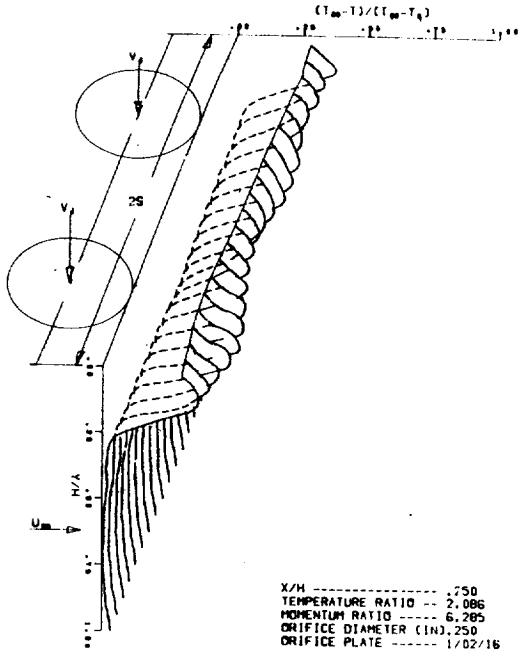

MULTIPLE JET TEST 17

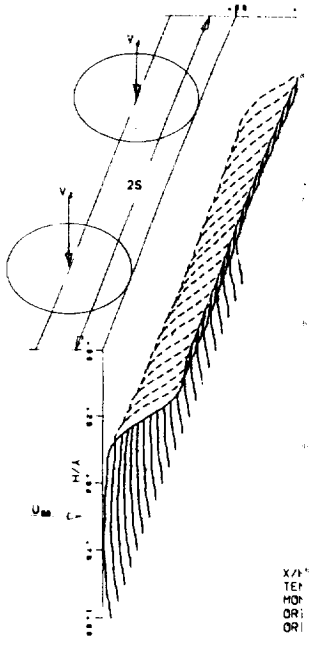

MULTIPLE JET T

MAINSTREAM VELOCITY = 25 m/SEC (70 FT/SEC)
NOMINAL MOMENTUM FLUX RATIO = 6

FIGURE

FOLDOUT FRAME 1

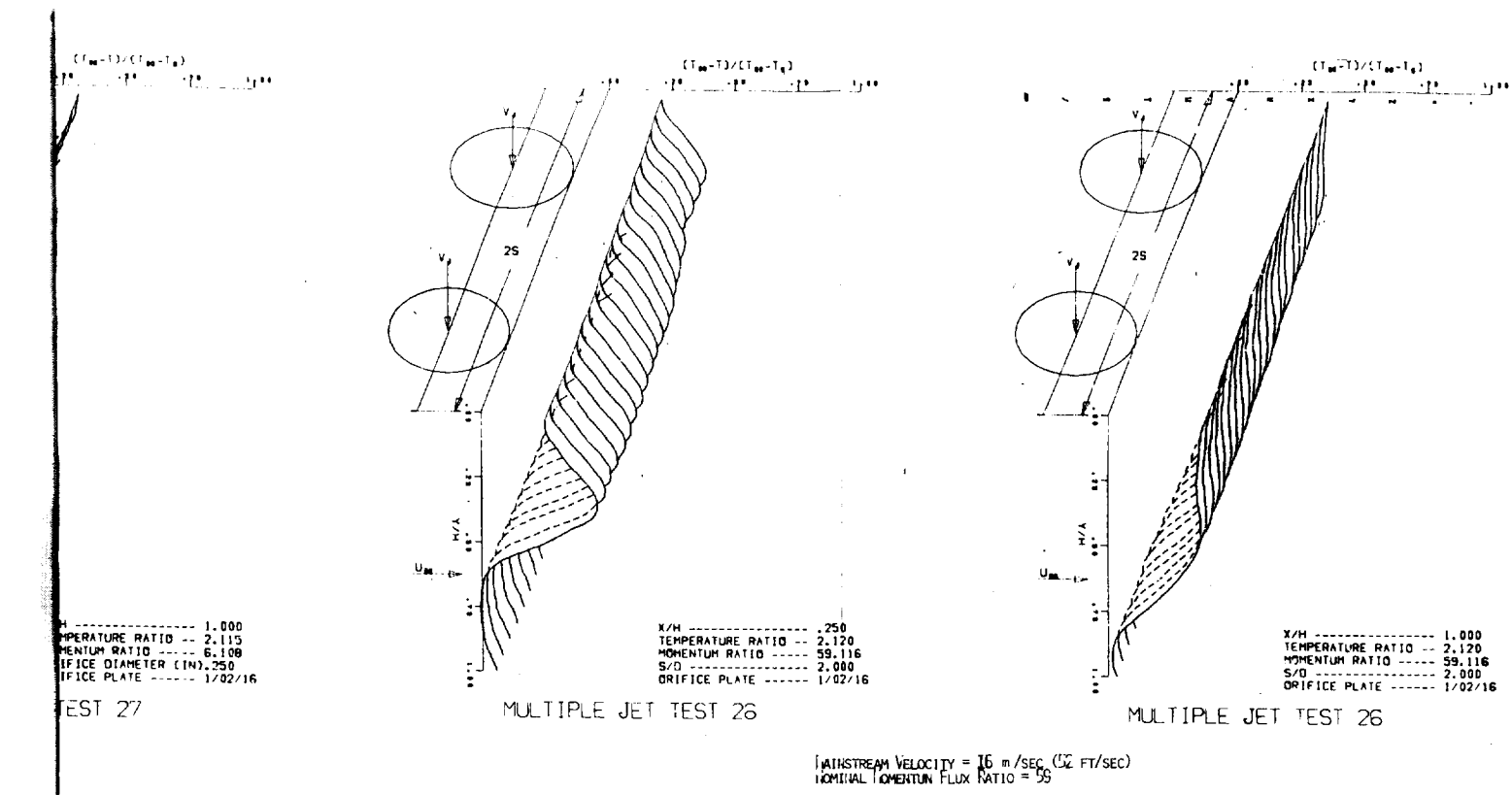

TEST 27 MULTIPLE JET TEST 28 MULTIPLE JET TEST 26

MAINSTREAM VELOCITY = 16 m/SEC (52 FT/SEC)
NOMINAL MOMENTUM FLUX RATIO = 55

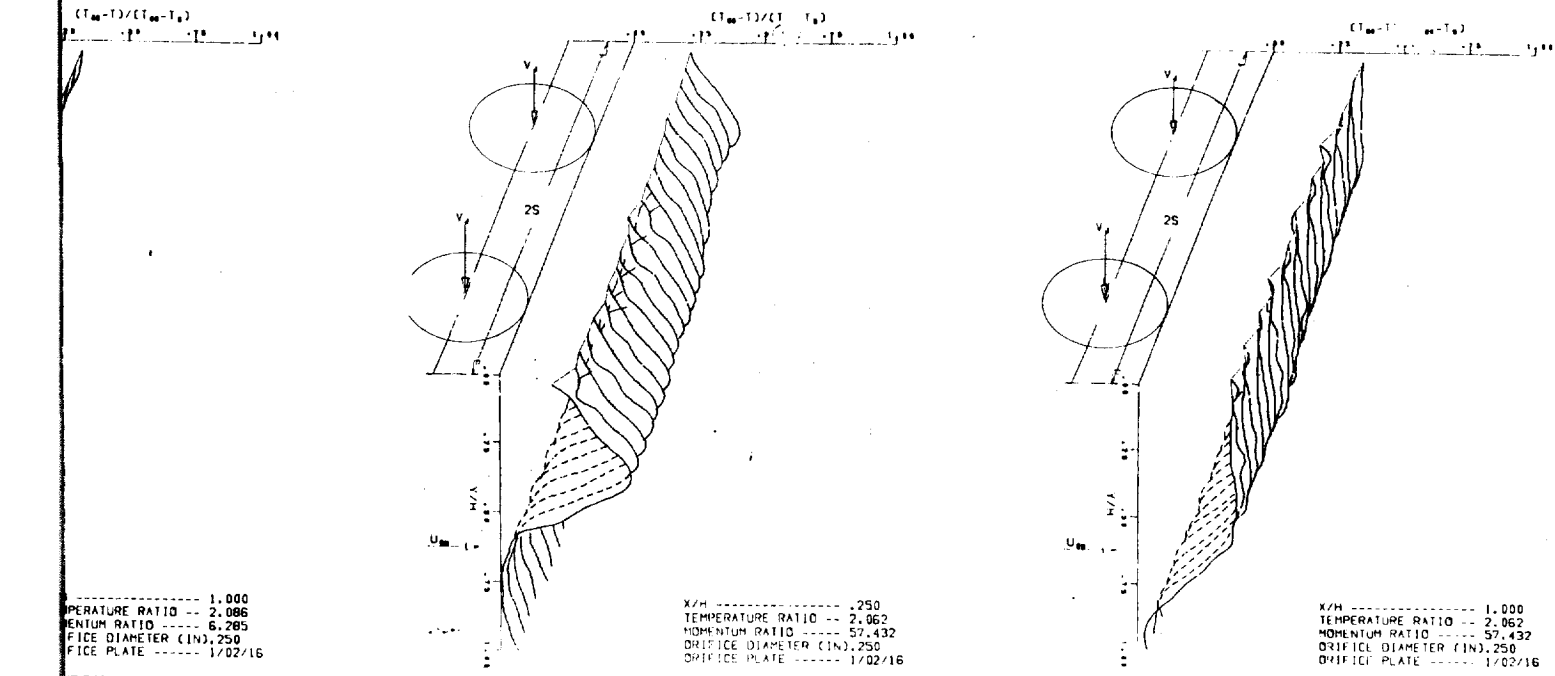

TEST 17 MULTIPLE JET TEST 4 MULTIPLE JET TEST 4

MAINSTREAM VELOCITY = 25 m/SEC (70 FT/SEC)
NOMINAL MOMENTUM FLUX RATIO = 57

E 13. EFFECT OF ABSOLUTE MOMENTUM LEVEL ON TEMPERATURE PROFILES

FIGURE 13

FOLDOUT FRAME 2

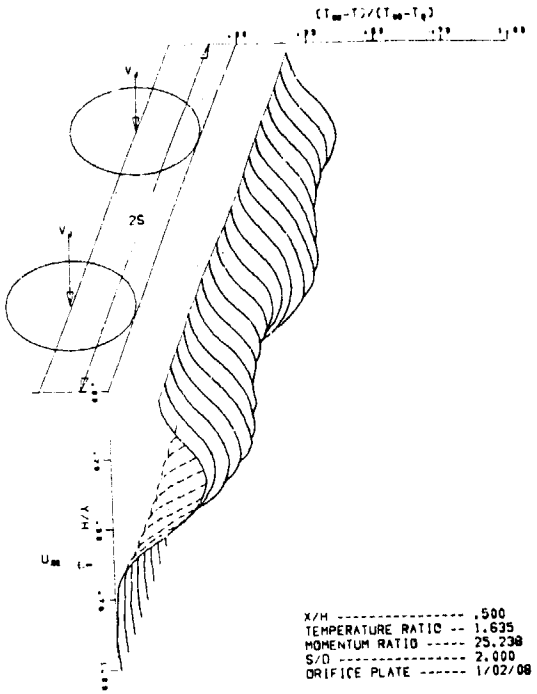

MULTIPLE JET TEST 60

X/h = 0.5

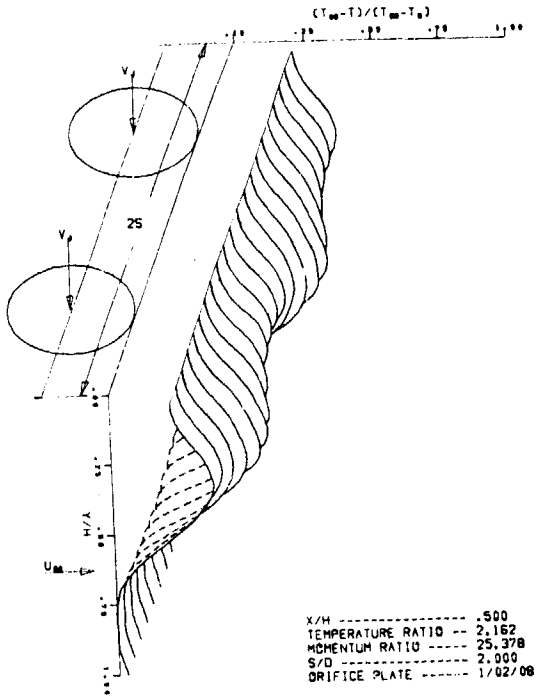

MULTIPLE JET TEST 59

X/h = 0.5

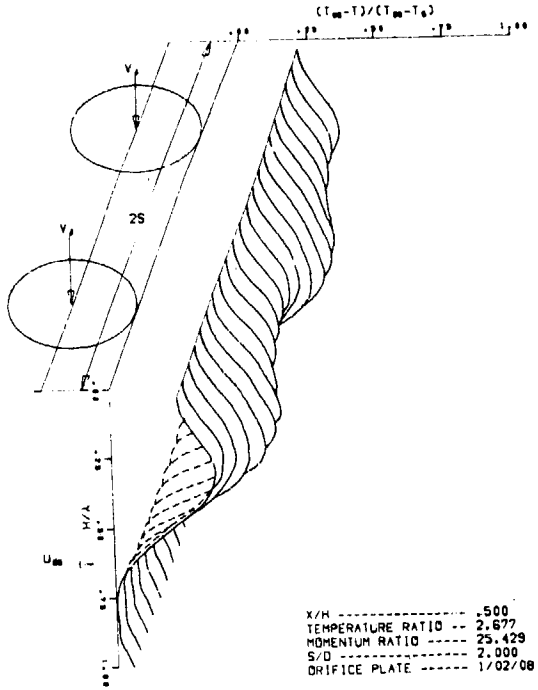

MULTIPLE JET TEST 61

X/h = 0.5

FOLDOUT FRAME

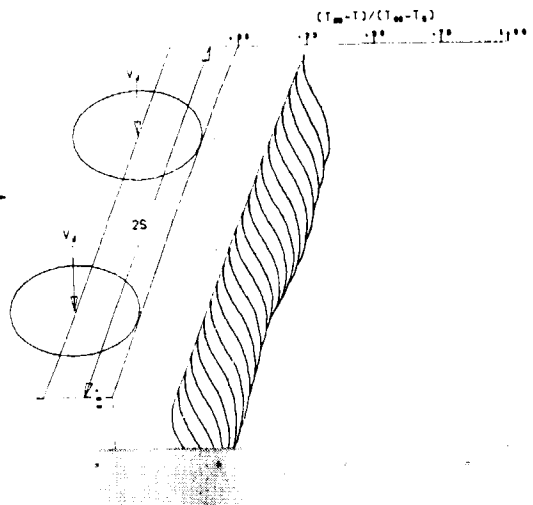

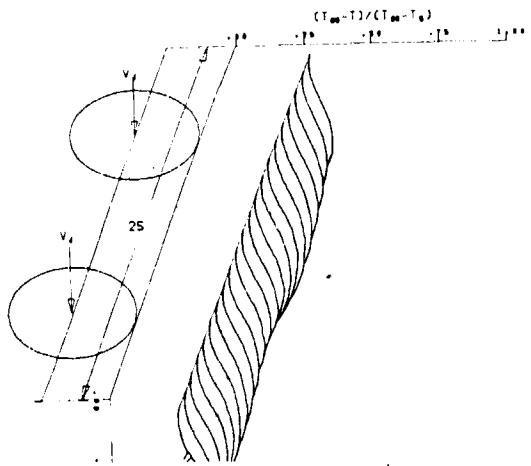

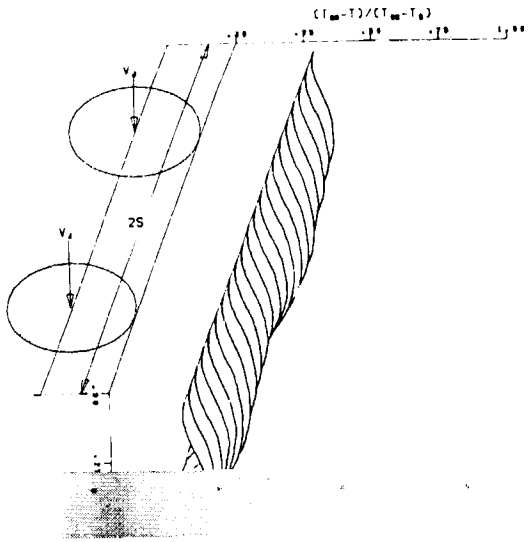

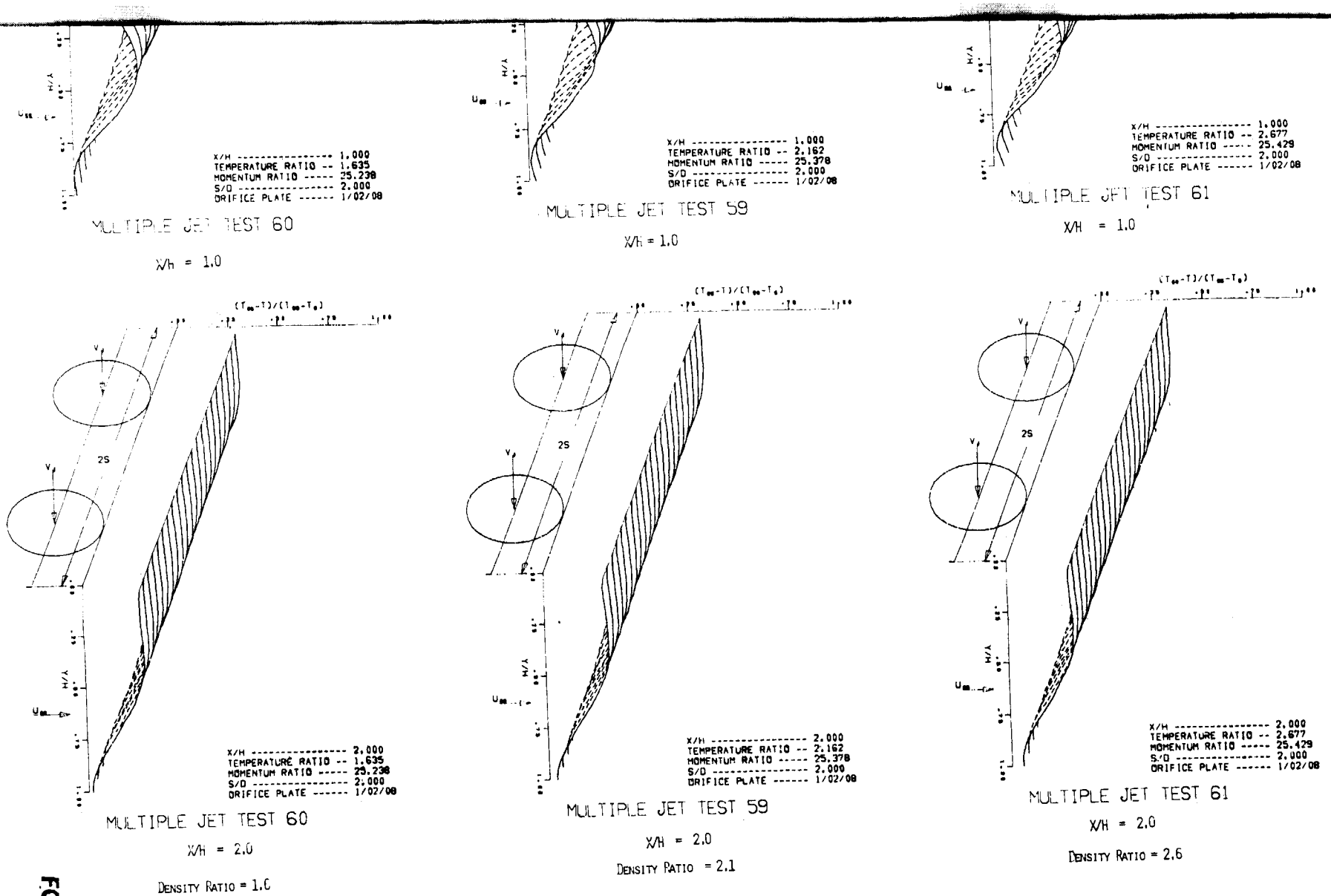

FIGURE 14. EFFECT OF DENSITY RATIO ON TEMPERATURE PROFILES

FOLDOUT FRAME

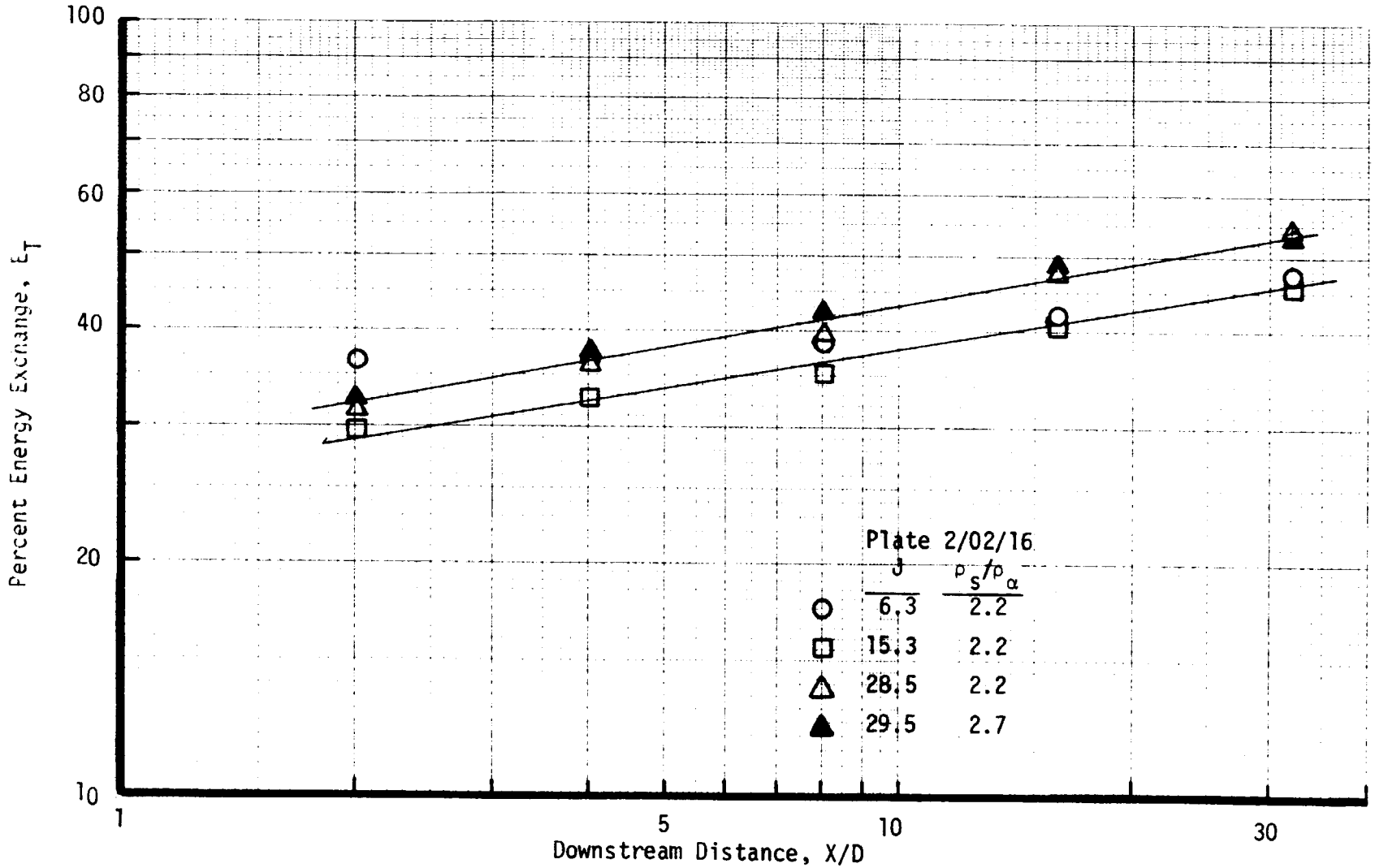

FIGURE 15. EFFECT OF X/D ON ENERGY EXCHANGE EFFICIENCY, ORIFICE PLATE 2/02/16

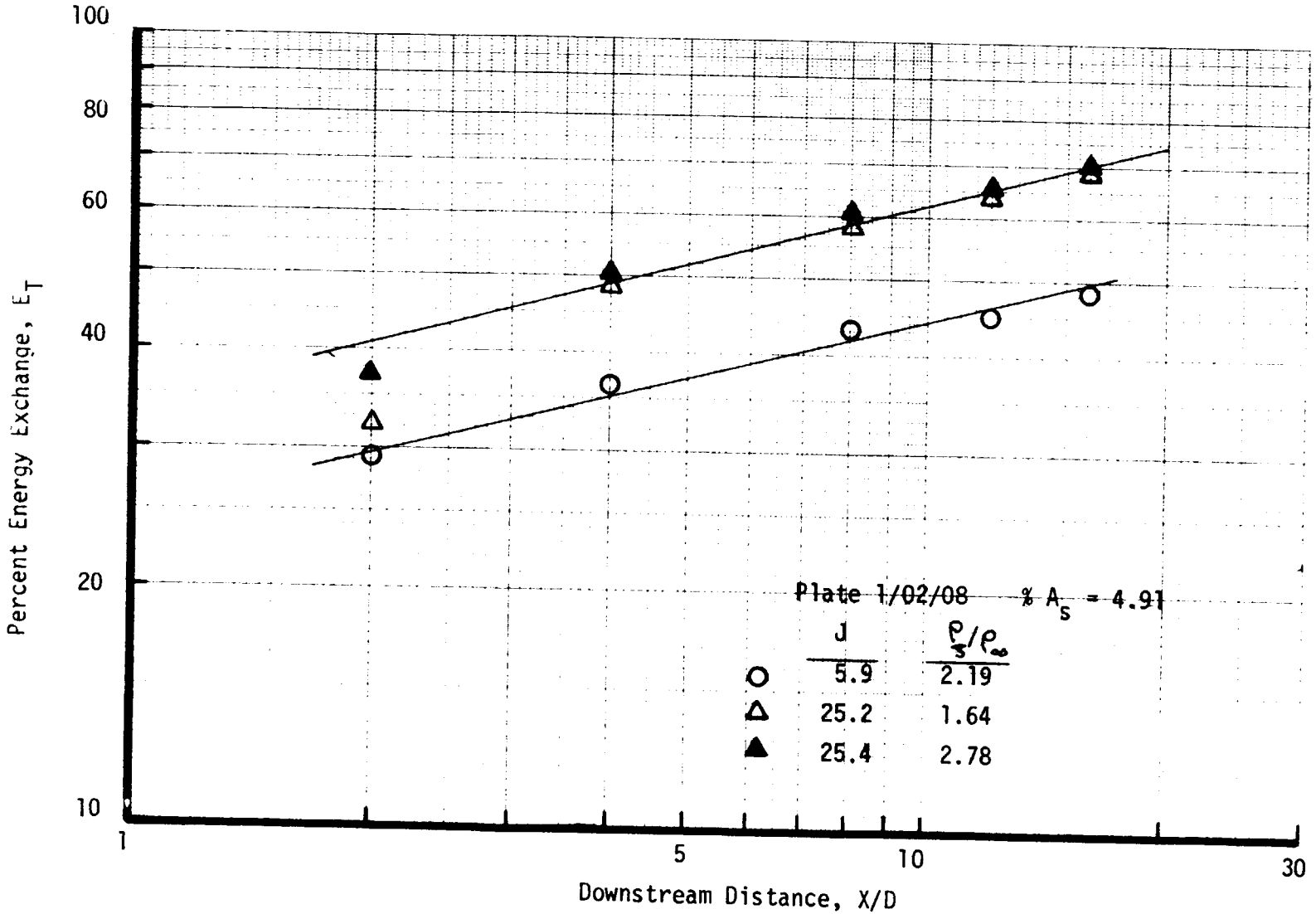

FIGURE 16. EFFECT OF X/D ON ENERGY EXCHANGE EFFICIENCY, ORIFICE PLATE 1/02/08

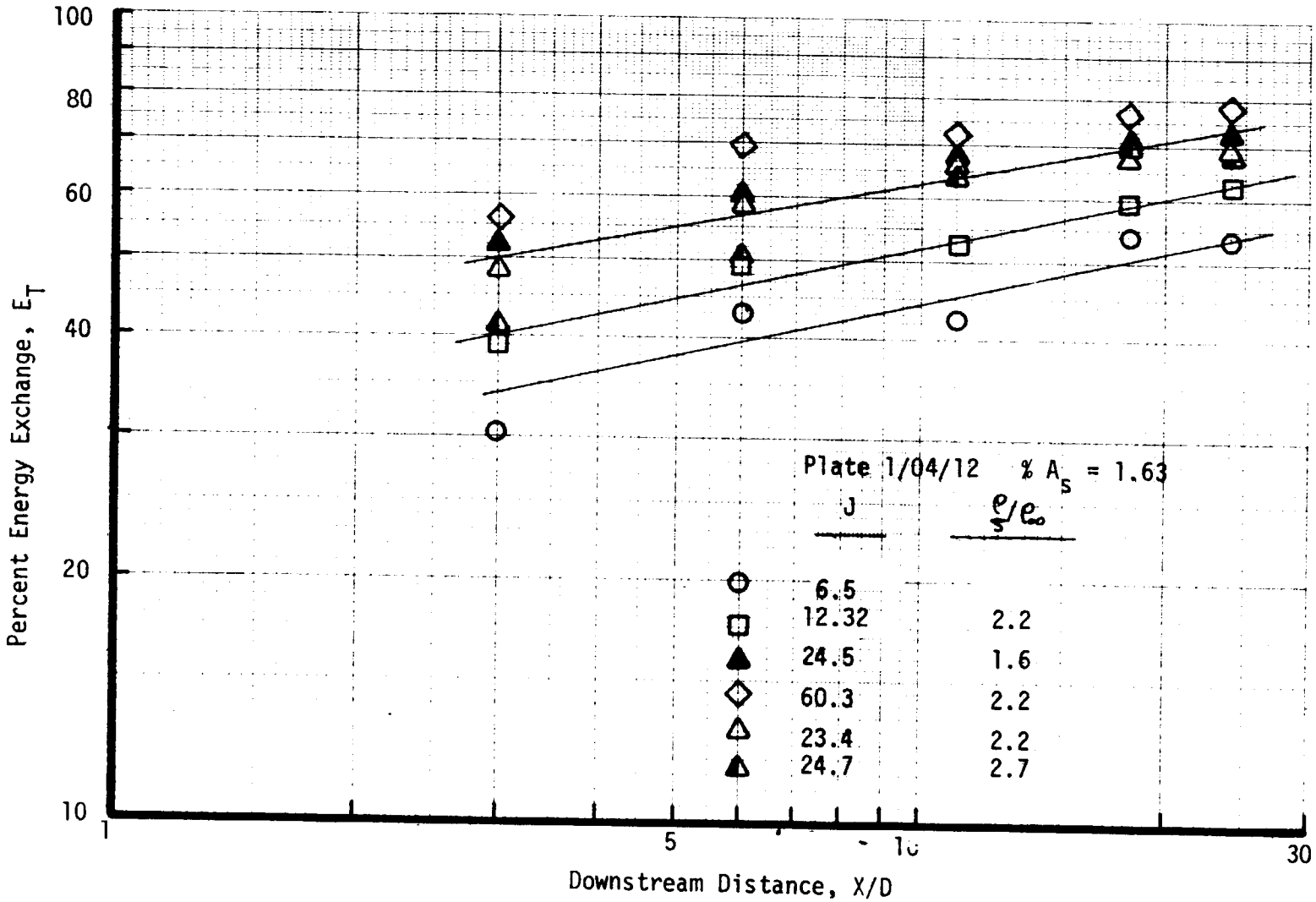

FIGURE 17. EFFECT OF X/D ON ENERGY EXCHANGE EFFICIENCY, ORIFICE PLATE 1/04/12

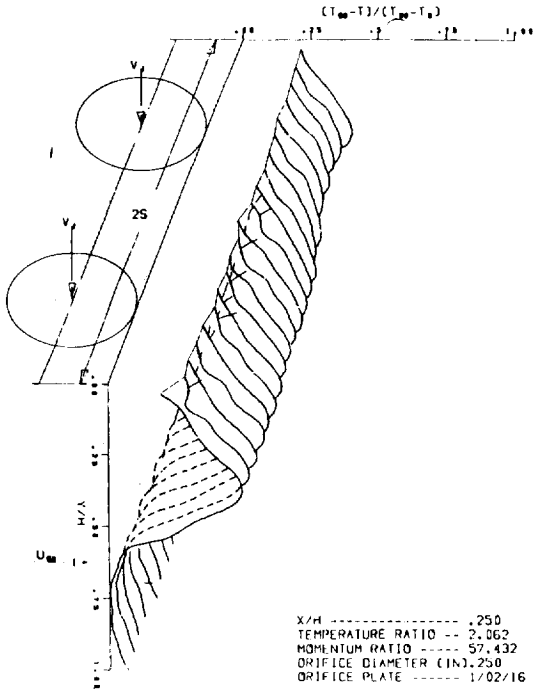

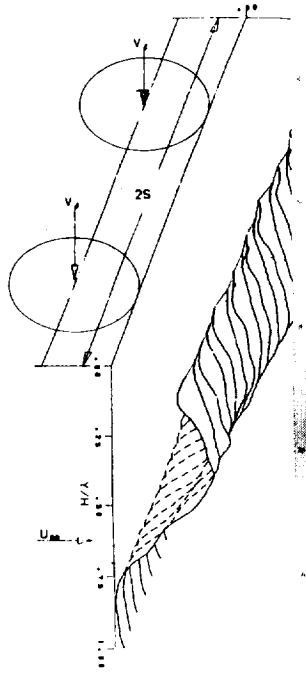

No Turbulence Grid, Nominal

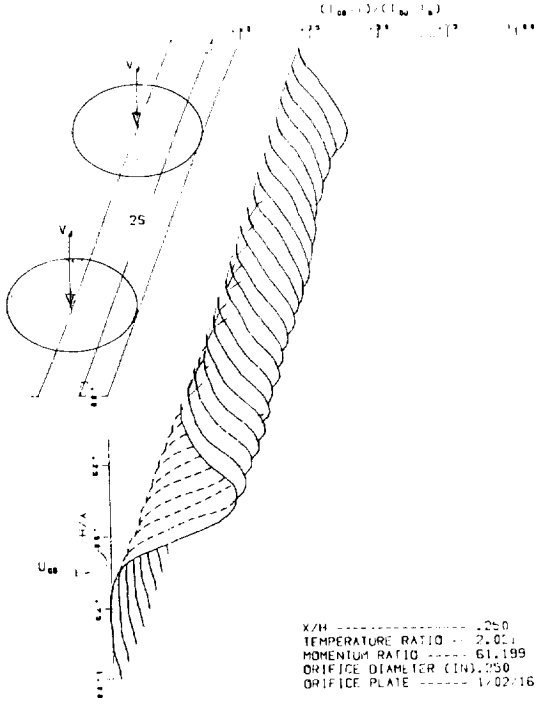

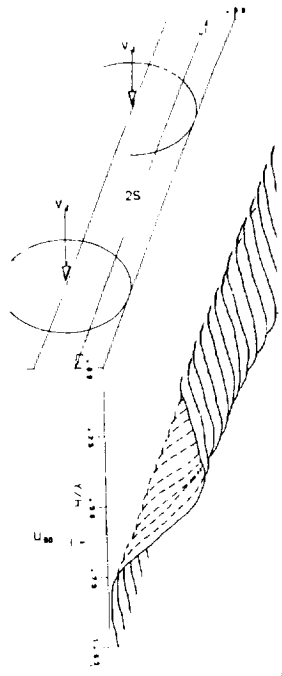

.75 cm (.29 IN) DIAMETER TU
NOMINAL MOMENTUM FLUX RATIO

FOLDOUT FRAME /

FIGURE 18. EFFECT OF TURBU

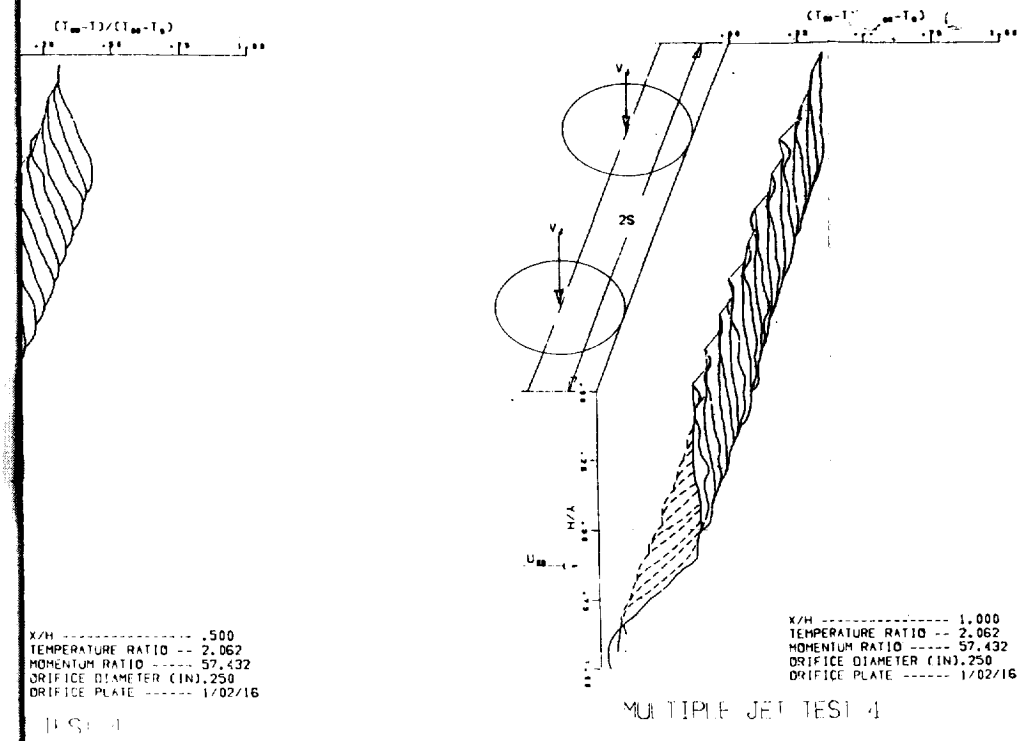

MULTIPLE JET TEST 4

MOMENTUM FLUX RATIO = 57, INCREASING X/h ⟶

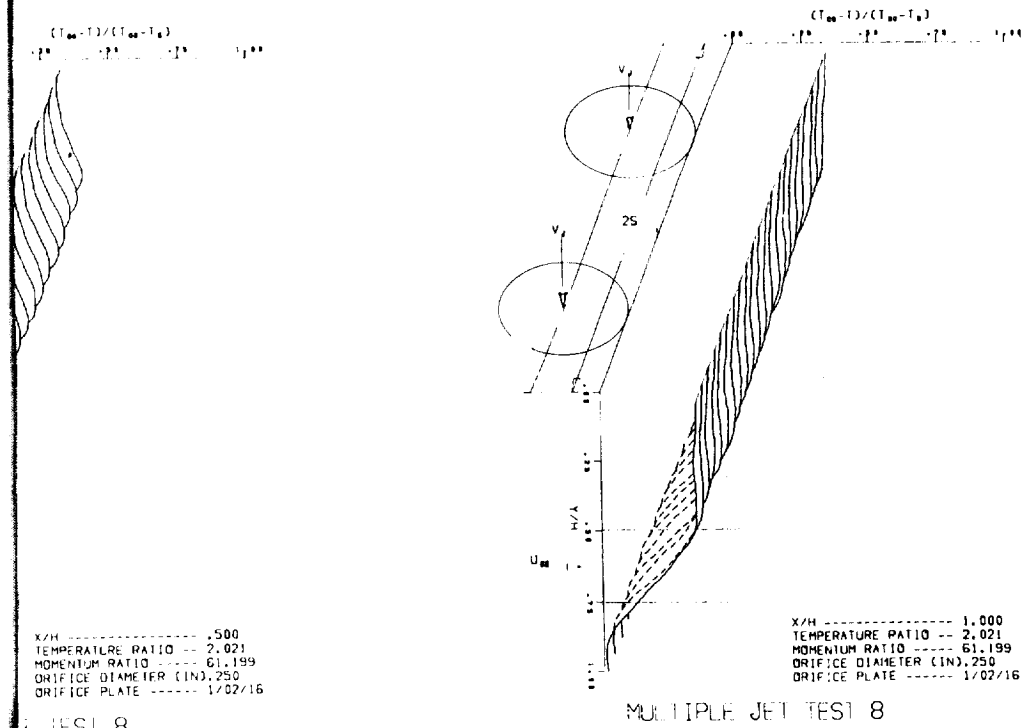

MULTIPLE JET TEST 8

BULENCE GRID (2.54 CM (1.0 IN) SPACING,
= 61, INCREASING X/h ⟶

Figure 18

LENCE GRID ON TEMPERATURE PROFILES

FOLDOUT FRAME 2

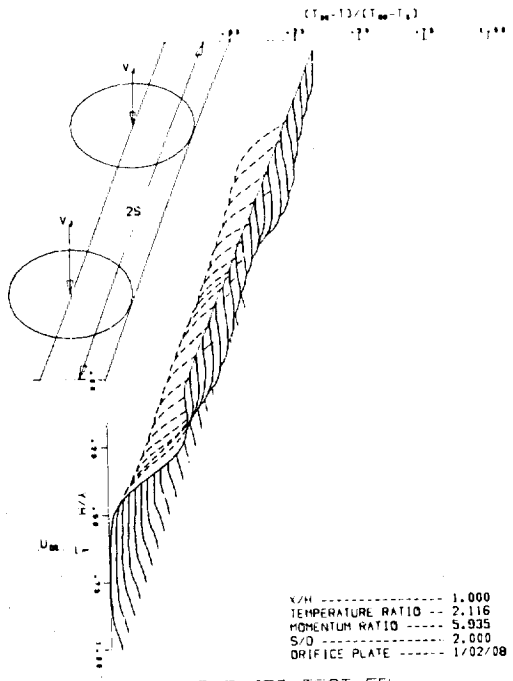

MULTIPLE JET TEST 57

H/D = 8

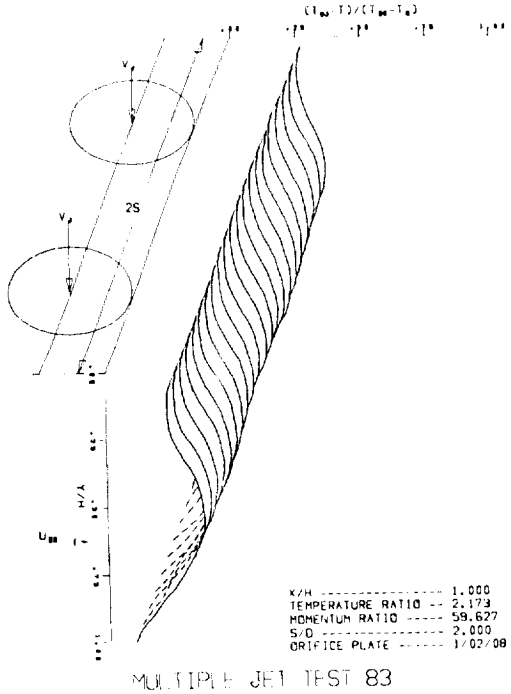

MULTIPLE JET TEST 83

H/D = 8

FIGUR

FOLDOUT FRAME 1

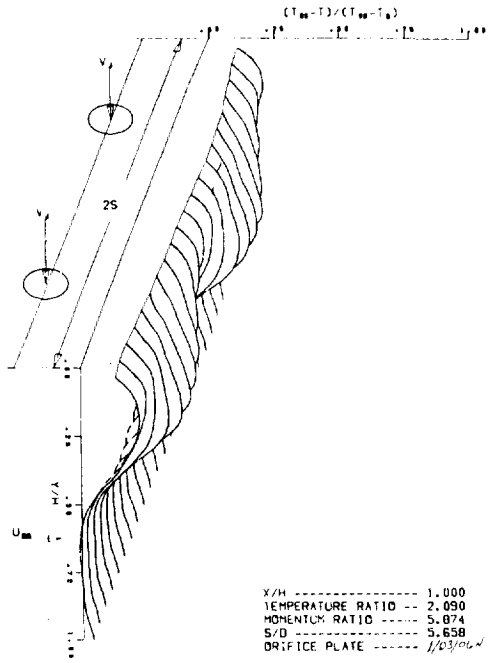

MULTIPLE JET TEST 94

A_j/A_∞ = .049 h/D = 0

Nominal Flow Ratio, $\dot{W}_j/\dot{W}_\infty$ = .12,
Nominal Momentum Flux Ratio = 6

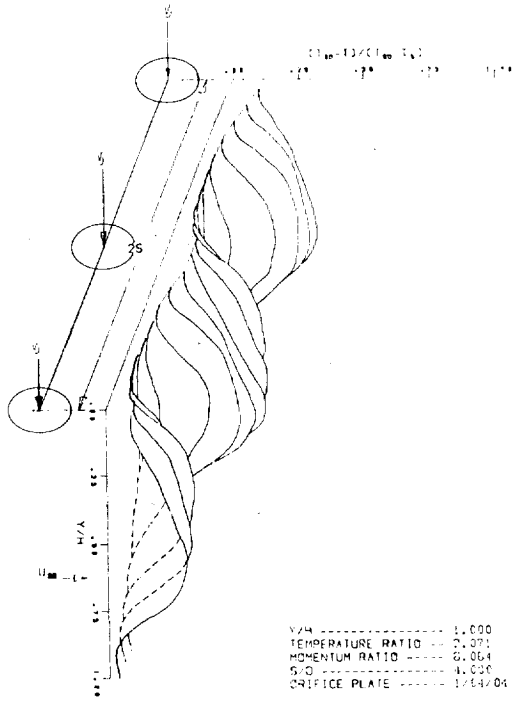

MULTIPLE JET TEST 86

h/D = 4

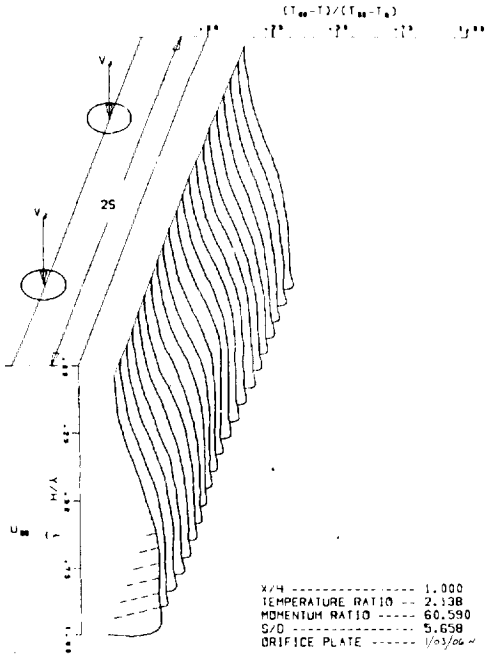

MULTIPLE JET TEST 97

h/D = 0

A_j/A_∞ = .049

Nominal Flow Ratio, $\dot{W}_j/\dot{W}_\infty$ = .36,
Nominal Momentum Flux Ratio = 60

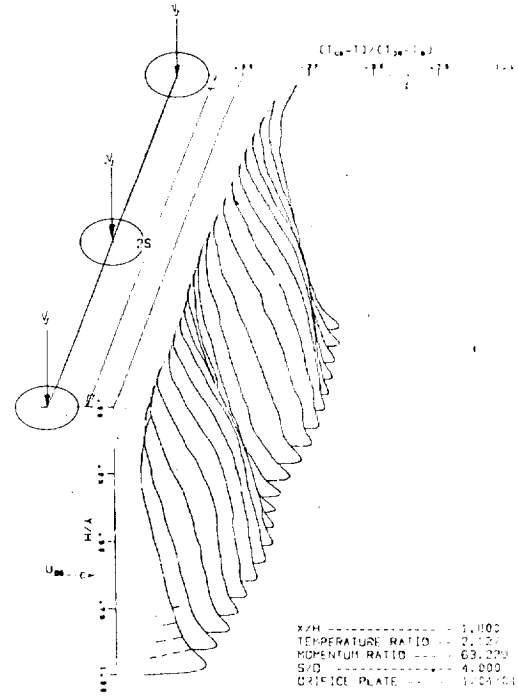

MULTIPLE JET TEST 89

h/D = 4

FIGURE 19

RE 19. TEMPERATURE PROFILES FOR CONSTANT ORIFICE AREA

FOLDOUT FRAME 2

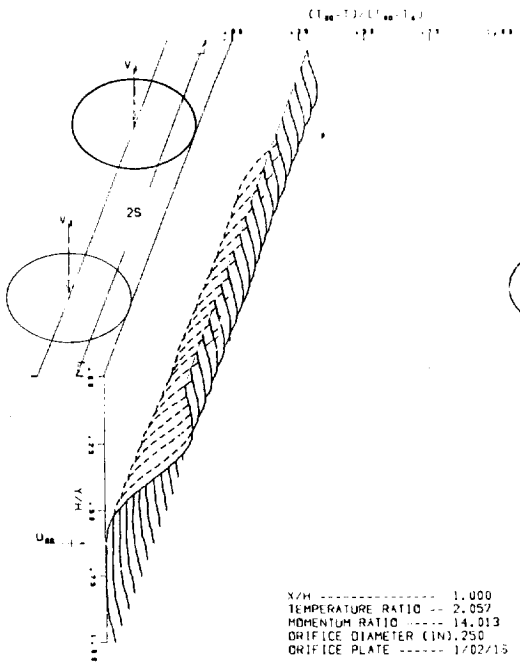

MULTIPLE JET TEST 2

H/D = 16

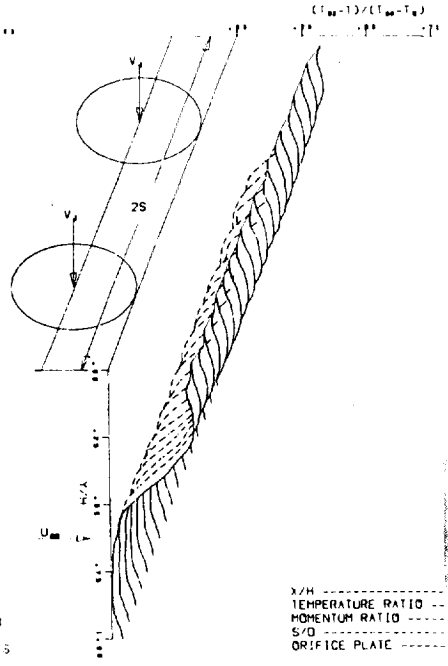

MULTIPLE JET TEST 46

H/D = 12

NOMINAL

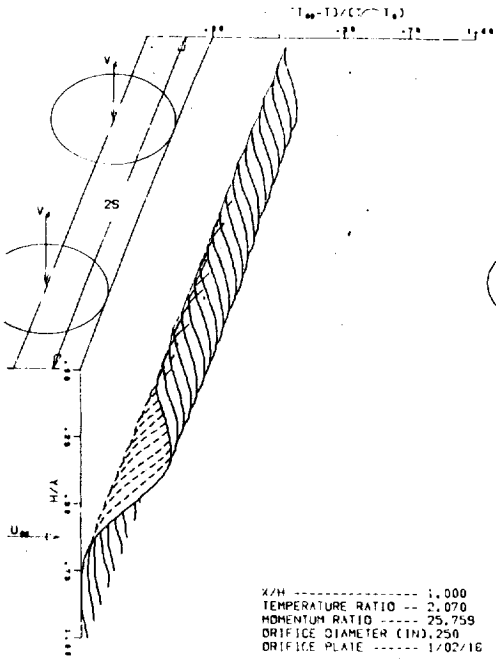

MULTIPLE JET TEST 3

H/D = 16

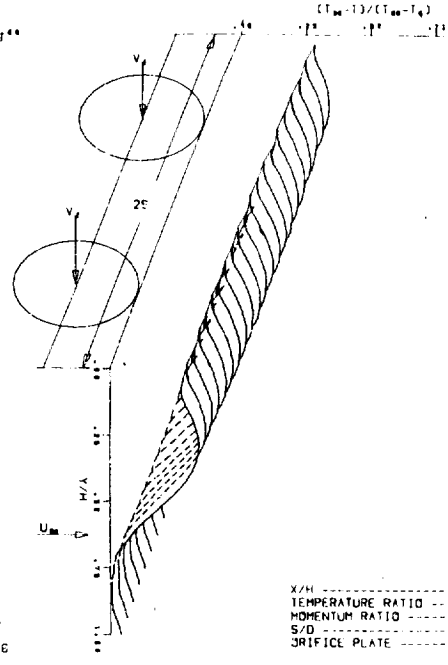

MULTIPLE JET TEST 47

H/D = 12

NOMINAL

FIGURE 20.

FOLDOUT FRAME 1

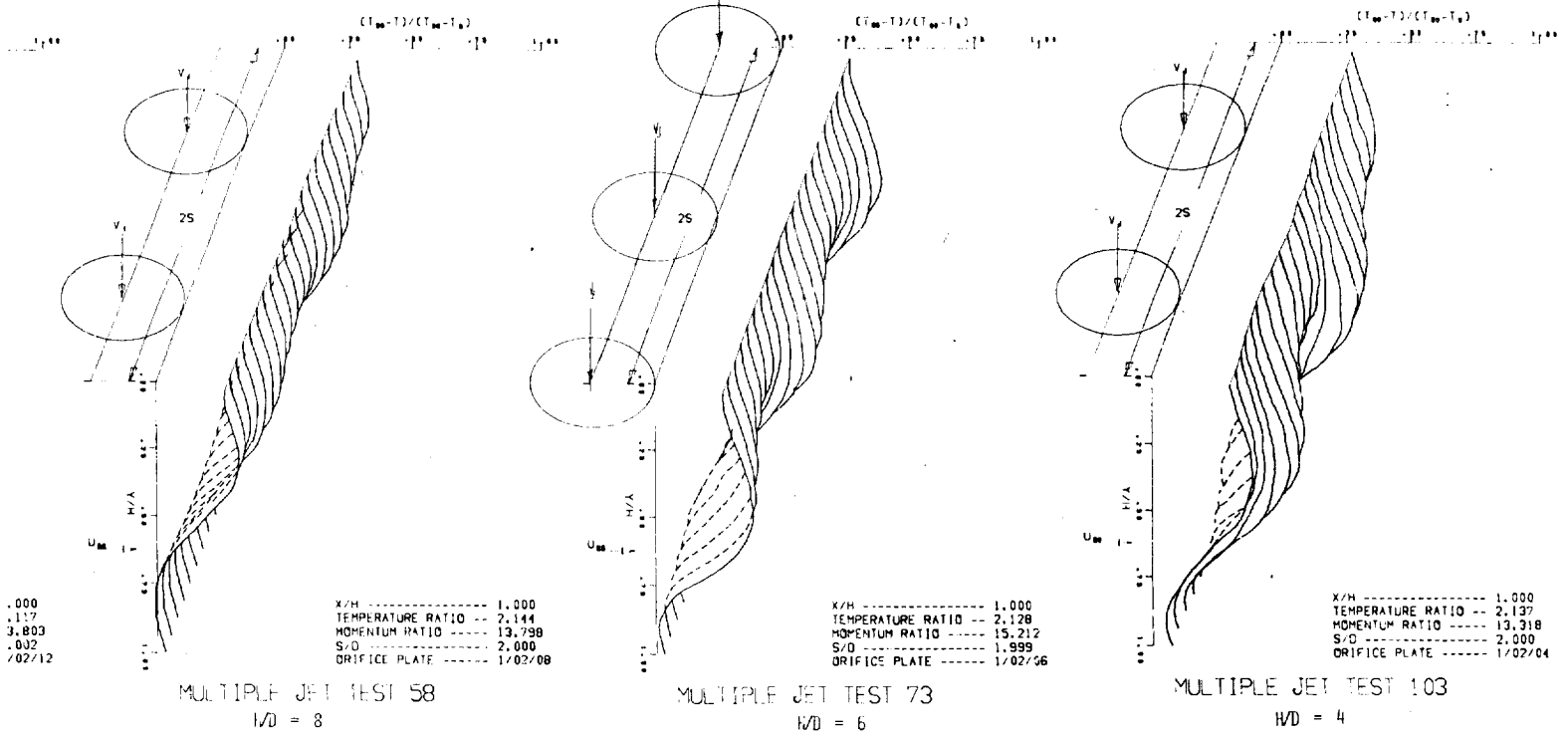

MENTUM FLUX RATIO = 14, X/H = 1.0, INCREASING ORIFICE DIAMETER ——→

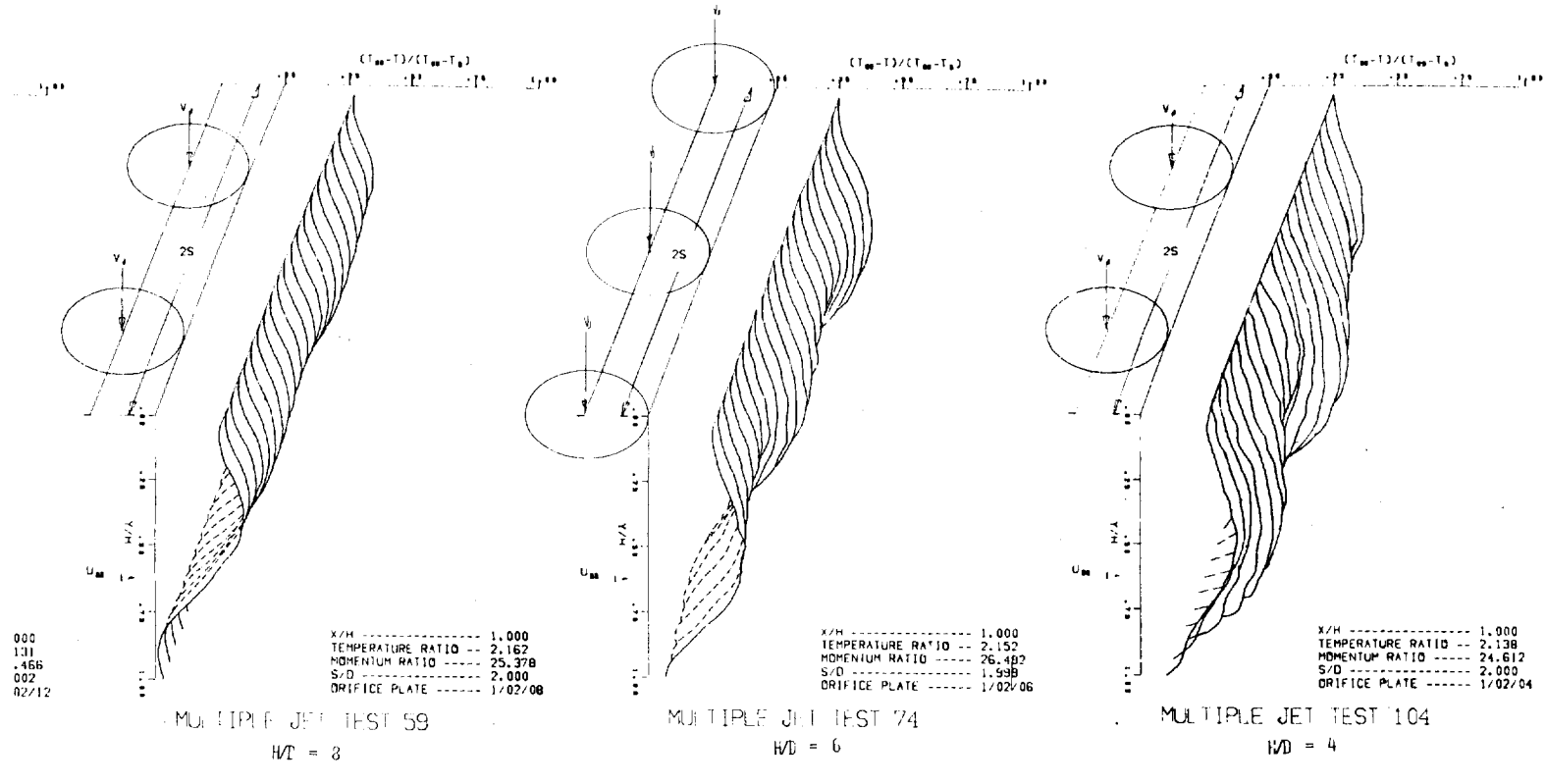

NTUM FLUX RATIO = 25, X/H = 1.0, INCREASING ORIFICE DIAMETER ——→

FIGURE 20

EFFECT OF ORIFICE DIAMETER ON TEMPERATURE PROFILES, CONSTANT S/D

FOLDOUT FRAME 2

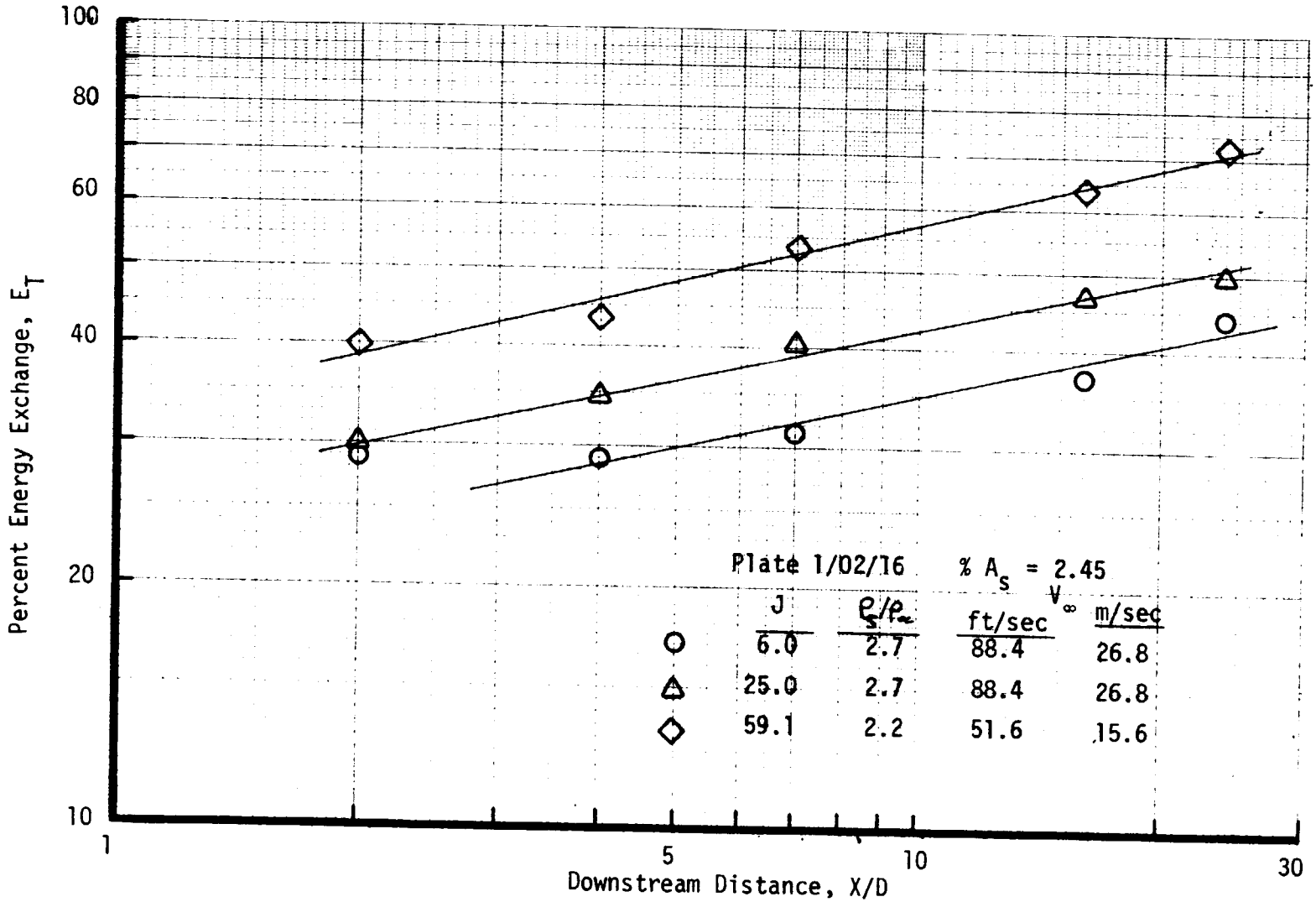

FIGURE 21. EFFECT OF X/D ON ENERGY EXCHANGE EFFICIENCY, ORIFICE PLATE 1/02/16

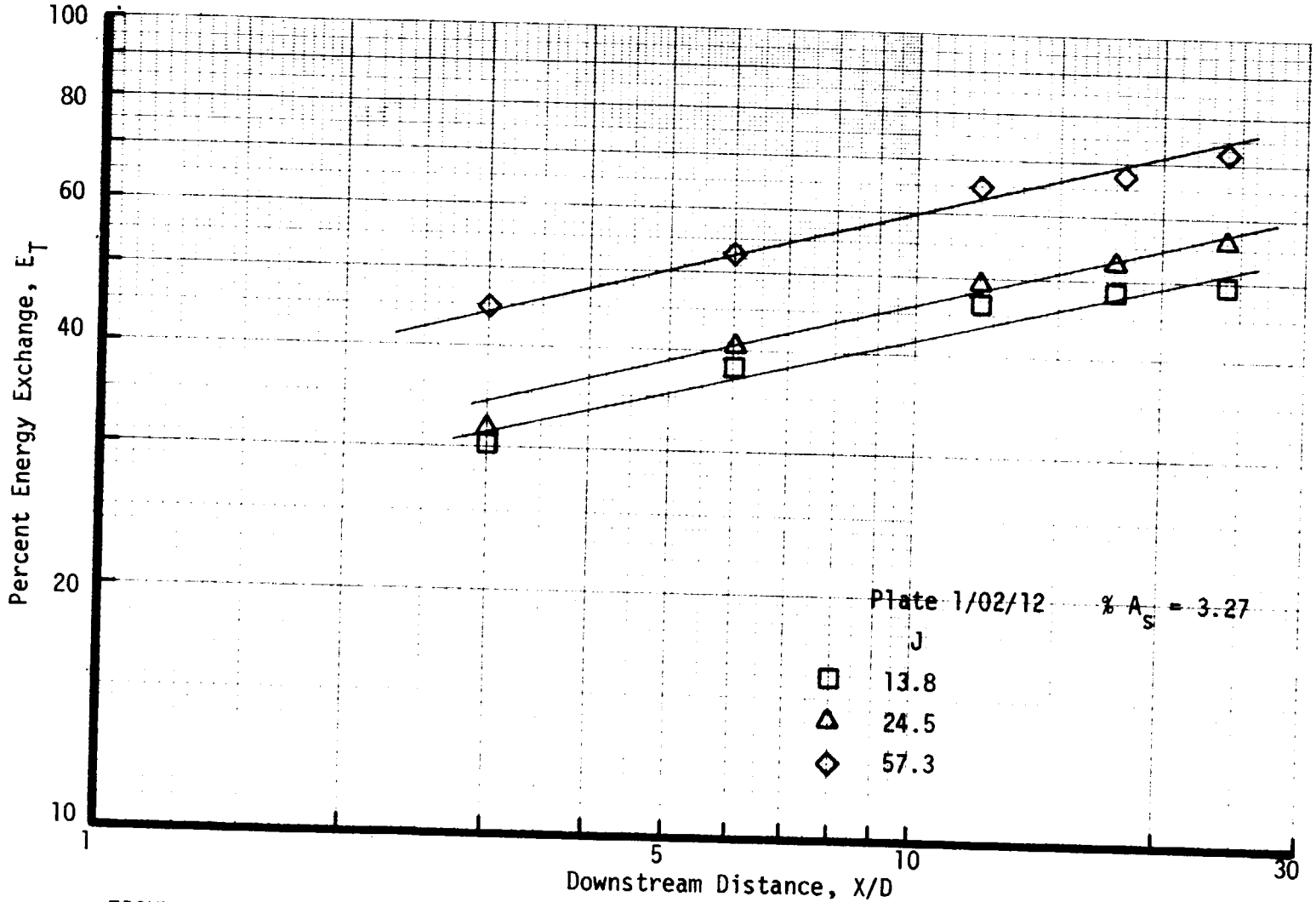

FIGURE 22. EFFECT OF X/D ON ENERGY EXCHANGE EFFICIENCY, ORIFICE PLATE 1/02/12

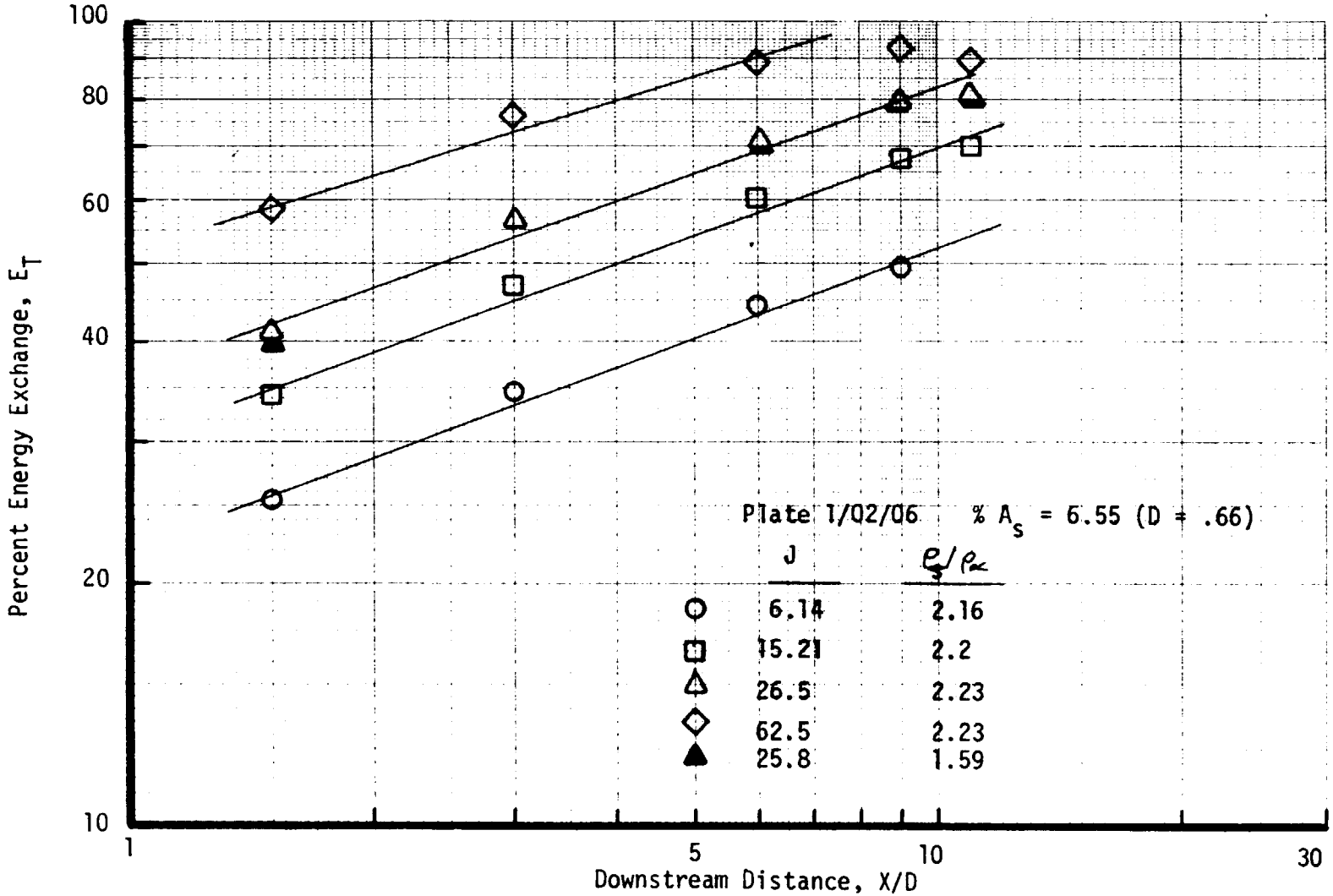

FIGURE 23. EFFECT OF X/D ON ENERGY EXCHANGE EFFICIENCY, ORIFICE PLATE 1/02/06

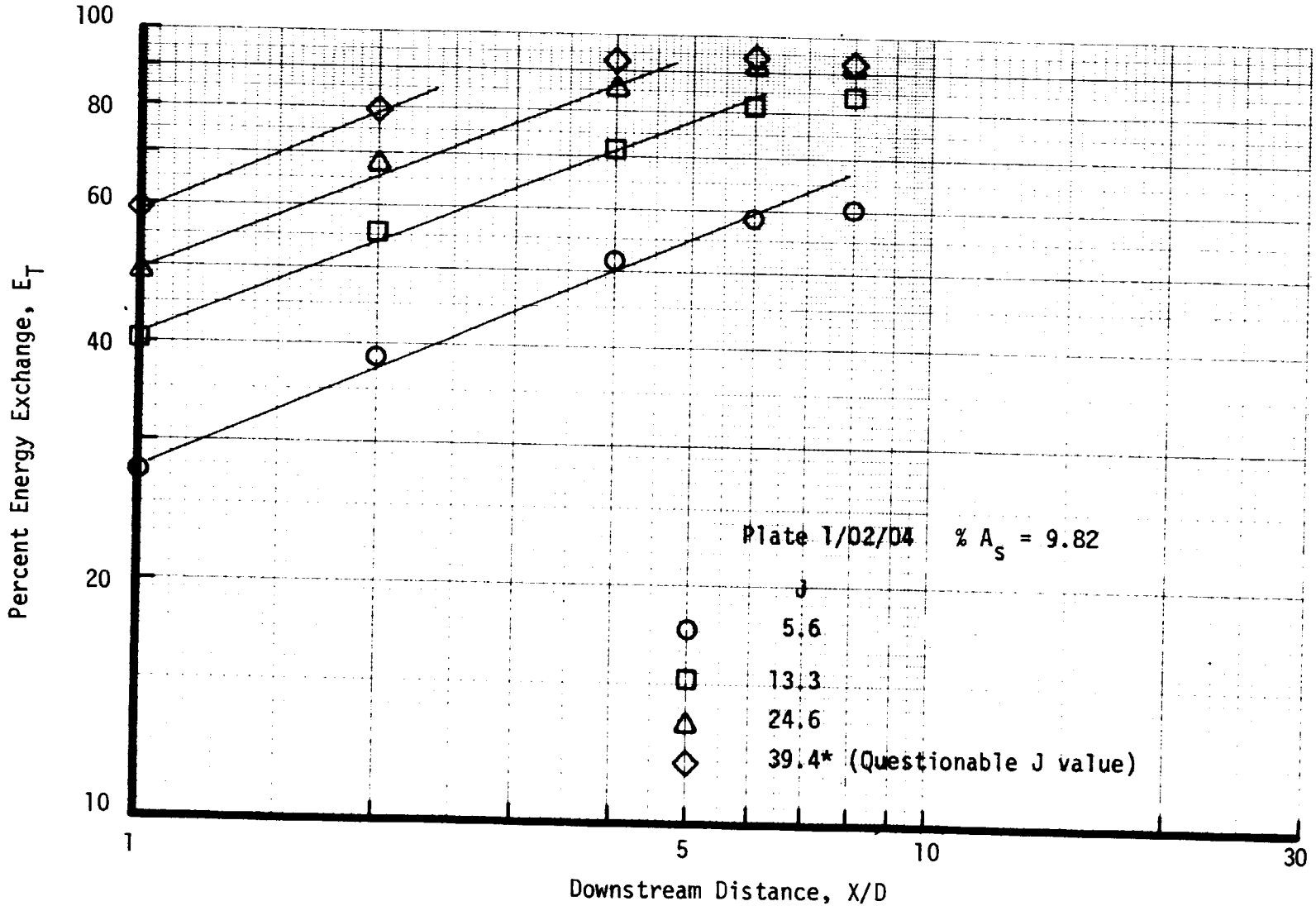

FIGURE 24. EFFECT OF X/D ON ENERGY EXCHANGE EFFICIENCY, ORIFICE PLATE 1/02/04

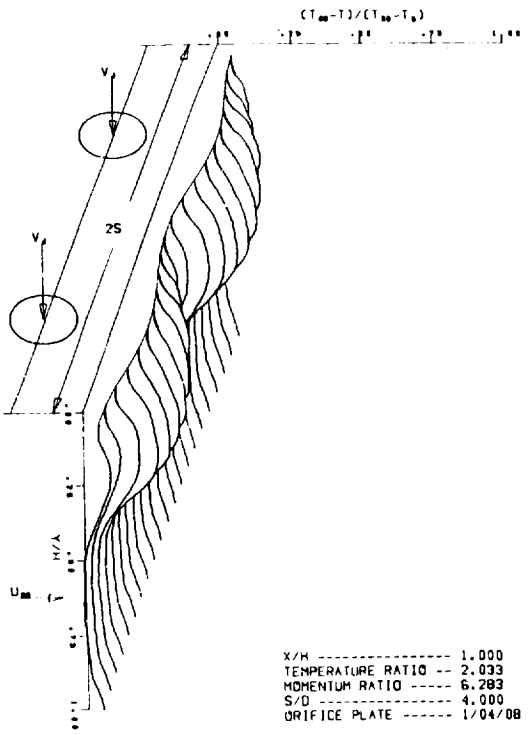

MULTIPLE JET TEST 67

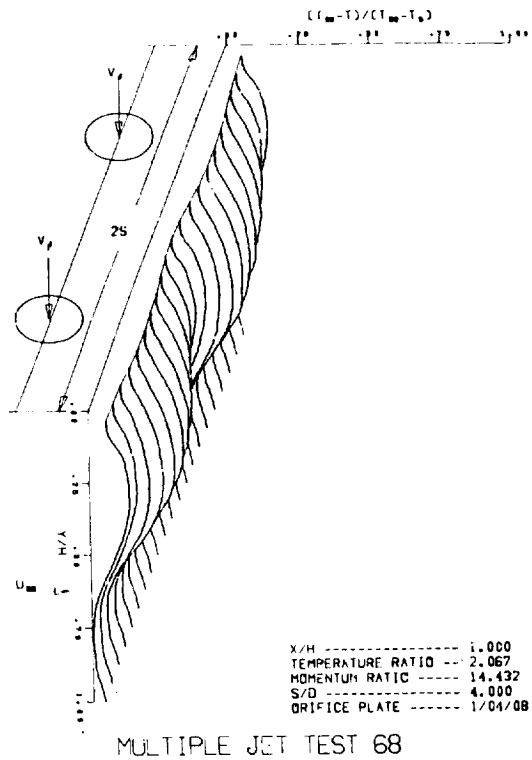

MULTIPLE JET TEST 68

ORIFICE PLATE 1/04/06, H/S =.5 , X/H

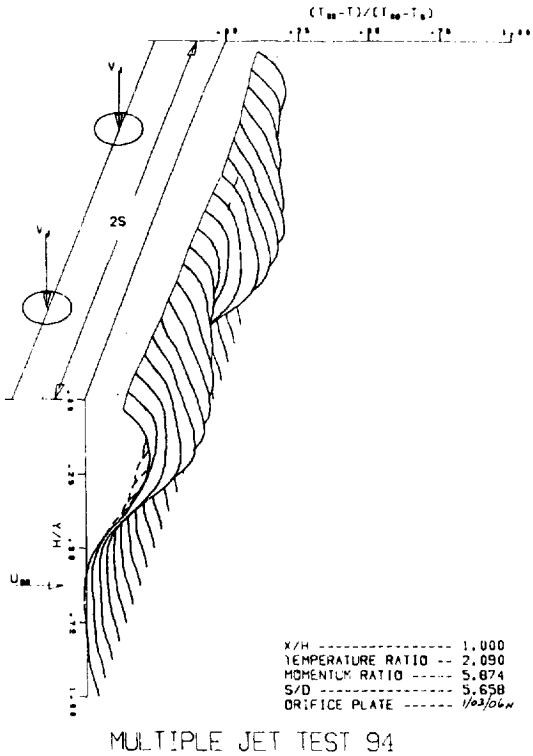

MULTIPLE JET TEST 94

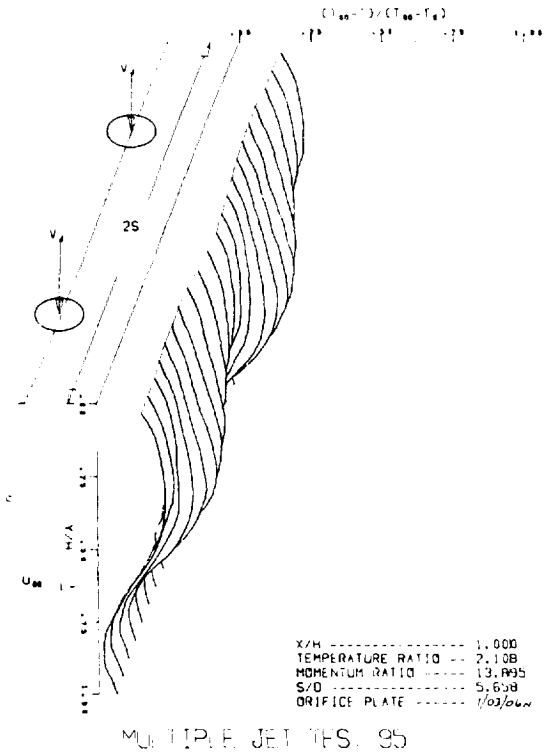

MULTIPLE JET TEST 95

ORIFICE PLATE 1/03/06N, H/S =.5 ,

FOLDOUT FRAME 1

FIGURE 25. COMPARISON

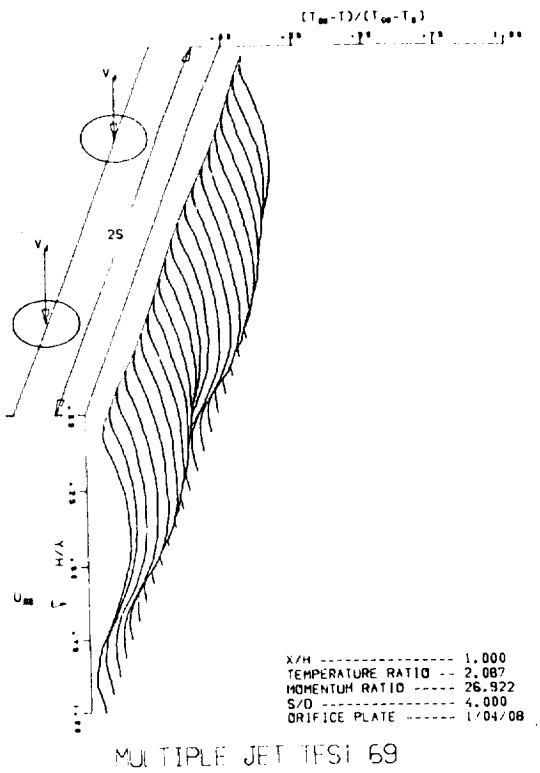

MULTIPLE JET TEST 69

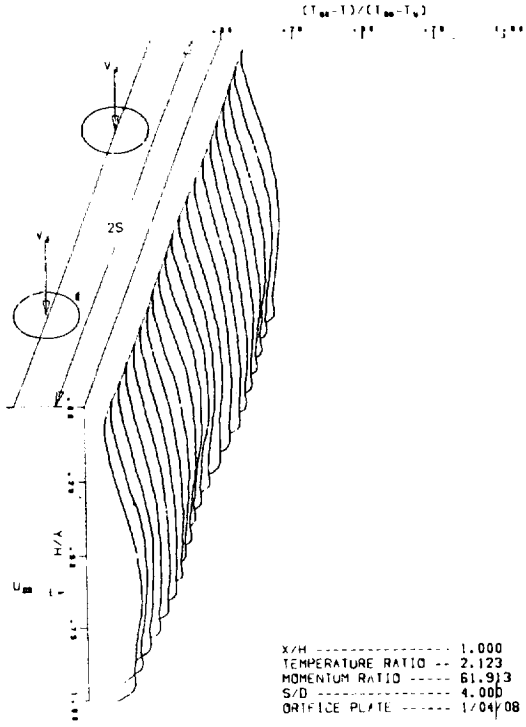

MULTIPLE JET TEST 84

= 1.0, INCREASING MOMENTUM FLUX RATIO ⟶

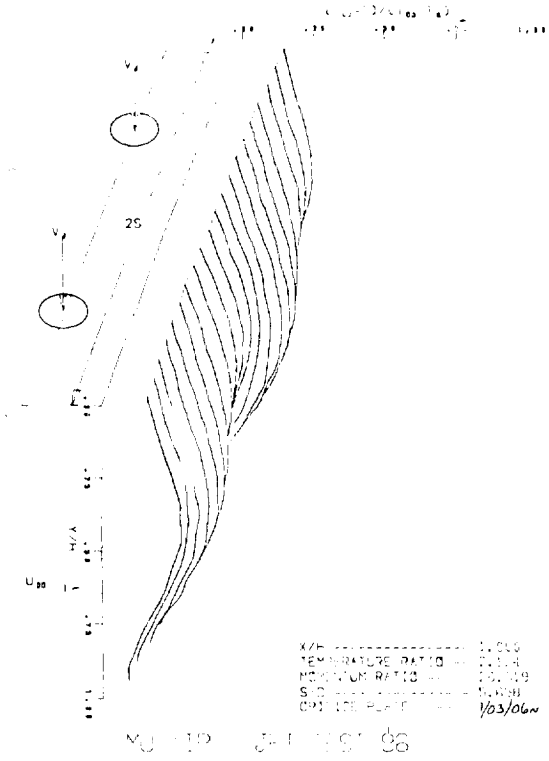

MULTIPLE JET TEST 88

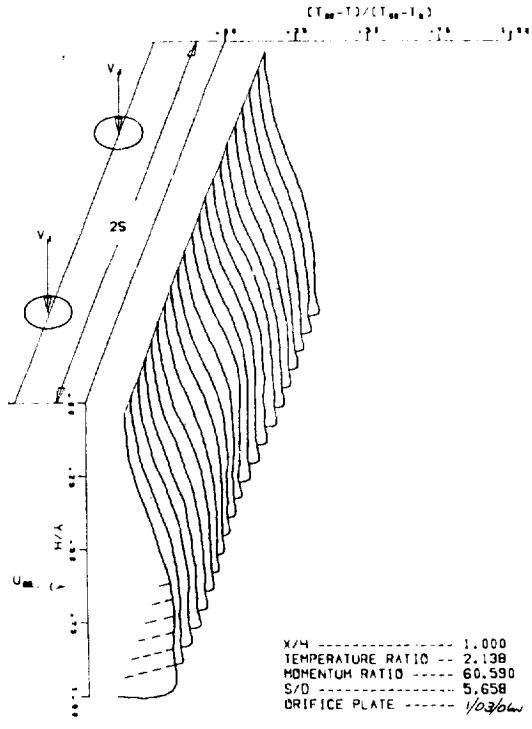

MULTIPLE JET TEST 97

S/H = 1.0, INCREASING MOMENTUM FLUX RATIO ⟶

FIGURE 25

OF TEMPERATURE PROFILES AT CONSTANT S/H

FOLDOUT FRAME 2

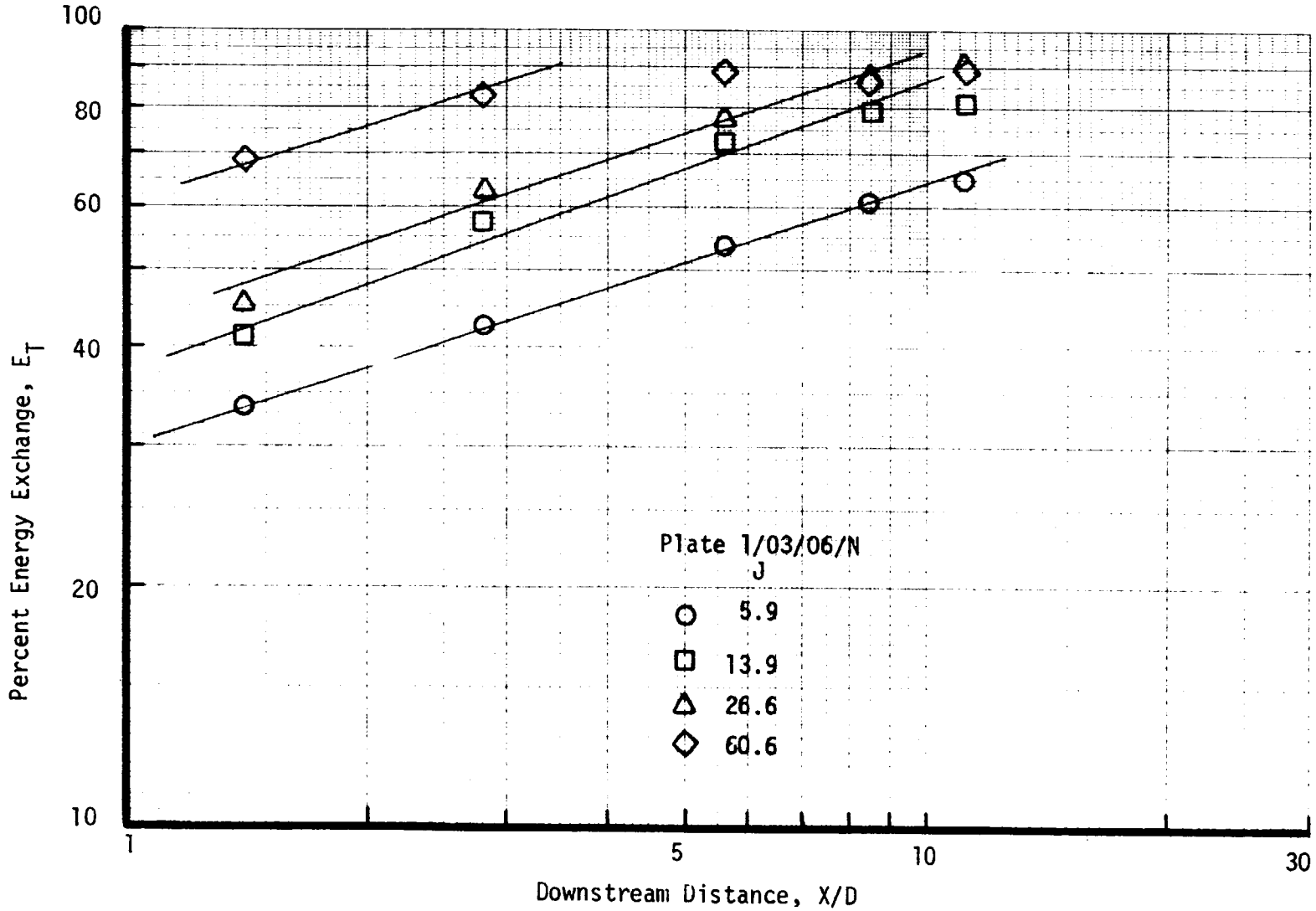

FIGURE 26. EFFECT OF X/D ON ENERGY EXCHANGE EFFICIENCY, ORIFICE PLATE $1/03/06_N$

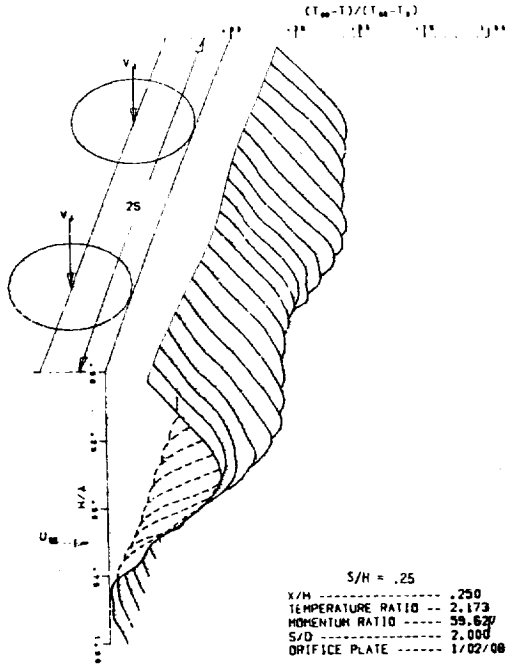

MULTIPLE JET TEST 83

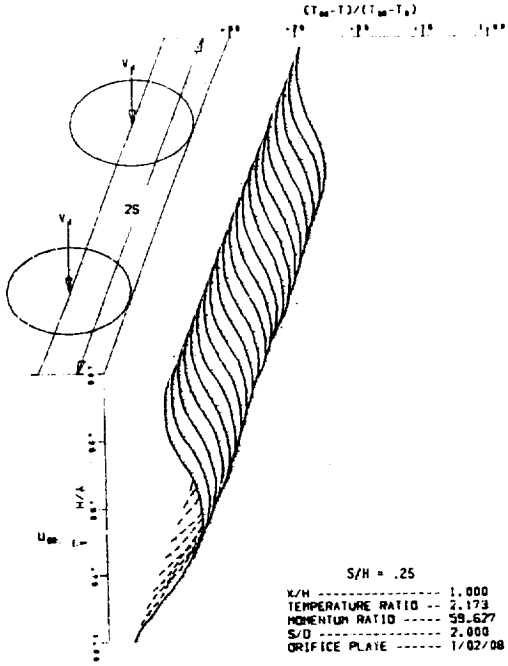

MULTIPLE JET TEST 83

FIGURE 27. E

FOLDOUT FRAME 1

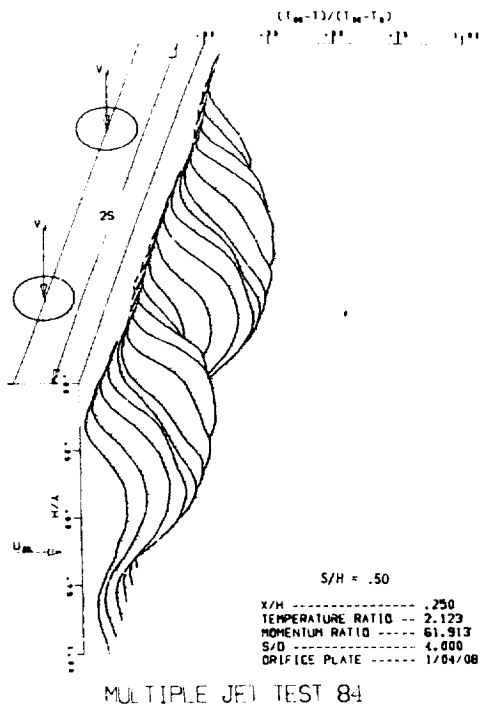

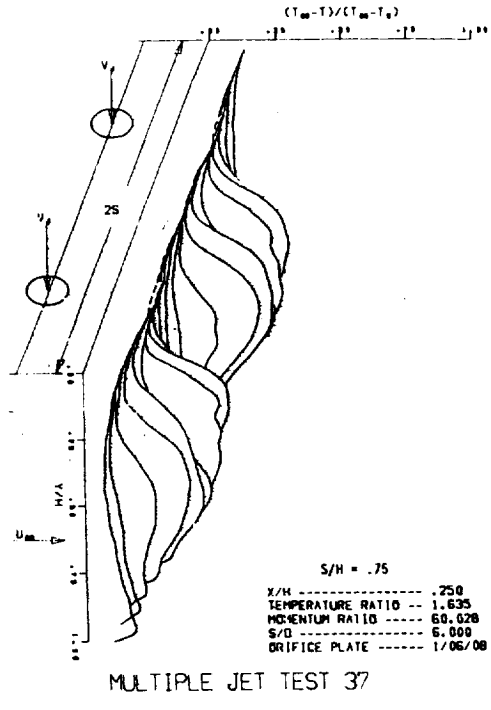

Temperature Profiles at X/H = .25, Increasing S/D and S/H ——→

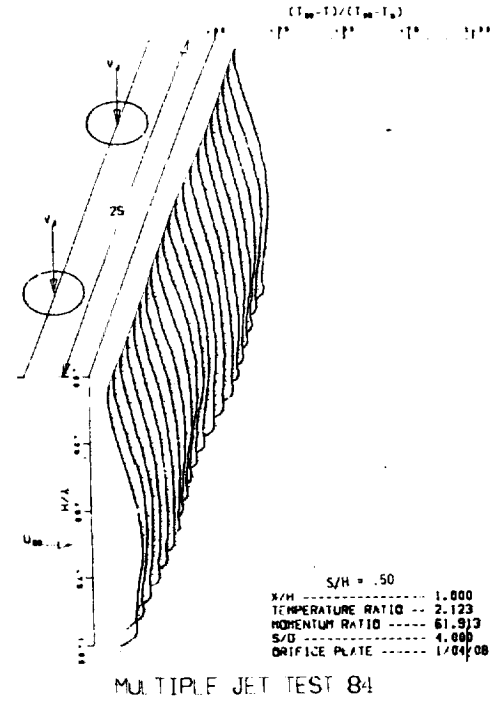

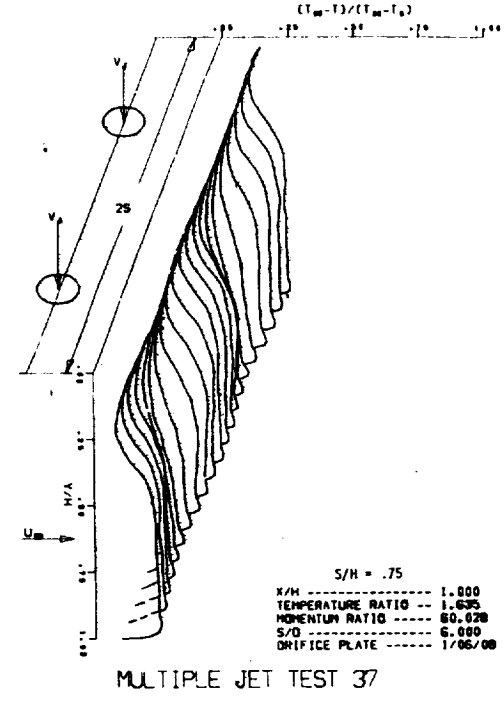

Temperature Profiles at X/H = 1.0, Increasing S/D and S/H ——→

FIGURE 27

EFFECT OF SPACING ON TEMPERATURE PROFILES FOR J=60, CONSTANT ORIFICE DIAMETER

FOLDOUT FRAME 2

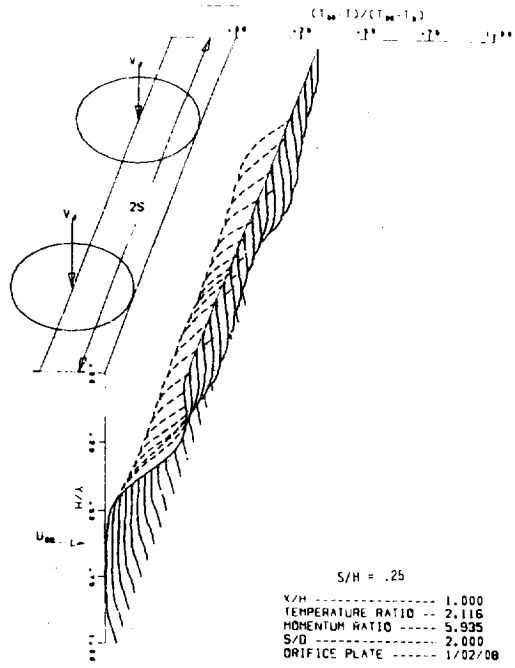

MULTIPLE JET TEST 57

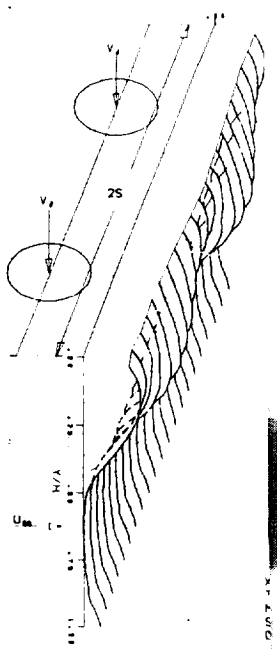

MULTIPLE JET

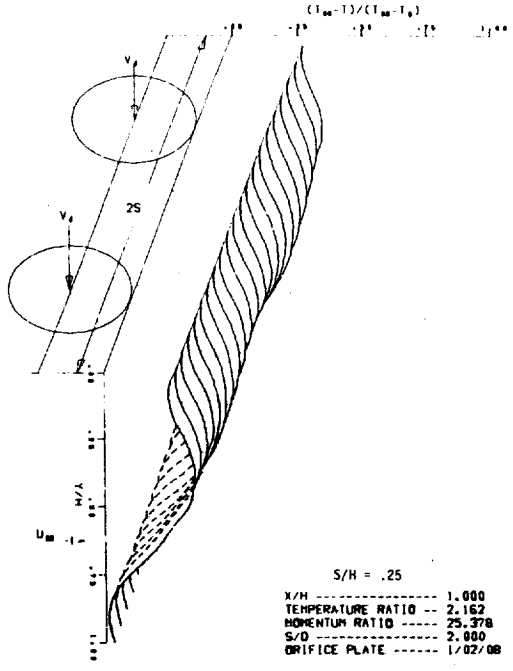

MULTIPLE JET TEST 59

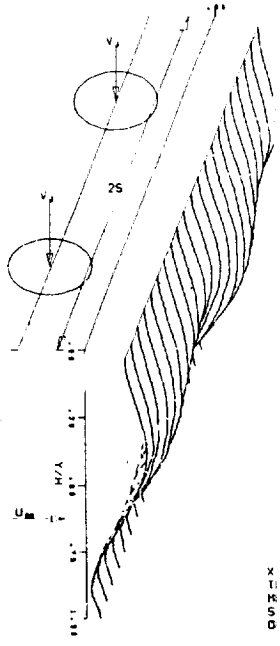

MULTIPLE JET

Nomi

FIGURE 28. EFFECT OF

FOLDOUT FRAME

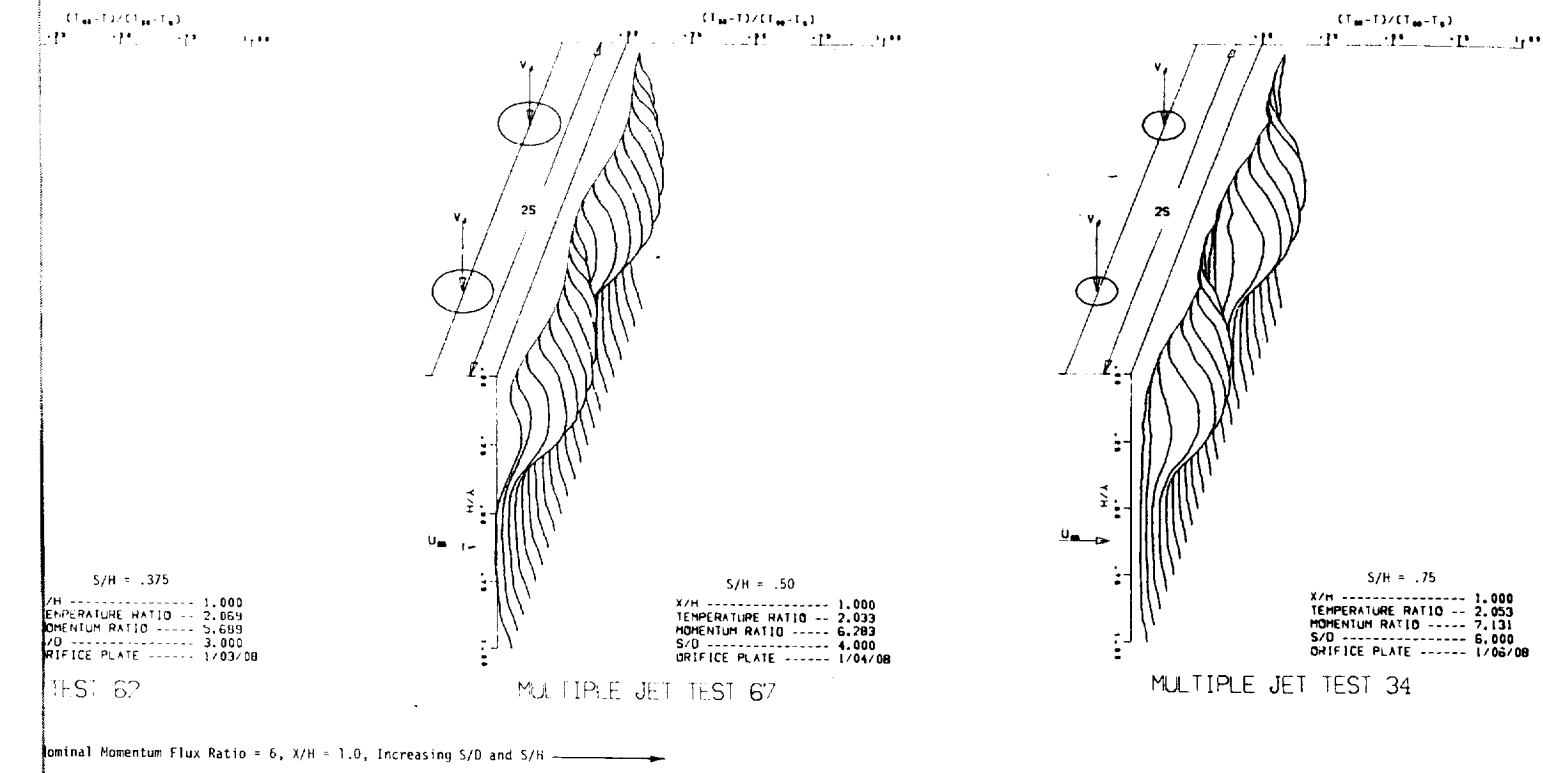

ominal Momentum Flux Ratio = 6, X/H = 1.0, Increasing S/D and S/H ⟶

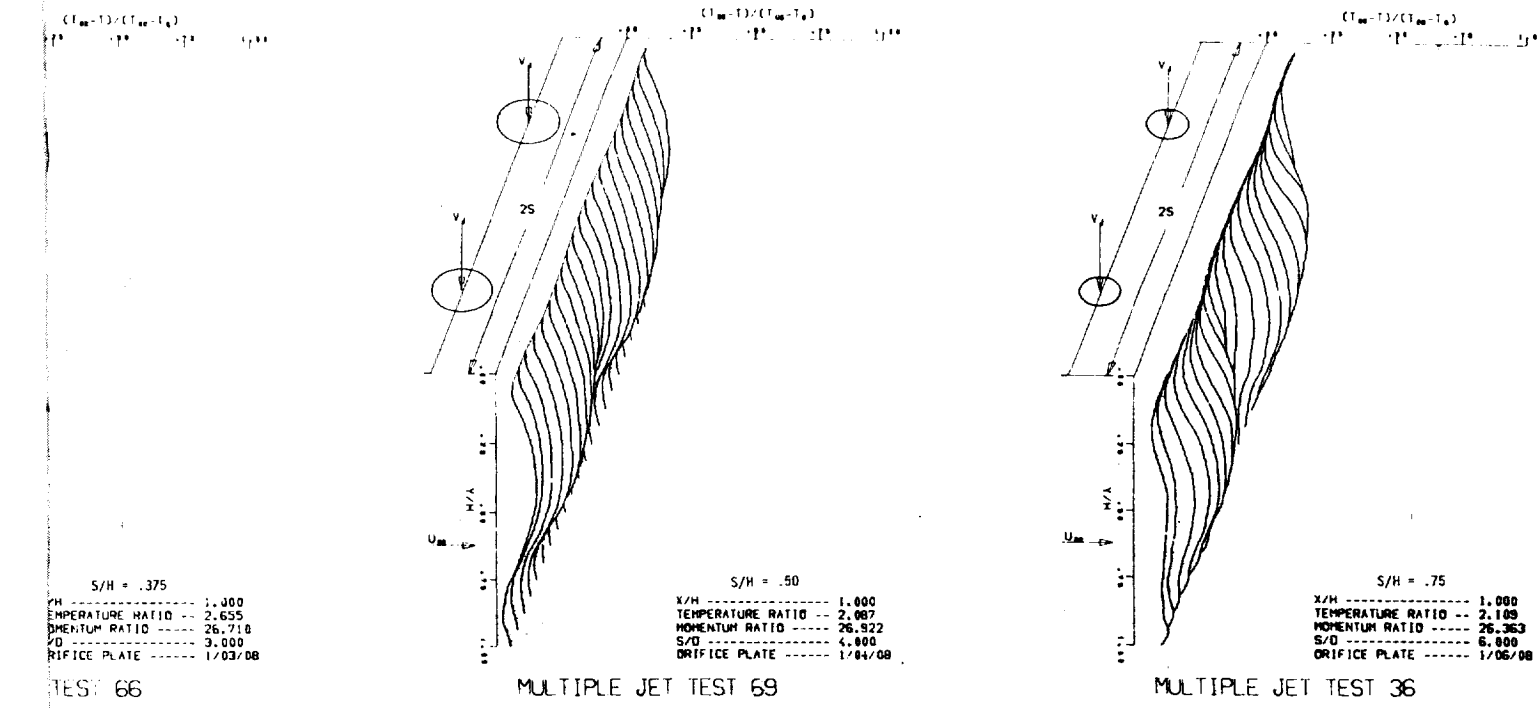

nal Momentum Flux Ratio = 26, X/H = 1.0, Increasing S/D and S/H ⟶

FIGURE 28

SPACING ON TEMPERATURE PROFILES FOR J=6 AND J=26, CONSTANT ORIFICE DIAMETER

FOLDOUT FRAME 2

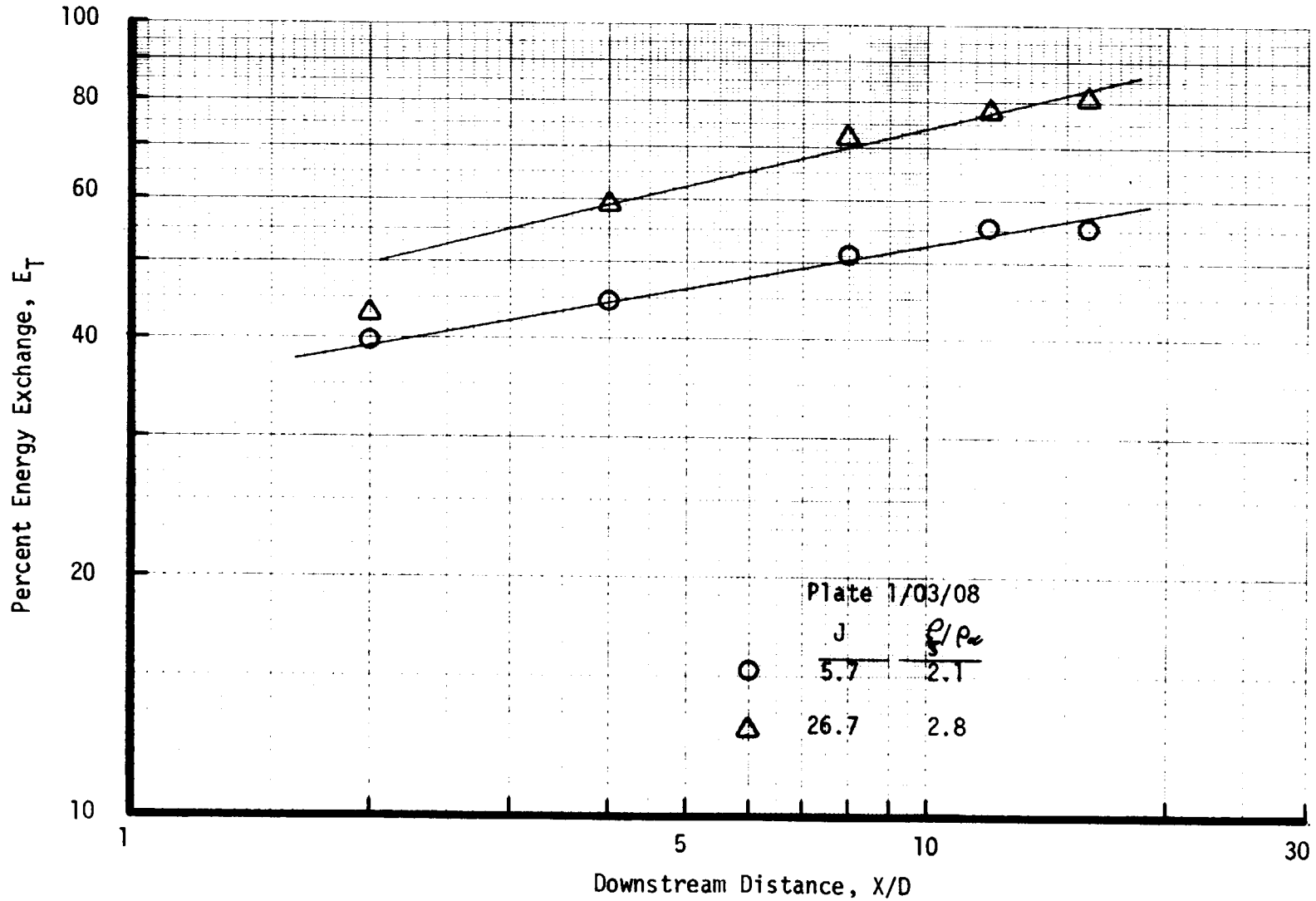

FIGURE 29. EFFECT OF X/D ON ENERGY EXCHANGE EFFICIENCY, ORIFICE PLATE 1/03/08

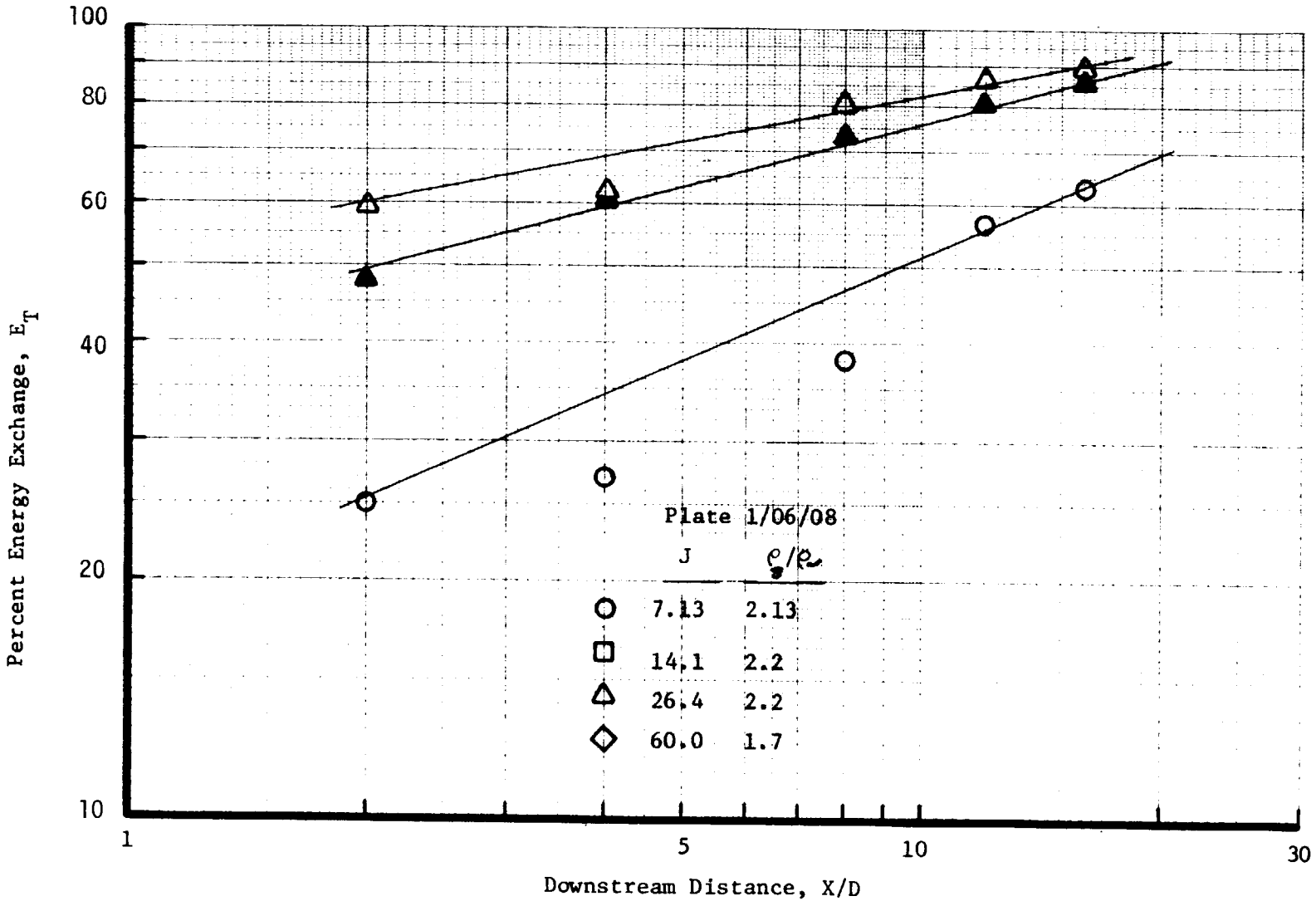

FIGURE 30. EFFECT OF X/D ON ENERGY EXCHANGE EFFICIENCY, ORIFICE PLATE 1/06/08

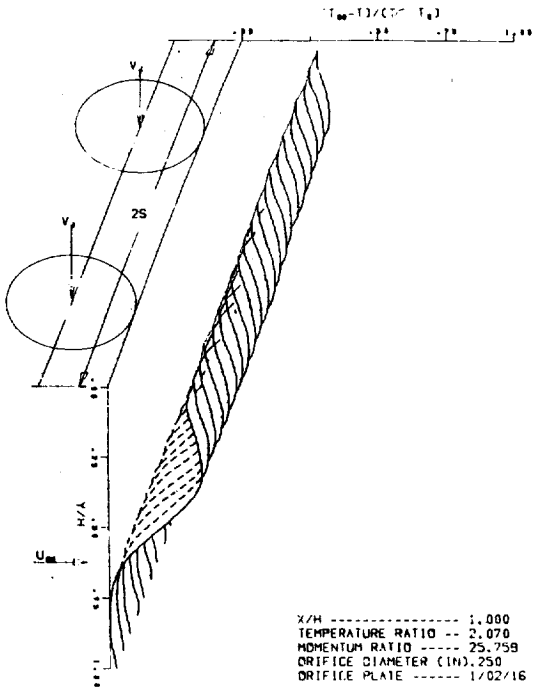

MULTIPLE JET TEST 3

CIRCULAR ORIFICE

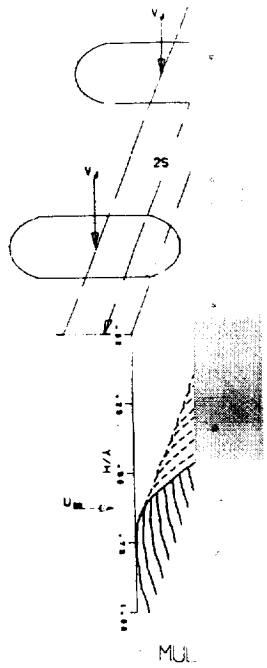

MUL

DIMENSIONLESS TEMPERATU

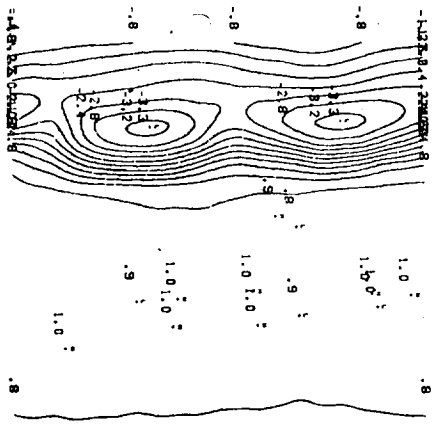

$1.-\theta/\theta_{AVG}$

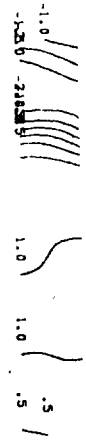

X/H ---------- .125
TEMPERATURE RATIO -- 2.070
MOMENTUM RATIO ----- 25.759
ORIFICE DIAMETER (IN).250
ORIFICE PLATE ------ 1/02/16

MULTIPLE JET TEST 3

CIRCULAR ORIFICE

MULT

DIMENSIONLESS TEMPERATURE C

FIGURE 31. EFFECT OF

FOLDOUT FRAME

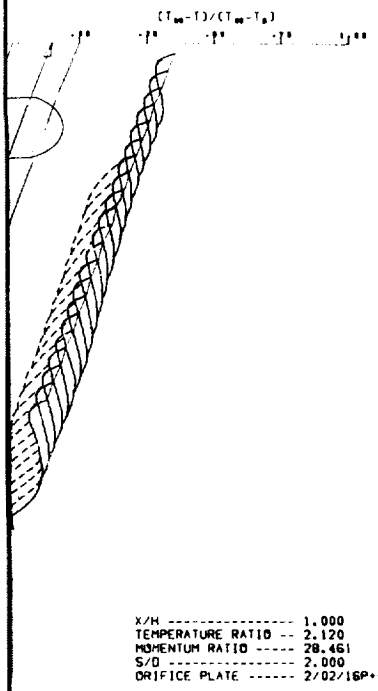

TIPLE JET TEST 79

ASPECT RATIO = 2 ORIFICE

RE PROFILES, NOMINAL MOMENTUM FLUX RATIO = 27, X/H = 1.0

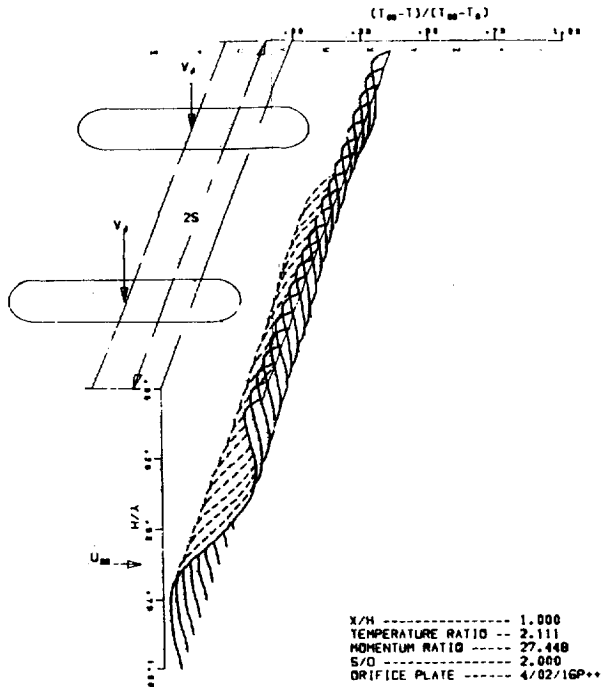

MULTIPLE JET TEST 30

ASPECT RATIO = 4 ORIFICE

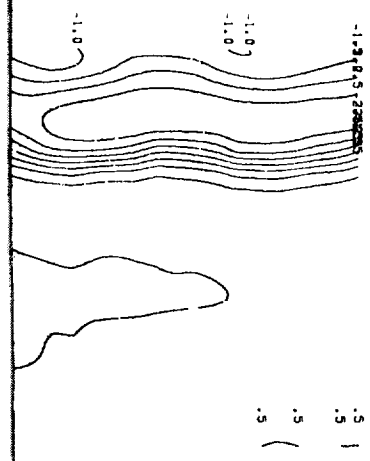

$1.-\Theta/\Theta_{AVG}$

INTERVAL = .5

X/H ---------- .125
TEMPERATURE RATIO -- 2.120
MOMENTUM RATIO ----- 28.461
S/O ---------- 2.000
ORIFICE PLATE ------ 2/02/16P++

PLE JET TEST 79

ASPECT RATIO = 2 ORIFICE

ONTOURS, NOMINAL MOMENTUM FLUX RATIO = 27, X/H = 0.125

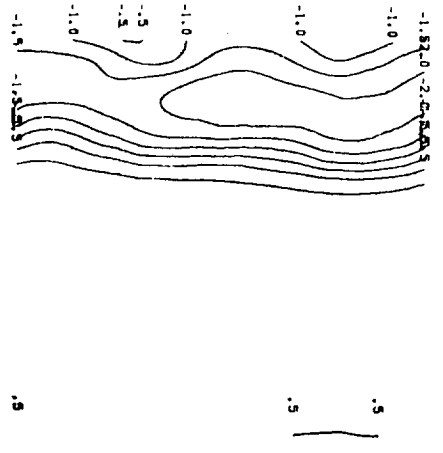

$1.-\Theta/\Theta_{AVG}$

INTERVAL = .5

X/H ---------- .125
TEMPERATURE RATIO -- 2.111
MOMENTUM RATIO ----- 27.448
S/O ---------- 2.000
ORIFICE PLATE ------ 4/02/16P++

MULTIPLE JET TEST 30

ASPECT RATIO = 4 ORIFICE

ORIFICE SHAPE ON TEMPERATURE PROFILES

Figure 31

FOLDOUT FRAME 2

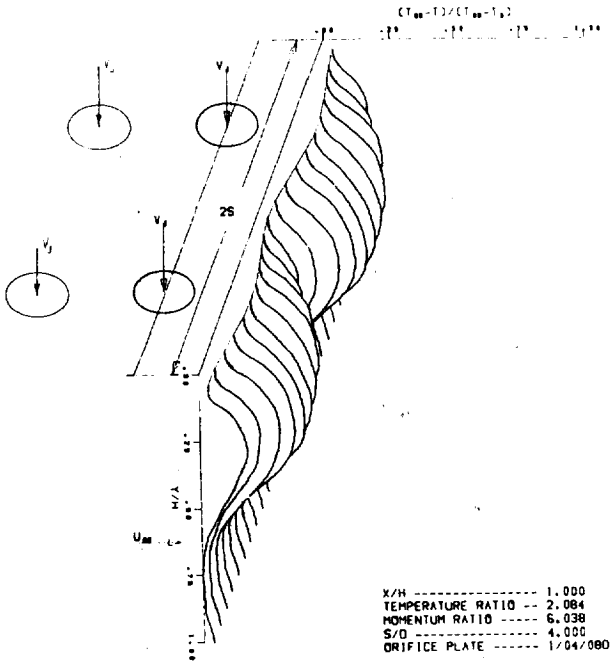

MULTIPLE JET TEST 90

DOUBLE ORIFICE ROW

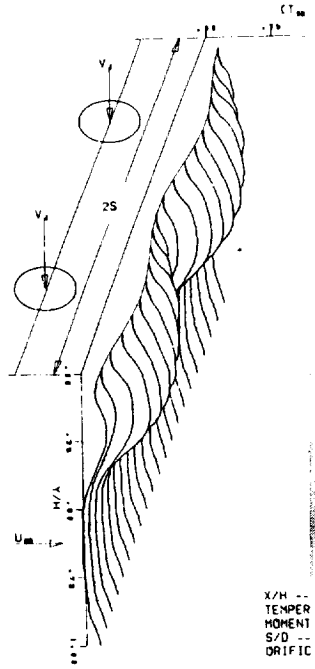

MULTIPLE JET TES

SINGLE ORIFICE ROW
A = 1/2 A OF DOUBLI

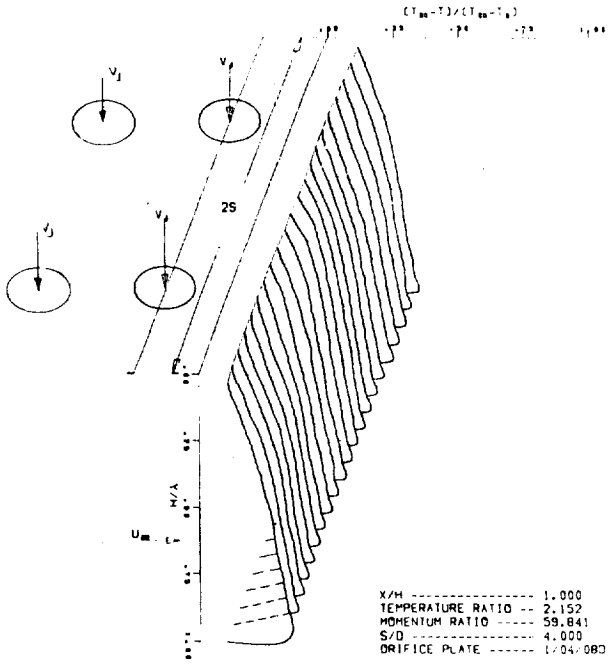

MULTIPLE JET TEST 93

DOUBLE ORIFICE ROW

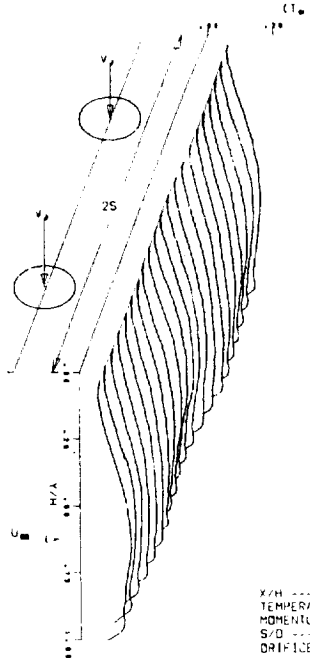

MULTIPLE JET TES

SINGLE ORIFICE RO
A = 1/2 A OF DOUB

FIGURE

FOLDOUT FRAME

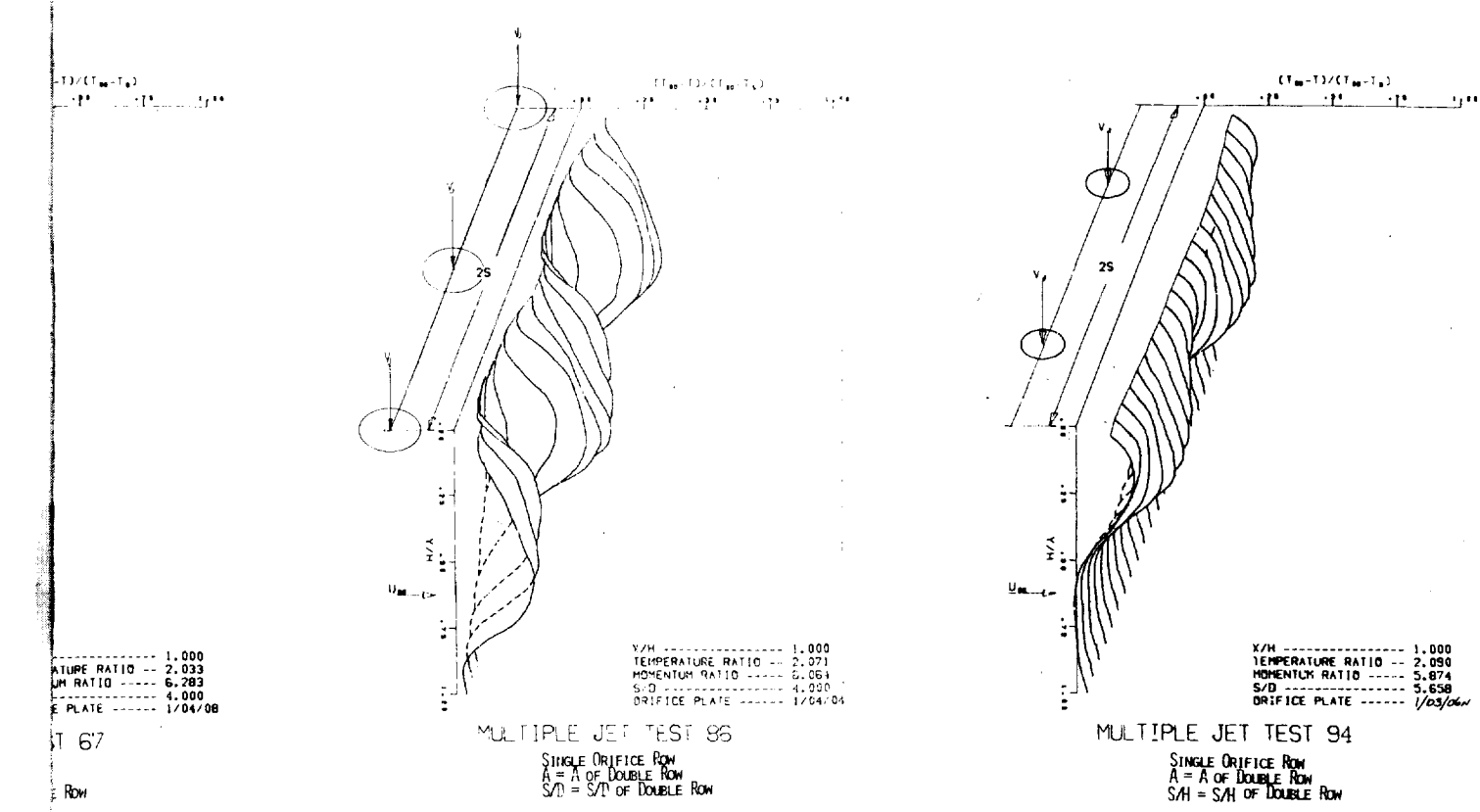

NOMINAL MOMENTUM FLUX RATIO = 6, X/H = 1.0

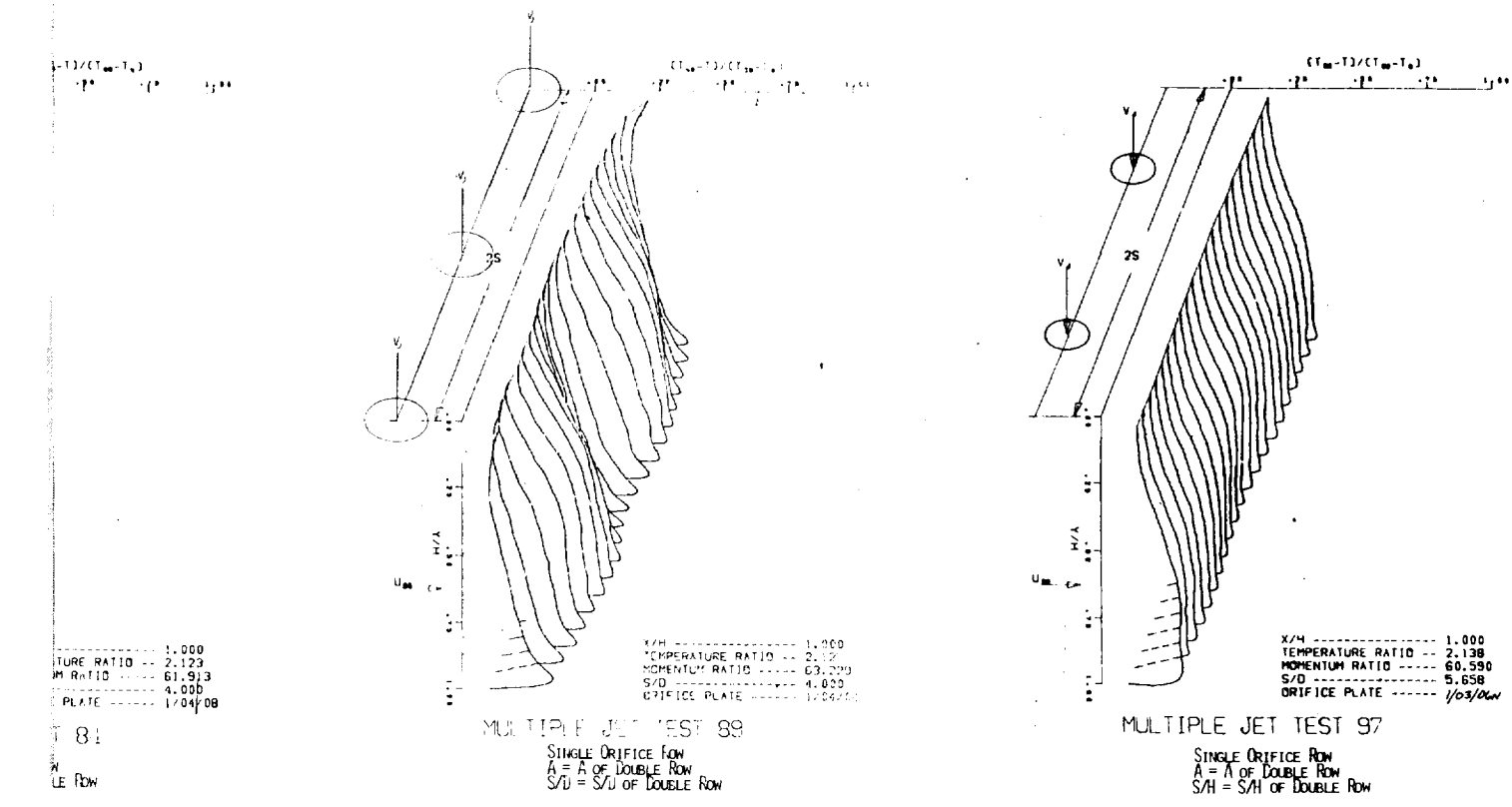

NOMINAL MOMENTUM FLUX RATIO = 60, X/H = 1.0

FIGURE 32

32. EFFECT OF DOUBLE ORIFICE ROWS ON TEMPERATURE PROFILE

FOLDOUT FRAME 2

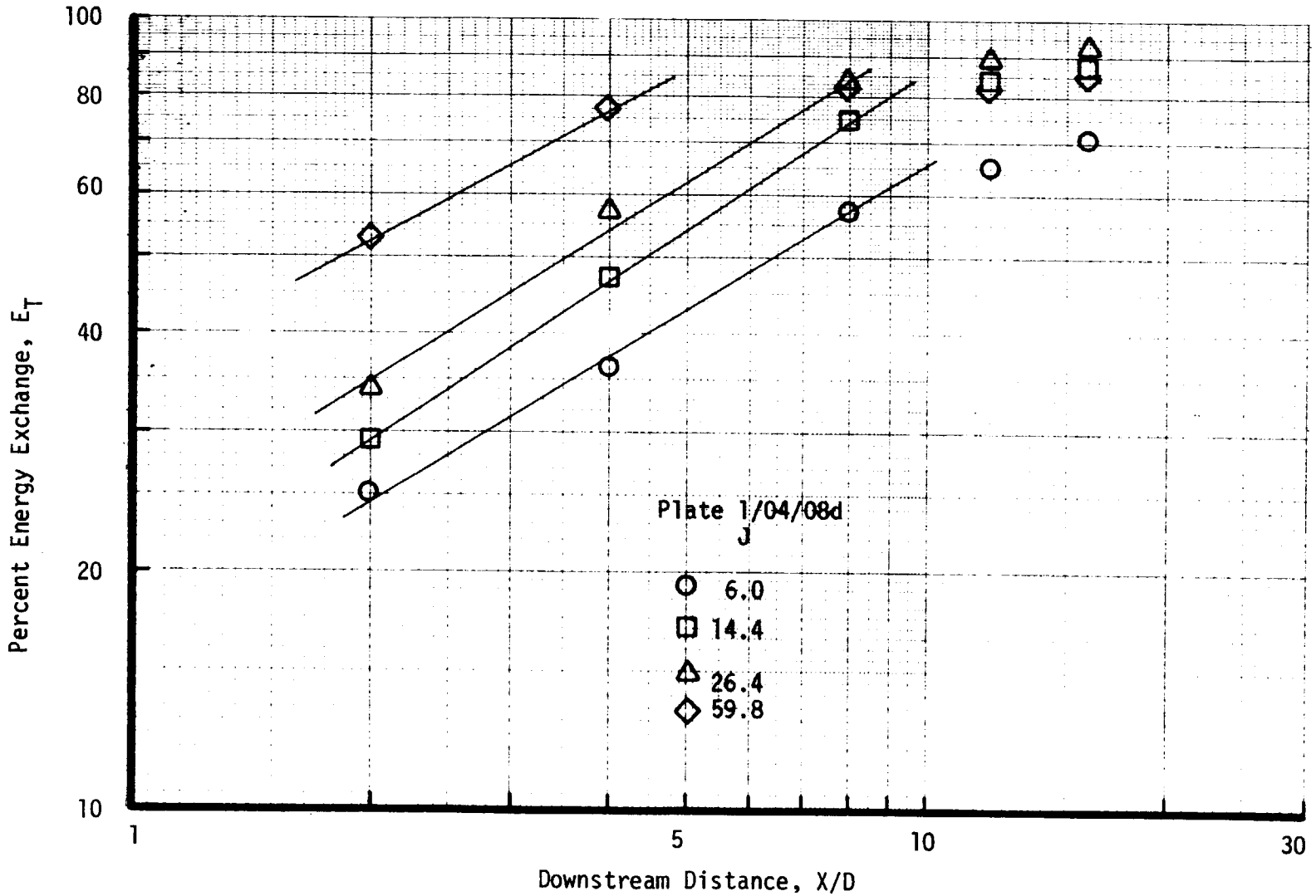

FIGURE 33. EFFECT OF X/D ON ENERGY EXCHANGE EFFICIENCY, ORIFICE PLATE 1/04/08d

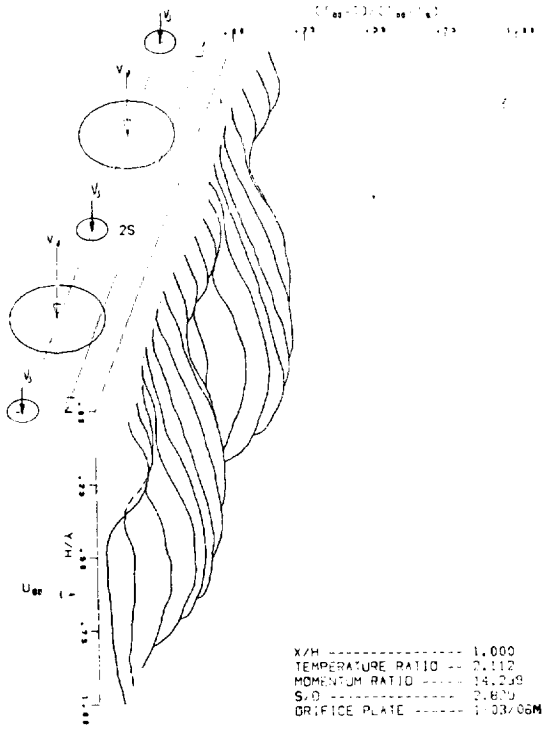

Mixed Orifice Size

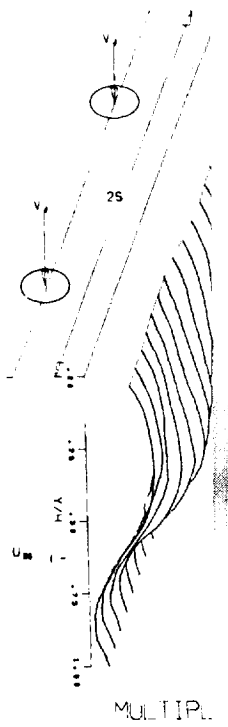

Single Or
A = A Mix
S/H = S/H

Nominal Momentu

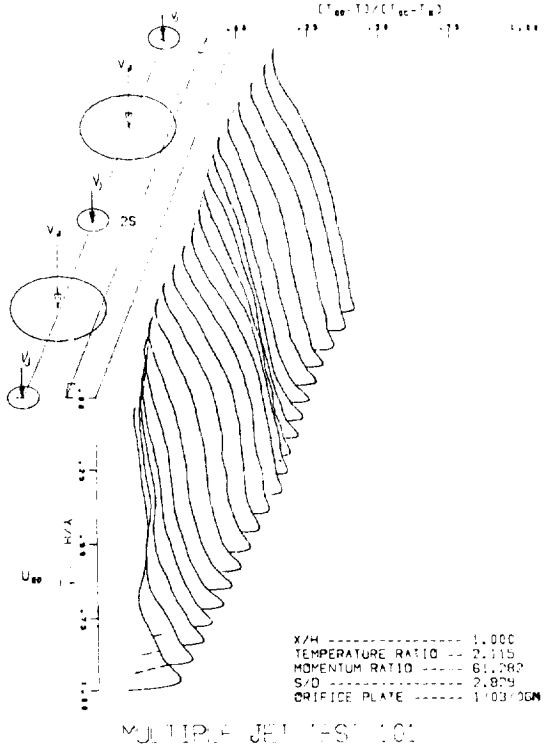

Mixed Orifice Size

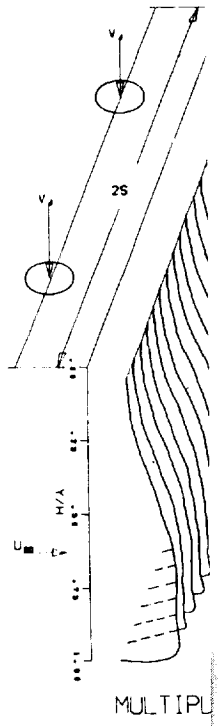

Single
A = A
S/H =

Nominal Mome

FOLDOUT FRAME

FIGURE 34. EFFECT OF MIXEI

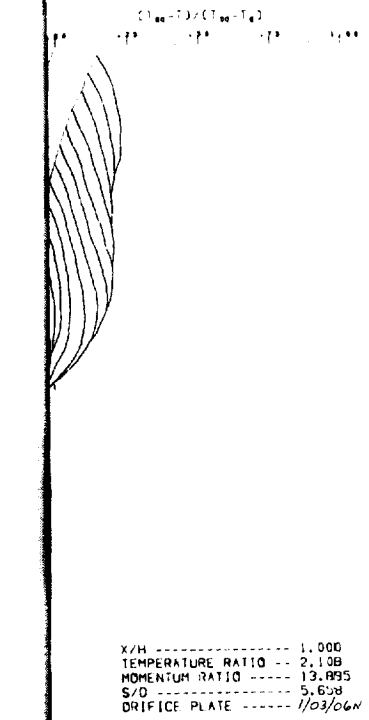

X/H ---------- 1.000
TEMPERATURE RATIO -- 2.108
MOMENTUM RATIO ----- 13.895
S/D ---------- 5.658
ORIFICE PLATE ------ 1/03/06N

E JET TEST 95

ifice Size
ed Orifice Size
Mixed Orifice Size Plate
m Flux Ratio = 14, X/H = 1.0

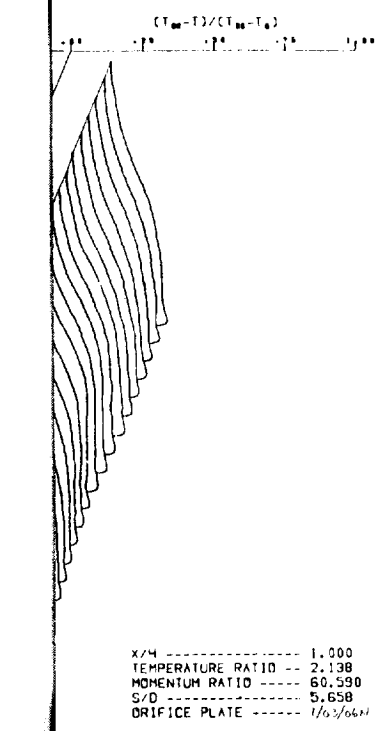

X/H ---------- 1.000
TEMPERATURE RATIO -- 2.138
MOMENTUM RATIO ----- 60.590
S/D ---------- 5.658
ORIFICE PLATE ------ 1/03/06N

E JET TEST 97

Orifice Size
Mixed Orifice Size
S/H Mixed Orifice Size Plate
ntum Flux Ratio = 60, X/H = 1.0

) ORIFICE SIZE ON TEMPERATURE PROFILE

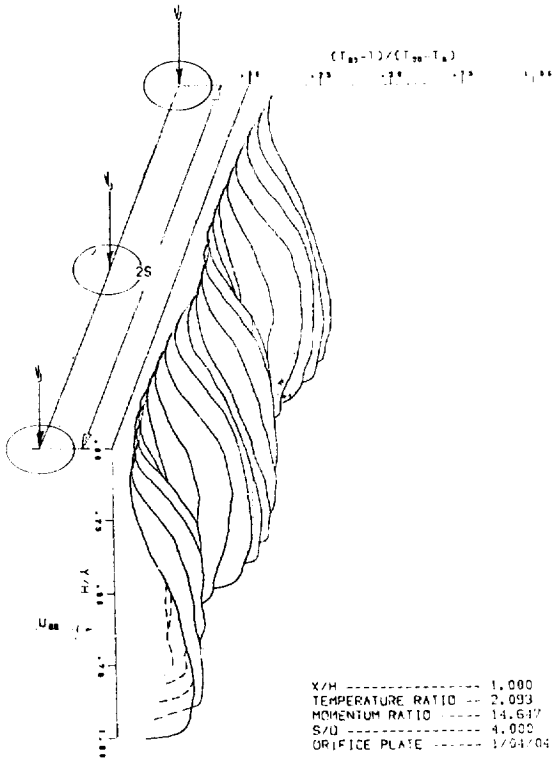

X/H ---------- 1.000
TEMPERATURE RATIO -- 2.093
MOMENTUM RATIO ----- 14.647
S/D ---------- 4.000
ORIFICE PLATE ------ 1/04/04

MULTIPLE JET TEST 87

Single Orifice Size
A = A Mixed Orifice Size
S/H = 2 S/H Mixed Orifice Size Plate

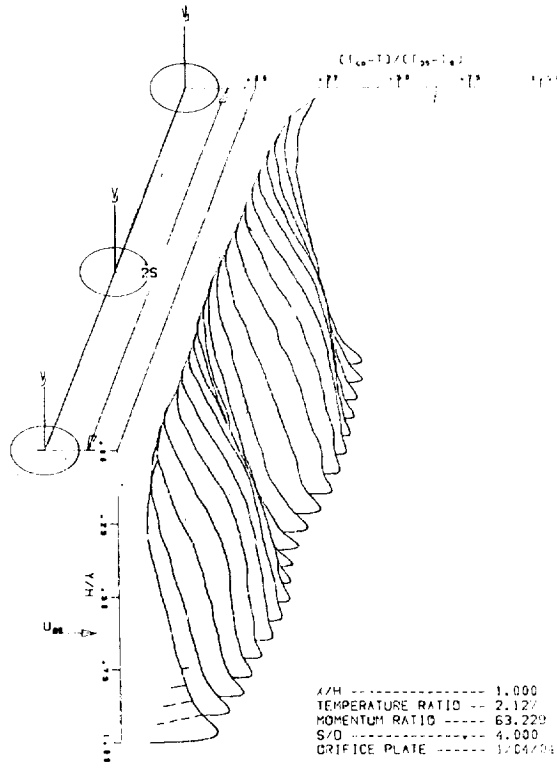

X/H ---------- 1.000
TEMPERATURE RATIO -- 2.12?
MOMENTUM RATIO ----- 63.229
S/D ---------- 4.000
ORIFICE PLATE ------ 1/04/04

MULTIPLE JET TEST 89

Single Orifice Size
A = A Mixed Orifice Size
S/H = 2 S/H Mixed Orifice Size Plate

FIGURE 34

FOLDOUT FRAME 2

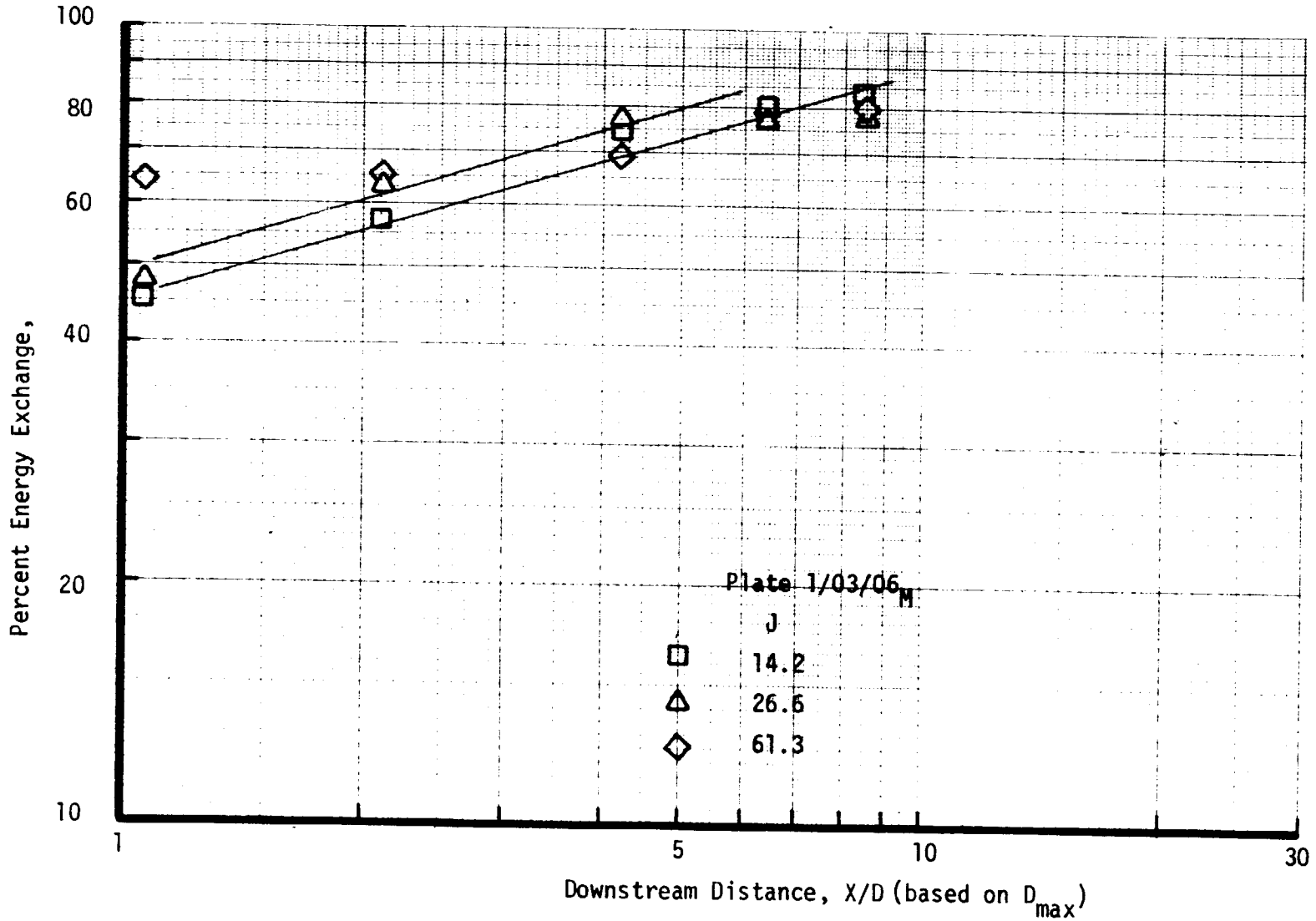

FIGURE 35. EFFECT OF X/D ON ENERGY EXCHANGE EFFICIENCY, ORIFICE PLATE $1/03/06_M$

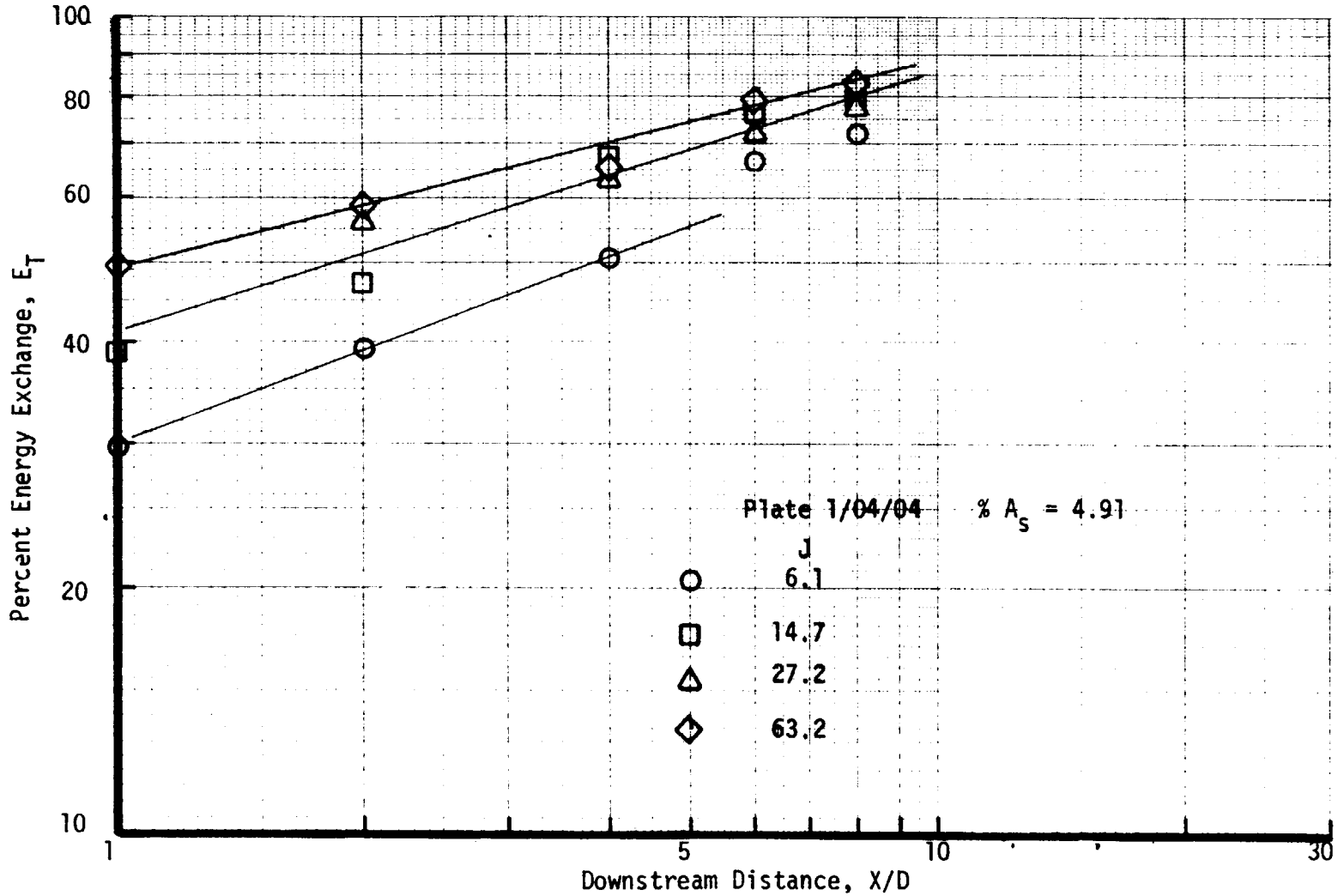

FIGURE 36. EFFECT OF X/D ON ENERGY EXCHANGE EFFICIENCY ORIFICE PLATE 1/04/04

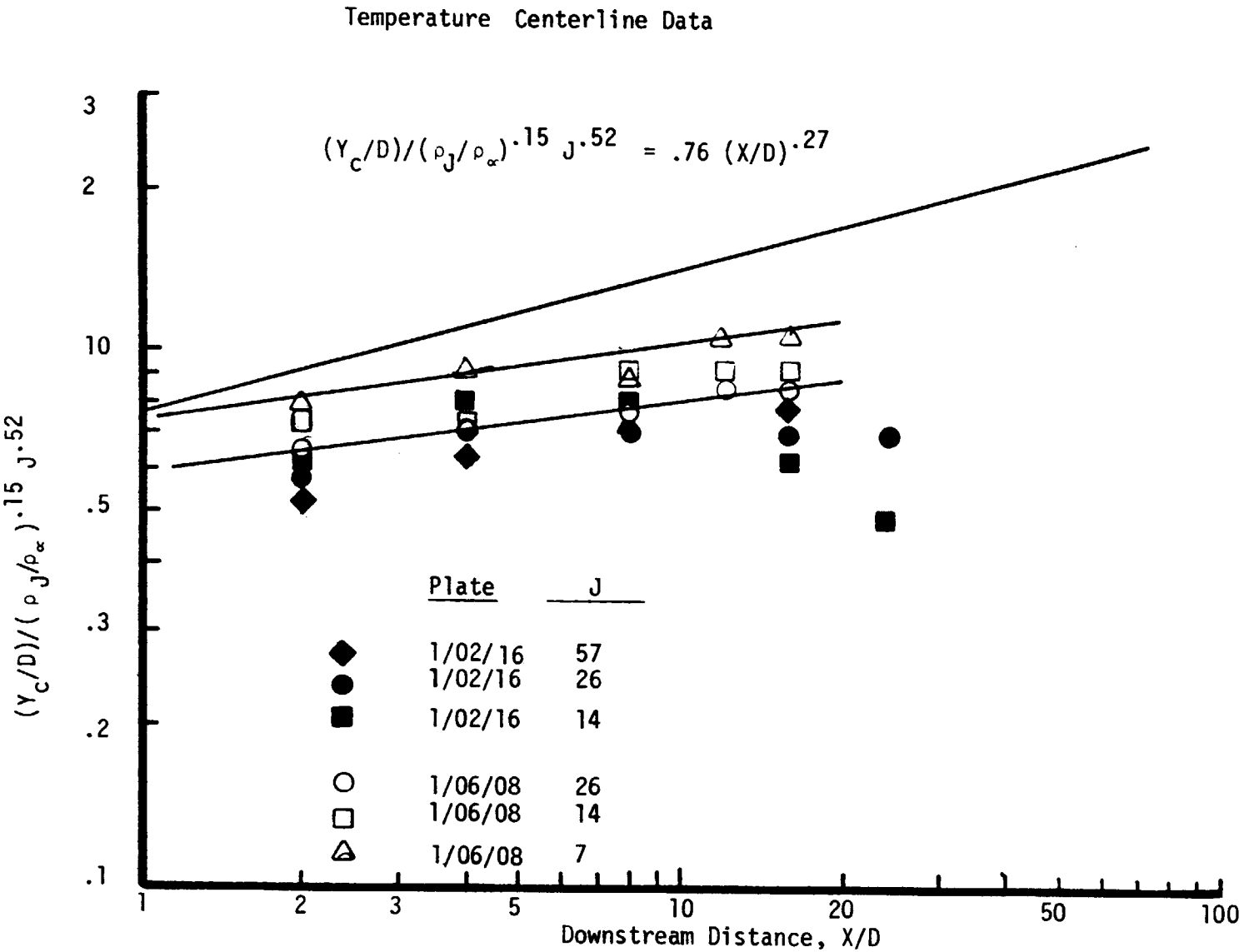

FIGURE 37. COMPARISON OF MULTIPLE JET AND SINGLE JET TEMPERATURE CENTERLINE DATA

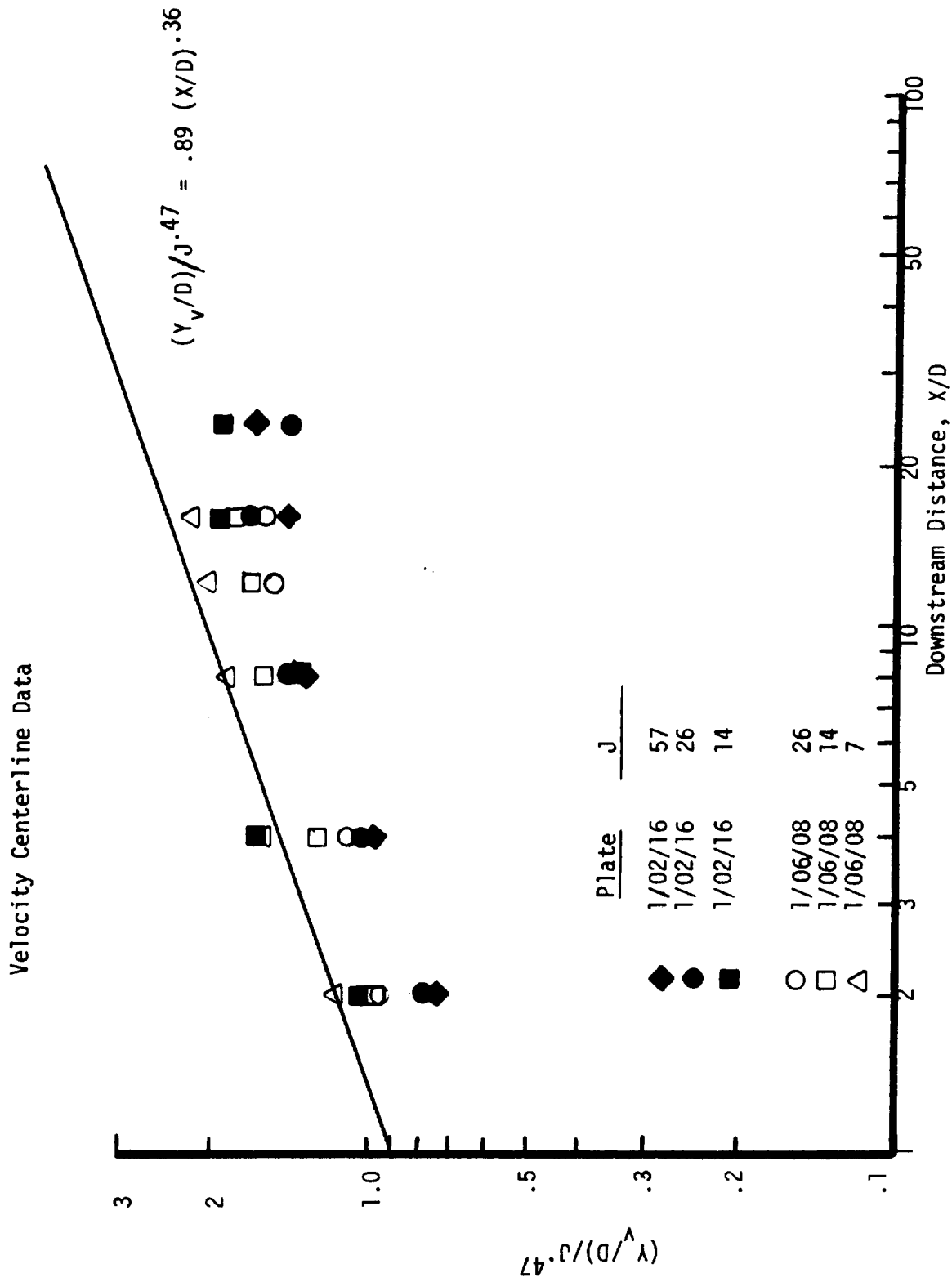

FIGURE 38. COMPARISON OF MULTIPLE JET AND SINGLE JET VELOCITY CENTERLINE DATA

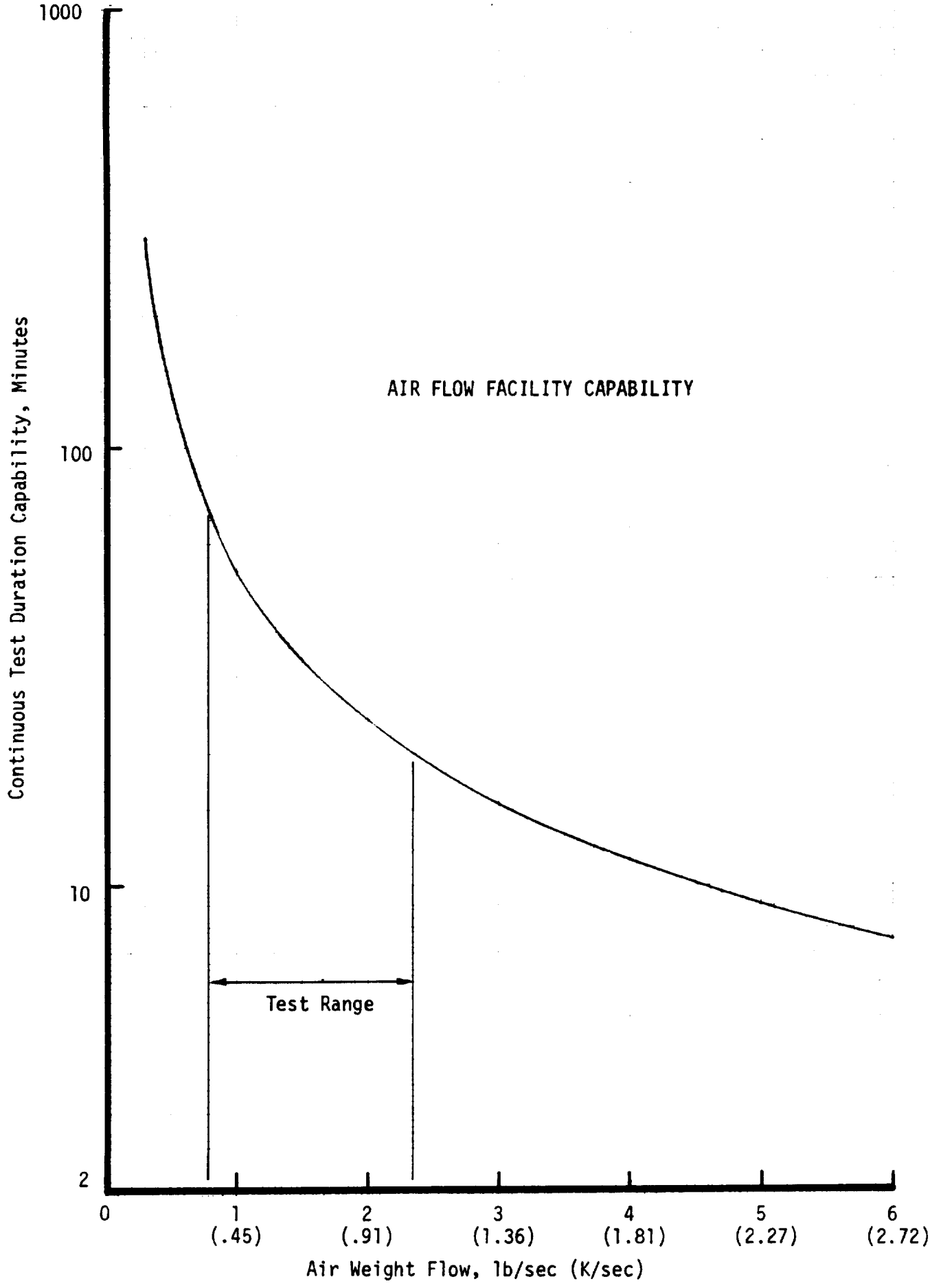

FIGURE 39. AIR FLOW FACILITY CAPABILITY

TEST DUCT REYNOLDS NUMBERS

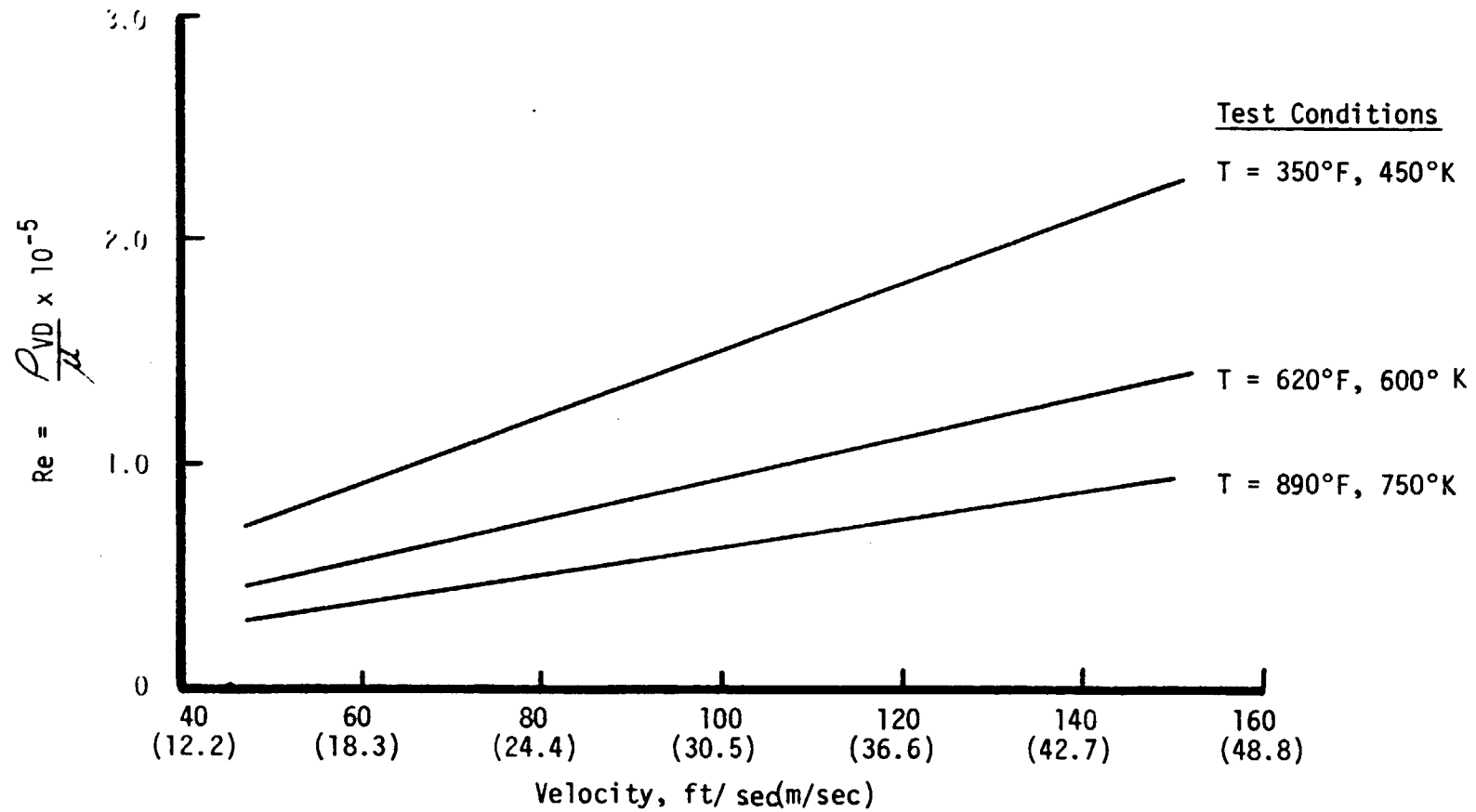

FIGURE 40. TEST DUCT REYNOLDS NUMBER

TEST DUCT
BOUNDARY LAYER DEVELOPMENT
AND
TRIP LOCATION

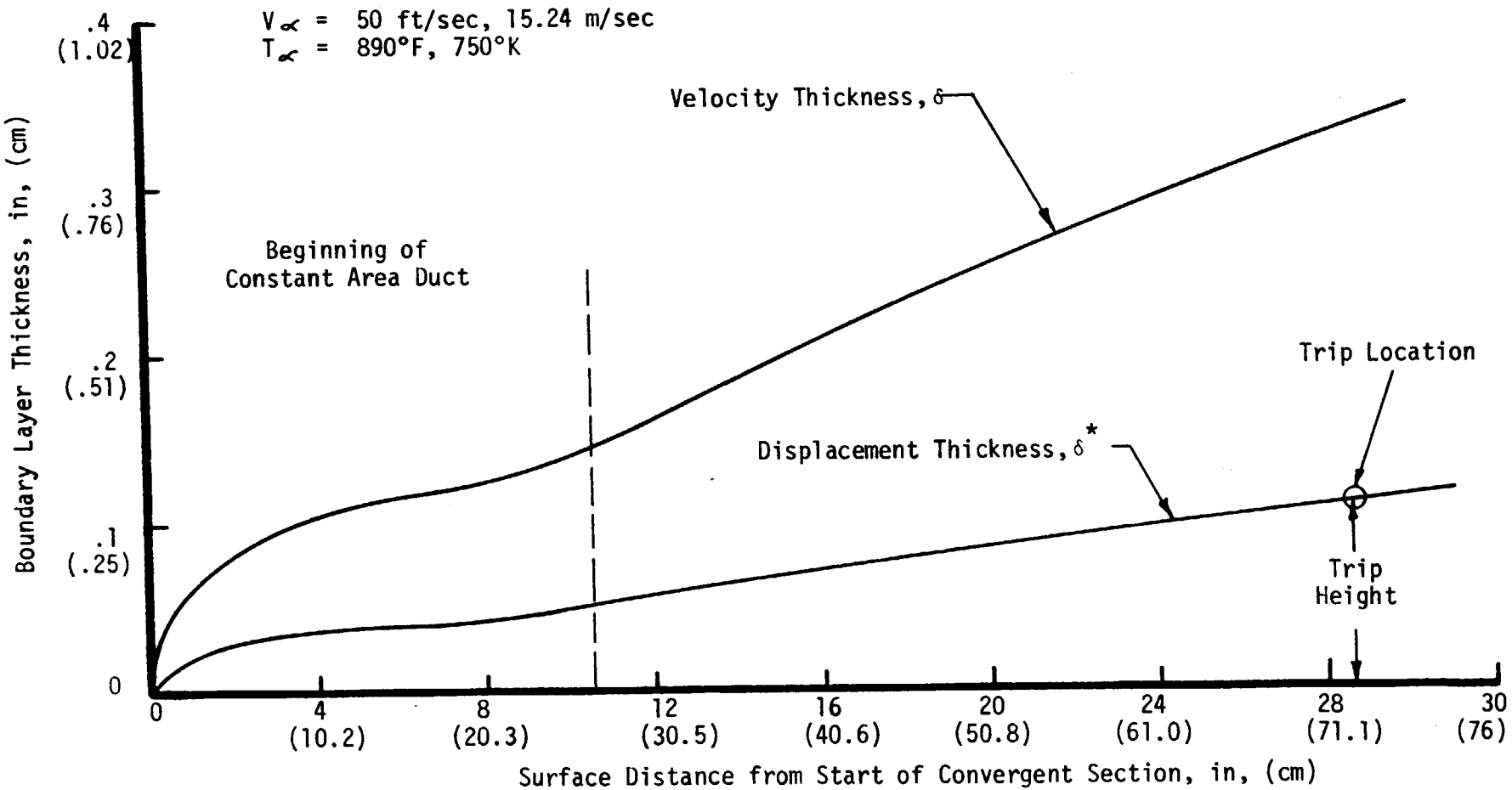

FIGURE 41. TEST DUCT BOUNDARY LAYER DEVELOPMENT AND TRIP LOCATION

DISTRIBUTION LIST FOR NASA CR-121217, Multiple Jet Study

NASA Scientific and Technical Information Facility P. O. Box 33 College Park, MD 20740 Attn: Acquisitions Branch			10
NASA - Lewis Research Center 21000 Brookpark Road Cleveland, OH 44135			
Attn:	Library	MS 60-3	2
	Technology Utilization	MS 3-19	1
	Report Control Office	MS 5-5	1
	Patent Counsel	MS 500-311	1
	Director of Aeronautics	MS 3-3	1
	Chief, Fluid Systems Components Division	MS 5-3	1
	Chief, V/STOL and Noise Division	MS 501-5	1
	Chief, Wind Tunnel and Flight Division	MS 86-1	1
	Chief, Airbreathing Engines Division	MS 60-4	1
	Chief, Physical Science Division	MS 301-1	1
	Head, Contract Section A, Technology Procurement Br.	MS 500-206	1
	AAMRDL	MS 500-317	1
	W. T. Olson	MS 3-16	1
	J. F. Dugan, Jr.	MS 86-1	1
	R. A. Rudey	MS 60-6	1
	R. E. Jones	MS 60-6	1
	J. S. Grobman	MS 60-6	1
	D. J. Poferl	MS 77-2	1
	J. E. Rohde	MS 77-2	1
	R. W. Graham	MS 301-1	1
	R. Siegel	MS 301-1	1
	W. H. Braun	MS 301-1	1
	C. J. Marek	MS 60-4	1
	C. T. Norgren	MS 60-6	1
	H. F. Butze	MS 60-6	1
	F. M. Humenik	MS 60-6	1
	J. A. Albers	MS 501-4	1
	J. D. Holdeman	MS 60-6	45

DISTRIBUTION LIST - NASA CR-121217 cont'd.

NASA Headquarters
600 Independence Ave., S.W.
Washington, D. C. 20546
Attn: N. F. Rekos (RAP) 1
Dr. W. H. Roudebush (RL) 1
J. Suddreth (RL) 1

NASA Langley Research Center
Langley Station
Hampton, VA 23365
Attn: Library 1
Dr. D. M. Bushnell 1
Dr. R. S. Levine 1

NASA Flight Research Center
P. O. Box 273
Edwards, CA 93523
Attn: J. Nugent, Code R 1

Jet Propulsion Laboratory
4800 Oak Grove Drive
Pasadena, CA 91103
Attn: Dr. James King, MS 183-401 1

NASA Ames Research Center
Moffett Field, CA 94035
Attn: Dr. I. G. Poppoff, MS 254-1 1
Library 1

Department of Transportation
400 7th Street, SW
Washington, D. C. 20590
Attn: Dr. R. Underwood, Code TST 1

FAA Headquarters
800 Independence Ave., S.W.
Washington, D. C. 20533
Attn: W. T. Westfield 1
Library 1

DOT Transportation Systems Center
55 Boradway
Cambridge, MA 02142
Attn: A. Broderick (TI) 1

DISTRIBUTION LIST - NASA CR-121217 cont'd.

Environmental Protection Agency
Research Triangle Park
Raleigh, NC 27711
Attn: E. E. Berkau 1
D. G. Lachapelle 1
D. Pershing 1
J. Wasser 1

Environmental Protection Agency
Advanced Automotive Power Systems Division
Ann Arbor, MI 48105
Attn: T. Sebestyen 1
Dr. W. Mirsky 1

United States Air Force
Aero Propulsion Laboratory
Area B, Bldg. 18D
Wright-Patterson A.F.B.
Dayton, OH 45433
Attn: R. E. Henderson AFAPL/TBC 1
Capt. W. Blazowski AFAPL/SFF 1
K. Mach 1

Air Force Office of Scientific Research
1400 Wilson Boulevard
Arlington, Virginia 22209
Attn: SREP 1

Department of the Army
U. S. Army Aviation Material Laboratory
Propulsion Division (SAUFE-PP)
Ft. Eustis, VA 23604
Attn: E. T. Johnson 1
Robert G. Dodd, SAVDL-EU-PP 1

Michigan State University
Department of Mechanical Engineering
201 Engineering Building
East Lansing, MI 48823
Attn: Professor J. F. Foss 1

Case Western Reserve University
Division of Fluid, Thermal, and Aerospace Sciences
Glennan Building
Cleveland, OH 44106
Attn: Professor Isaac Greber 1
Dr. Y. Kamotani 1

Bell Aerospace Company
Advanced Technology Research
P. O. Box 1
Buffalo, NY 14240
Attn: Dr. S. W. Zelazny 1

Northern Research and Engineering Corp.
219 Vassar Street
Cambridge, MA 02139
Attn: Dr. E. R. Norster 1
Dr. D. M. Dix 1

General Electric Company
Flight Propulsion Division
Cincinnati, OH 45215
Attn: Technical Info. Center N-32 1
D. Bahr 1

Detroit Diesel Allison Division
Department 8894, Plant 8
P. O. Box 894
Indianapolis, Indiana 46206
Attn: Dr. H. J. Brandon 1
Library 1

General Applied Science Labs
Merrick and Stewart Avenues
Westbury, Long Island, NY 11590
Attn: Dr. R. Edelman 1

Fluidyne Engineering Corporation
5900 Olson Memorial Highway
Minneapolis, Minnesota 55422
Attn: O. P. Lamb 1

AiResearch Manufacturing Company of Arizona
Division of the Garrett Corporation
402 South 36th Street
Phoenix, Arizona 85034
Attn: J. M. Haasis 1

Massachusetts Institute of Technology
Department of Mechanical Engineering
Cambridge, MA 02139
Attn: Professor J. A. Fay 1
Professor J. B. Heywood 1

DISTRIBUTION LIST - NASA CR-121217 cont'd.

Advanced Technology Laboratory
400 Jericho Turnpike
Jericho, NY 11753
Attn: Dr. A. Ferri — 1

Virginia Polytechnic Institute
and State University
Department of Aerospace Engineering
Blacksburg, VA 24061
Attn: Professor J. A. Shetz — 1

Arnold Engineering Development Center
J. Division, Engine Test Facility
Arnold Air Force Station, Tenn. 37389
Attn: Dr. C. E. Peters — 1
Dr. P. T. Harsha — 1
D. W. Male — 1

The University of Tennessee Space Institute
Tullahoma, Tennessee 37388
Attn: Professor G. W. Braun — 1

Georgia Institute of Technology
School of Aerospace Engineering
Atlanta, Georgia 30332
Attn: Professor L. H. Bangert — 1

Washington State University
College of Engineering Research Division
Pullman, Washington 99163
Attn: Dr. C. T. Crowe — 1

Surface Combustion Division
Midland-Ross Corporation
2375 Dorr Street
Toledo, OH 43691
Attn: Dr. Klaus H. Hemsath — 1

University of Minnesota
Mechanical Engineering Department
Minneapolis, Minnesota 55455
Attn: Professor R. J. Goldstein — 1

Purdue University
School of Mechanical Engineering
West Lafayette, Indiana
Attn: Professor V. W. Goldschmidt — 1

Polytechnic Institute of Brooklyn
Department of Aerospace Engineering
and Applied Mechanics
Long Island Graduate Center
Route 110, Farmingdale, NY 11735
Attn: Professor P. M. Sforza 1

Lockheed Missile and Space Company
Palo Alto Research Laboratory
3251 Hanover Street
Palo Alto, CA 94304
Attn: Dr. R. J. Conti 1

Solar Division
International Harvester Company
2200 Pacific Highway
San Diego, CA 92138
Attn: W. Compton 1

General Motors Research Laboratories
12 Mile and Mound Roads
Warren, MI 48090
Attn: W. Cornelius 1

University of Illinois at Urbana - Champaign
Department of Aeronautical and Astronautical Engineering
Urbana, Illinois 61801
Attn: Professor R. A. Strehlow 1

University of California at Berkeley
Department of Mechanical Engineering
Berkeley, CA 94720
Attn: Professor R. F. Sawyer 1

Northwestern University
Department of Mechanical Engineering
Evanston, Illinois 60201
Attn: Professor A. A. Kovitz 1

United Aircraft Corporation
400 Main Street
East Hartford, Connecticut 06108
Attn: R. L. O'Brien(UARL) 1
L. S. Cohen (UARL) 1
Library (UARL) 1
R. Marshall (P&WA) 1

Pratt and Whitney Aircraft
Florida Research and Development Center
Box 2691
West Palm Beach, Florida 33402
Attn: G. B. Cox, Jr. 1
D. J. Nielsen 1

AVCO Lycoming Division
550 South Main Street
Stratford, Conn. 06497
Attn: D. Eckber 1